FAIRCHILD IMAGING SYSTEMS
A Division of Fairchild Camera and Instrument Corporation

(4)

(14) Technical Report No. ED-AX-82

(6) CCD PERISCOPE PROGRAM

(9) FINAL REPORT, MAY 75-MAY 77.

(11) 6 June 77 (12) 164p.

This document is furnished in response to the Naval Electronics System Command Contract No. N00039-75-C-0410. The Government shall have the right to duplicate, use, or disclose the data to the extent provided in the contract. This restriction does not limit the Government's right to use information contained in the data if it is obtained form another source.

for

Naval Electronics System Command

(15) Contract No. N00039-75-C-0410

A. Approved for public release, distribution unlimited

409993

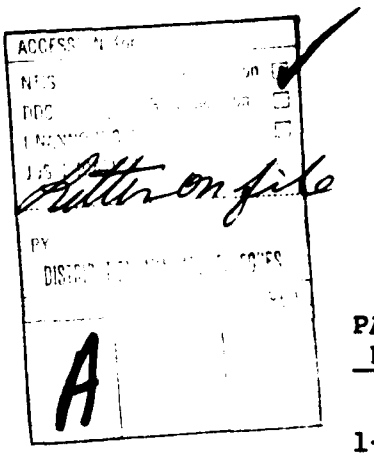

TABLE OF CONTENTS

TABLE OF CONTENTS (Continued)

TABLE OF CONTENTS (Continued)

LIST OF ILLUSTRATIONS

LIST OF ILLUSTRATIONS (Continued)

LIST OF ILLUSTRATIONS (Continued)

SECTION I

1.0 INTROUDCTION

This report describes, in detail, the work performed by Fairchild on the CCD Periscope Program, Navy Contract No. N00039-75-C-0410, from the period of May 1975 to May 1977. The results of this effort clearly demonstrate the advantages of utilizing a specialized time delay and integration charge coupled device (TDI-CCD) visual spectrum sensor for detecting and recognizing sea-surface target under low light level starlight or higher illumination, low contrast conditions.

The work described includes a) the initial contract requirements, i.e., feasibility demonstrations, stabilization and display studies, system definition efforts, b) an add-on modification to the contract, i.e., a 2-chip hybrid sensor test/demonstration effort and the incorporation of a "falling raster" display into the feasibility demonstration equipment. The falling raster or "moving window" display segment of the add-on program effort was provided by Fairchild at no cost to the Navy and c) a second modification to the referenced contract requiring the incorporation of calibrated vibration-inducing mechanisms into the feasibility model equipment to evaluate imaging performance of the CCD Periscope feasibility system under typical periscope motion conditons. This segment of work was designed to provide guidance to practical stabilization designs.

Section II presents a brief summary of the CCD Periscope Program and the conclusions derived; the technical details of the program are presented in Section III. Each of the key elements of the feasibility demonstration model equipment is described in detail in this section. Also provided in this section are the test results from the two prescribed feasibility model configurations, i.e., both the high resolution and the low light level CCD electro-optical camera configurations.

Section IV presents the results of stabilization studies related to a type 16 periscope mast. These analyses were based on inputs provided by Navy-supplied literature referenced in the study. Display and recording studies conducted during the program are discussed in detail in Section V. These investigations include both "real time" and "relaxed time replay" modes of operation and how they relate to sensor operation.

System definition efforts are discussed in Section VI; these include system parameters and tradeoffs considered, optical/mechanical configuration investigations for potential periscope mast installations of a CCD System, and preliminary CCD low light level performance analyses.

SECTION II

2.0 SUMMARY AND CONCLUSIONS

A key objective of the Day/Night Periscope program was to demonstrate the feasibility of using charge coupled devices to provide low light level, high resolution sensing in periscopes that would solve operational surveillance problems.

The procedures used to demonstrate feasibility were two specified investigations, i.e., High Resolution Scanning and Integrating Mode Low Light operation, using a 1 x 1728 linear CCD sensor and a 128 x 128 TDI CCD Integrating Mode Sensor, respectively.

A simulation of a panoramic scan about a vertical axis was also prescribed for the feasibility investigations with the following Navy specifications:

FEASIBILITY TEST INSTRUMENTATION PARAMETERS

	Integrating Mode	High Resolution Mode
Sensor Array	128 x 128	1 x 1728
Number of Elements	128	1728
Element Pitch	20 μm (.00079")	13 μm).00051")
Focal Length	1"	3"
Vertical Angle	5.86°	16.77°
Scan Rate	18°/sec	37.3°/sec
Exposure Time	325 ms	260 μs
Lines per 180° Scan	3932	18547
Data Rate	10^6 elem/sec	6.9 x 10^6 elem/sec
Scene Irradiance/ Brightness	3 x 10^{-9} W/cm^2	100 ft. lamberts

In addition, the following design studies were specified: 1) analysis of Navy field results to aid in defining an image stabilization system, 2) a design study of "real time" and "replay" display configurations, and 3) a preliminary system definition for the CCD Periscope.

Additional efforts added to the program were a "2-chip Hybrid TDI Sensor" to be incorporated in the periscope feasibility model system and a "falling raster" or "moving window" display implementation.

2.1 PERISCOPE PANORAMIC SCANNER INSTRUMENTATION

The feasibility test instrumentation designed and fabricated for demonstrating system sensor performance for the periscope application is shown in the block diagram of Figure 2-1 and in the photograph of Figure 2-2. It inlcudes a rotating table to simulate periscope scanning, controllable light source, lens, array sensors, array logic and drive circuits, signal processing amplifiers and image display equipment. The display equipment consists of both a direct CRT display with a polaroid camera recorder and a scan converter for single frame storage and TV monitor display of the image at 30 frames per second. It also incorporates a moving window display. Each sensor, the high resolution and/or the integrating sensor configuration, with its lens and control electronics, is interchangeable on the rotating table.

The high resolution arrangement was operated, however, with its own scanner arrangement as shown in Figure 2-3 to avoid testing schedule conflicts.

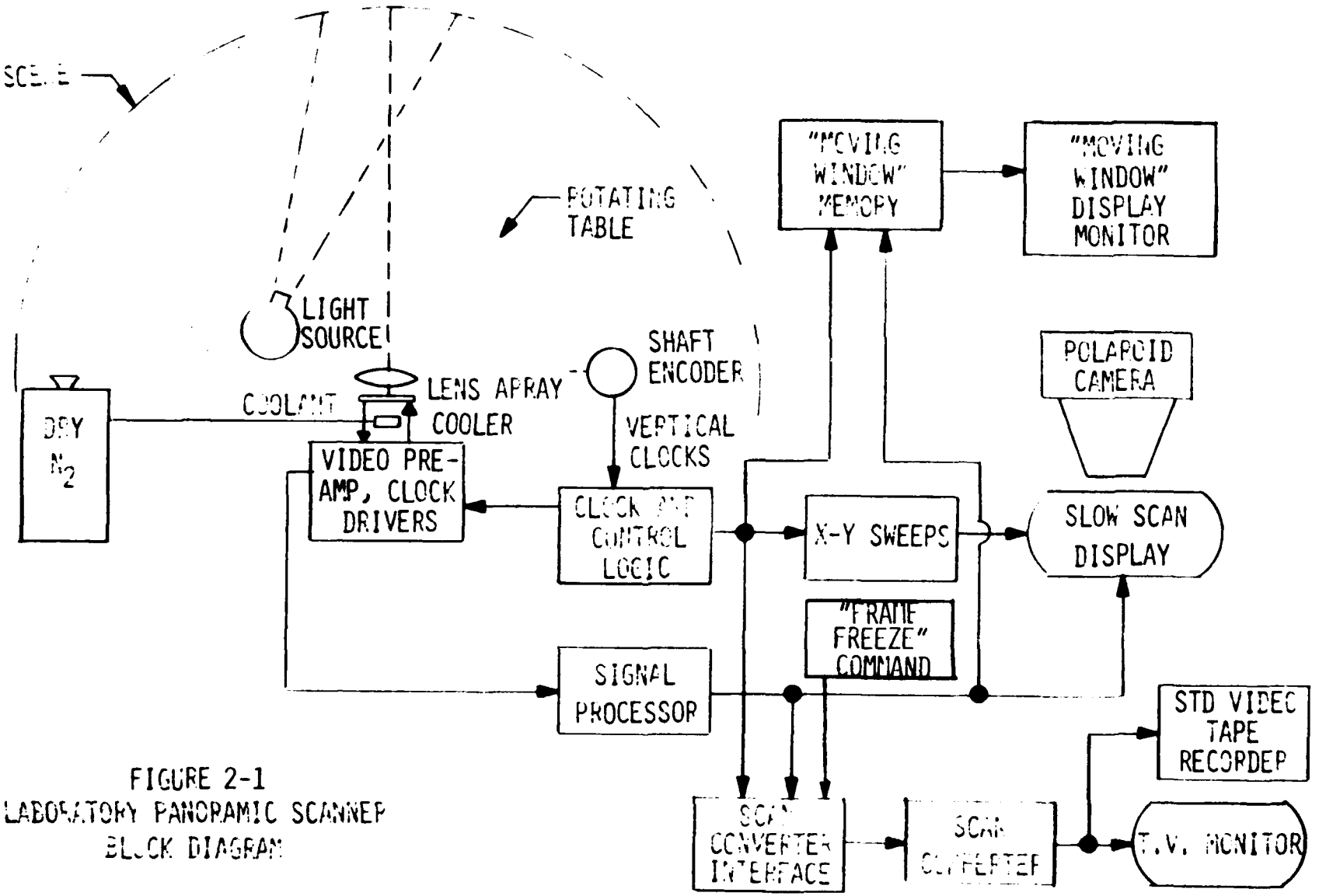

FIGURE 2-1
LABORATORY PANORAMIC SCANNER
BLOCK DIAGRAM

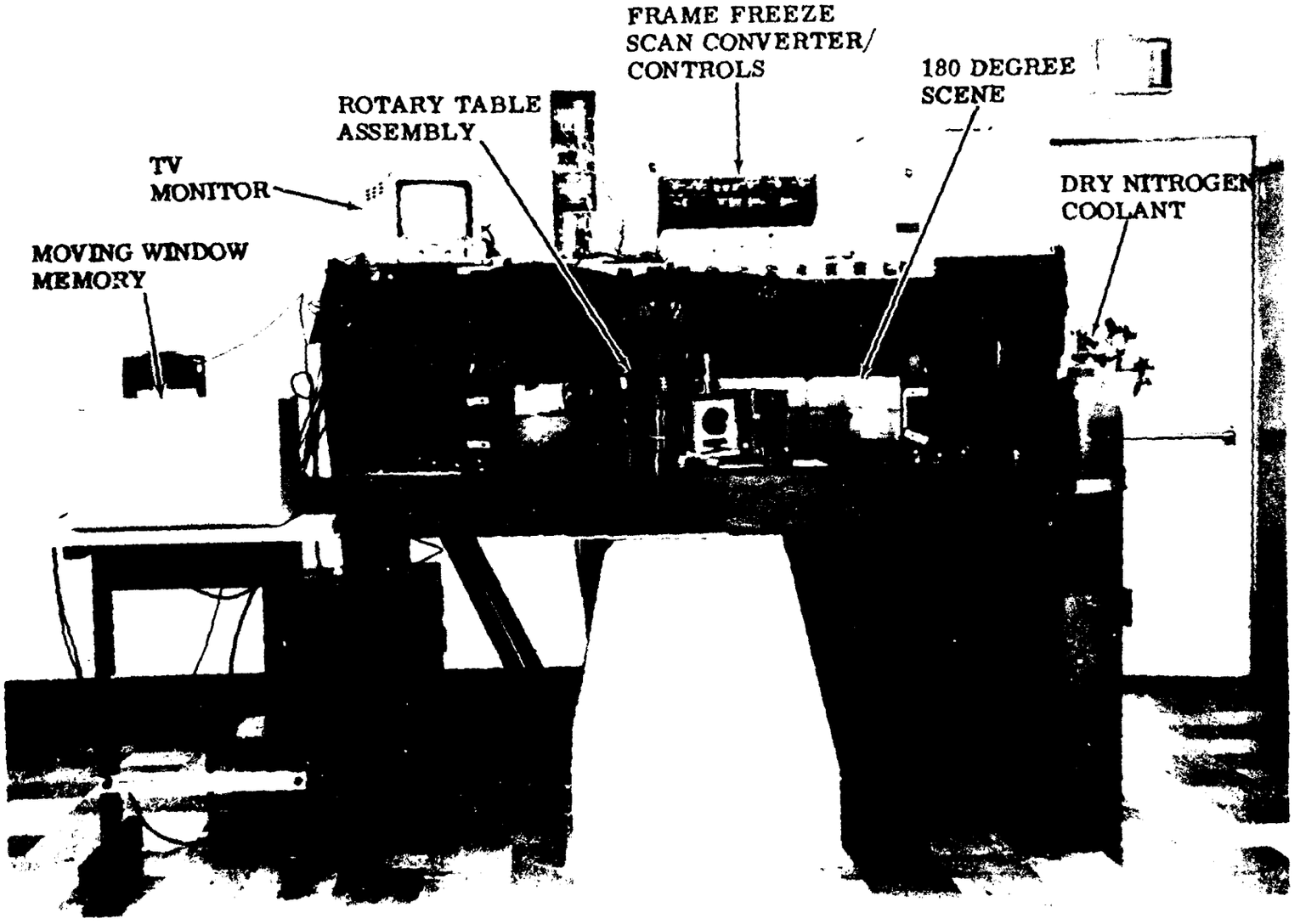

FIGURE 2-2. CCD PERISCOPE PANORAMIC SCANNER

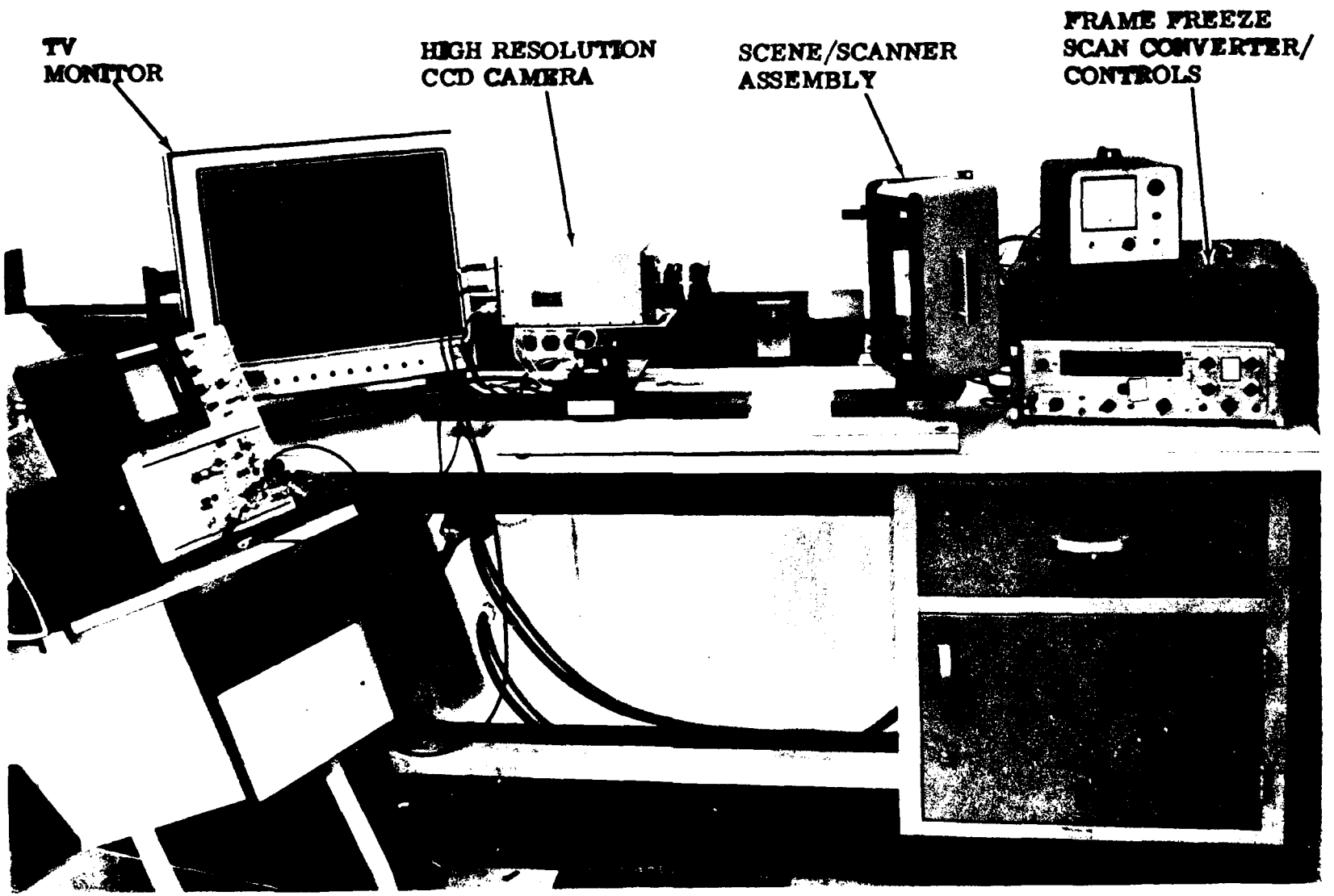

FIGURE 2-3. PHOTOGRAPH OF HIGH RESOLUTION SCANNER

Clocking voltages used to transfer signal charges from row-to-row in synchronism with the image motion at the array plane of the 128 x 128 line sensor are driven from a shaft encoder coupled to the rotating table. Temperature control of the array, required to reduce dark current under low light input conditions, is provided by a cooled dry nitrogen system.

The test instrumentation operation is described briefly in the following paragraphs.

2.1.1 Sensor Arrays

The scanner arrays used in the Day/Night Periscope configurations were the 128 x 128 TDI CCD array (for integrating mode operation) and the 1 x 1728 CCD linear array (for high resolution mode operation). The general characteristics of these CCD arrays are shown in Section III.

2.1.2 Rotary Stage/Encoder

The rotary stage, simulating a panoramic scan about a vertical axis, is a high accuracy rotary table of 12" diameter, driven by a servo motor, for constant velocity operation. The speed of the table is adjustable by a front panel control using a precision potentiometer and dial. The system is designed to operate in the forward direction for 180°; after completion of the half cycle, the table is driven back to the starting position. This operation can be continuously performed when the "run" control switch is on. However, when only one cycle is desired, the operator pushes the single cycle momentary switch.

A high precision angular encoder is directly connected by a worm drive to the table. Based on the encoder resolution and the worm wheel drive ration, the total number of counts derived is 180,000 per a 360° rotation of the table or a resolution of 0.12' of arc.

The encoder output pulses are used, after processing in a digital adjusting circuit, to clock the TDI arrays. This arrangement assures synchronism between image motion and clocking rates thereby allowing the "summing" or integration of signal charge as the array scans the scene.

2.1.3 Array & Display Electronics

The array and display electronics consist of the digital control logic, signal processing electronics, scan converter controls and standard television monitors.

The control logic for the operation of the TDI array is designed to synchronize the encoder outputs to an internal clock and generate the array clocks.

The off-chip signal processor electronics was set up to operate with a 2-stage floating-gate amplifier (FGA) configuration. The off-chip processor consists of a X10 low noise amplifier, line driver, matched filter, DC restorer and sample and hold circuit. The X10 amplifier and the line driver are packaged on the same printed card as the 128 x 128 TDI device for noise minimization.

The display electronics consists of a Hughes Model 639-H Scan Converter, the external controls necessary for its operation, and a standard television monitor. An interface video amplifier converts the video levels to those required by the scan converter.

The horizontal and vertical sweep generators provide the proper external sweeps required by the scan converter for the XY writing mode, which is used to write information at other than standard television rates.

The write control takes over after the manual WRITE switch is depressed, and synchronizes the writing operation so that one full video frame is written into the scan converter. At the end of the write cycle, the read control automatically takes over and presents the information stored in the scan converter on a standard television monitor.

2.1.4 Optics/Light Source/Scene Simulation

The lens and light source shown in Figure 2-1 are mounted in the rotary table. The lens is an Anginieux Type M1 (f/0.95; focal length: 1 inch). The light source is projected onto the segment of the 180° scene that reflects back to the TDI sensor array. The lamp is calibrated in illumination level and color temperature (2854°K). Neutral density filters are used to vary the test light levels. A diffuser is also incorporated into the lamp housing to establish uniform light distribution on the scene.

The 180° scene simulation was made up of a photographed strip scene of many-size ships on the water (New York Harbor). In one segment of the scene, however, are calibrated cutouts of three ships representing different distance ranges as shown in Figure 2-4. The reflectance from each ship target was 36% and corresponded to the value used in calculation of a horizon silhouette model.

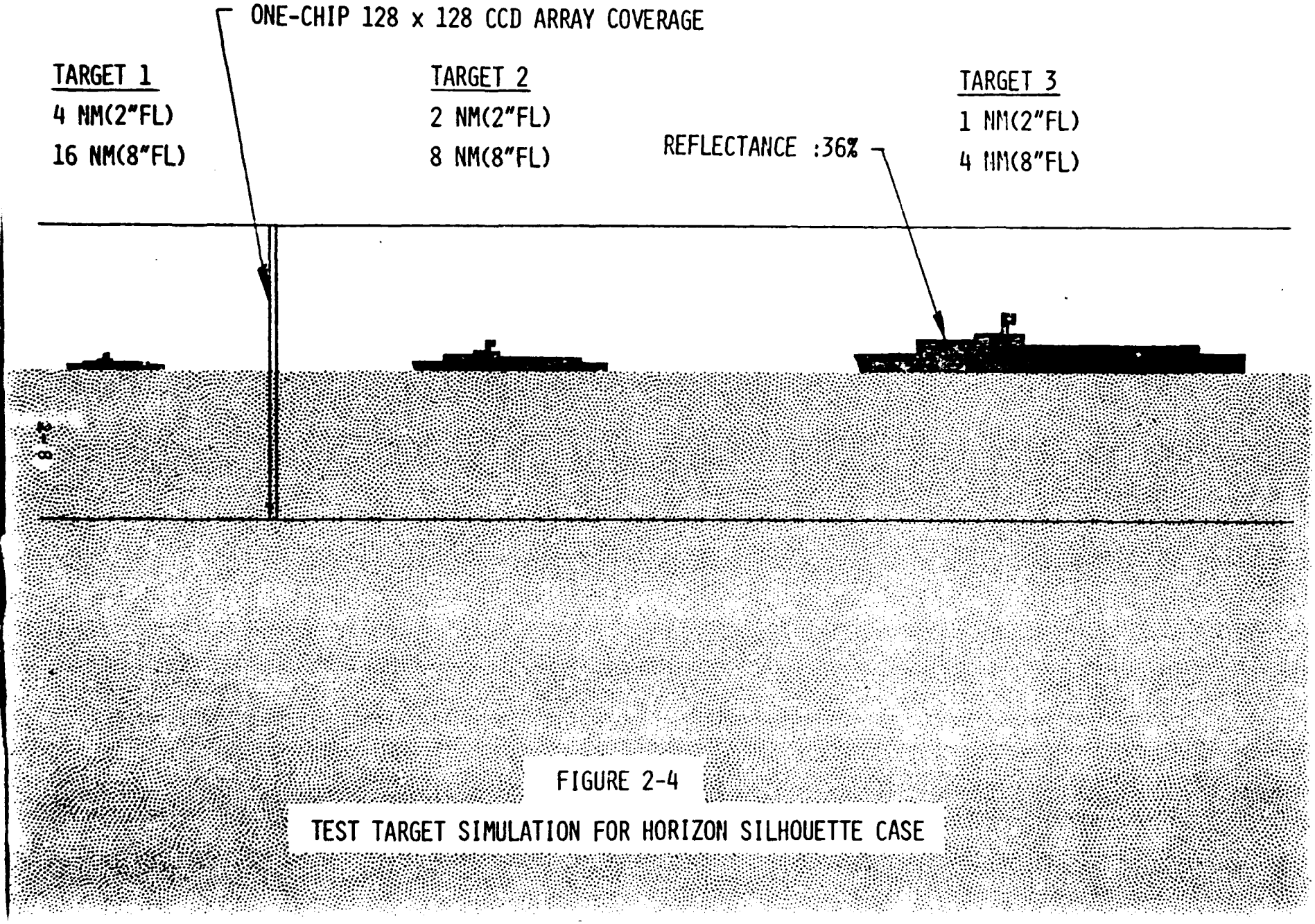

FIGURE 2-4

TEST TARGET SIMULATION FOR HORIZON SILHOUETTE CASE

2.2 SUMMARY OF PANORAMIC SCANNER TEST RESULTS

Under simulated panoramic scan conditions as shown on page 2-1 the following performance results were demonstrated to the Navy.

2.2.1 High Resolution Scanning

With the prescribed 100 foot lambert brightness levels imagery was displayed that verified full Nyquist frequency performance, i.e., a limiting resolution of 38 lp/mm.

2.2.2 Integrating Mode Low Light Operation

The laboratory periscope scanner was tested at several light levels with emphasis on moonlight and starlight illumination conditions.

The targets shown in Figure 2-4 were used as a test target with detection of target No. 1 (smallest ship) set as a goal. Target No. 1 shows a silhouette of a 400 foot destroyer as seen by the 128 x 128 TDI array. The height of the ship corresponds to 4 pixels at the array plane.

The test conditions under all illumination levels were; scan rate of 18° per second, integration time of 325 msec. and the lens aperture at f/.95.

Each target was displayed on the monitor under every light level tested, and all were clearly detectable. The right hand monitor in Figure 2-5 displays the image of test target No. 1 taken with 1.5×10^{-4} foot candles (2854°K source) incident on the target, which approximates starlight under clear sky condition. For a reference, the left hand monitor displays the same target as recorded by a standard 525 line TV Camera under daylight illumination.

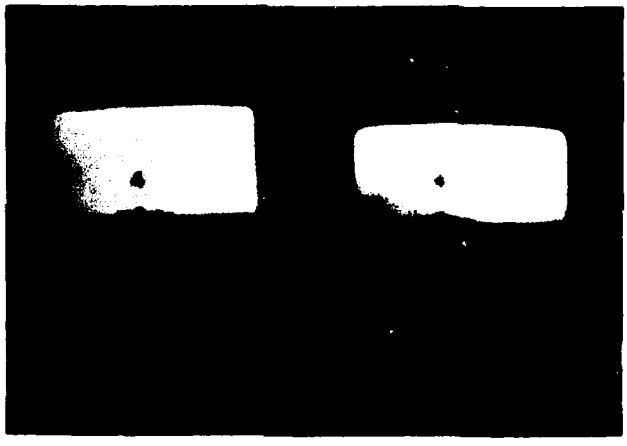

FIGURE 2-5. STARLIGHT IMAGERY OF SHIP TARGET

The numeral above the ship (4) indicates the simulated distance of the target to the periscope in nautical miles. The starlight image shows a slight degradation, but the target is easily recognizable. In fact, the signal-to-noise ratio for this condition was greater than 30:1, which indicates that targets of even lower contrasts or illuminated levels can also be detected.

The same ship targets were displayed on the Fairchild "moving window" display under the same illumination conditions. Although the fall-through rate of the image was less than 1 second per frame width, it was found that at this rate the target was still recognizable "on the fly". There was also sufficient operator reaction time to freeze the ship target image (via a manual control) on the "frame freeze" electronics before it moved off the screen.

2.3 STABILIZATION DESIGN STUDY

In the stabilization design study effort, Navy measurement and modeling data on periscope motions due to hydrodynamic forces was analyzed. The following are key results derived from the investigation:

a) Calculations were made, using a Type 16 Periscope model, and values for the following parameters were determined:

- Static Deflection versus Velocity
- Deep Water Wave Velocity versus Wavelength and Amplitude
- Peak Vibration Amplitude versus Periscope Speed (Vortex Shedding Analysis)
- Peak Angular Velocity versus Periscope Speed

The following analyses were also made:

- Monitor View of a Horizon Scene as a function of Periscope deflection
- Analysis of parameters considered for detection in compensation method

This initial study has provided information and insight into typical ranges of vibration and deflection to expect in a real periscope environment, and has given thought to candidate methods to achieve stabilization. The study report is presented in Section IV.

2.4 DISPLAY CONFIGURATION STUDY

This design investigation effort has reviewed the "real time" and "relaxed time" methods of displaying periscope data. These included "falling raster" direct view display and optical projection methods. Recording methods including laser beam, light emitting diode, and electron beam techniques, were also reviewed. Several of the considerations for the selection of a periscope display and record system, e.g., "fall through" time, field of view, writing speed, etc. are discussed in Section V.

2.5 HYBRID OPERATION

Hybrid testing was completed using the same operating conditions specified for the integrating mode low light level operation. Two 128 x 128 TDI arrays from six provided on special carrier mounts, were selected and mounted as a hybrid assembly at Fairchild, Syosset. The bilinear mounting was such that during panoramic scanning, chip number one was aligned to scan a 5.86 x 180 degree band just above and 256 lines ahead of chip number two.

All of the display systems were designed to present a 256 x 256 element picture when handling output from the hybrid assembly. Figure 2-6 is a photo taken from the "frame freeze" monitor of output from the 2-chip hybrid. The image was made under 1/4 moon illumination, 1.63×10^{-3} foot lamberts. The silhouettes of ships, scaled to 2 and 4 nautical mile distances, are clearly visible.

2.6 IMAGE MOTION SIMULATION TESTING

Image motion simulation testing was completed, using a specially constructed vibrating platform to provide image motion while a CCAID 128-A array was used in a snapshot mode to record the smeared imagery. Single shot photos from a variety of image motions were captured by the frame freeze recording system for analysis. The amounts of image degradation resulting from target motions during the array integration time were evaluated using a specially constructed test target. Subjective results were compared to theoretical predictions with good correlation. In general, uncompensated image vibrations above one pixel, peak-to-peak are highly undesireable when Nyquist limit resolution is required. For ship-like targets encompassing several pixels on the minimum dimension, an MTF degradation is encountered of 45 percent for sinusoidal vibrations equal in amplitude at the image plane to the ship minimum dimensions. This effectively halves the target detection capability in noise limited situations. Section 3.6 contains the details of this testing.

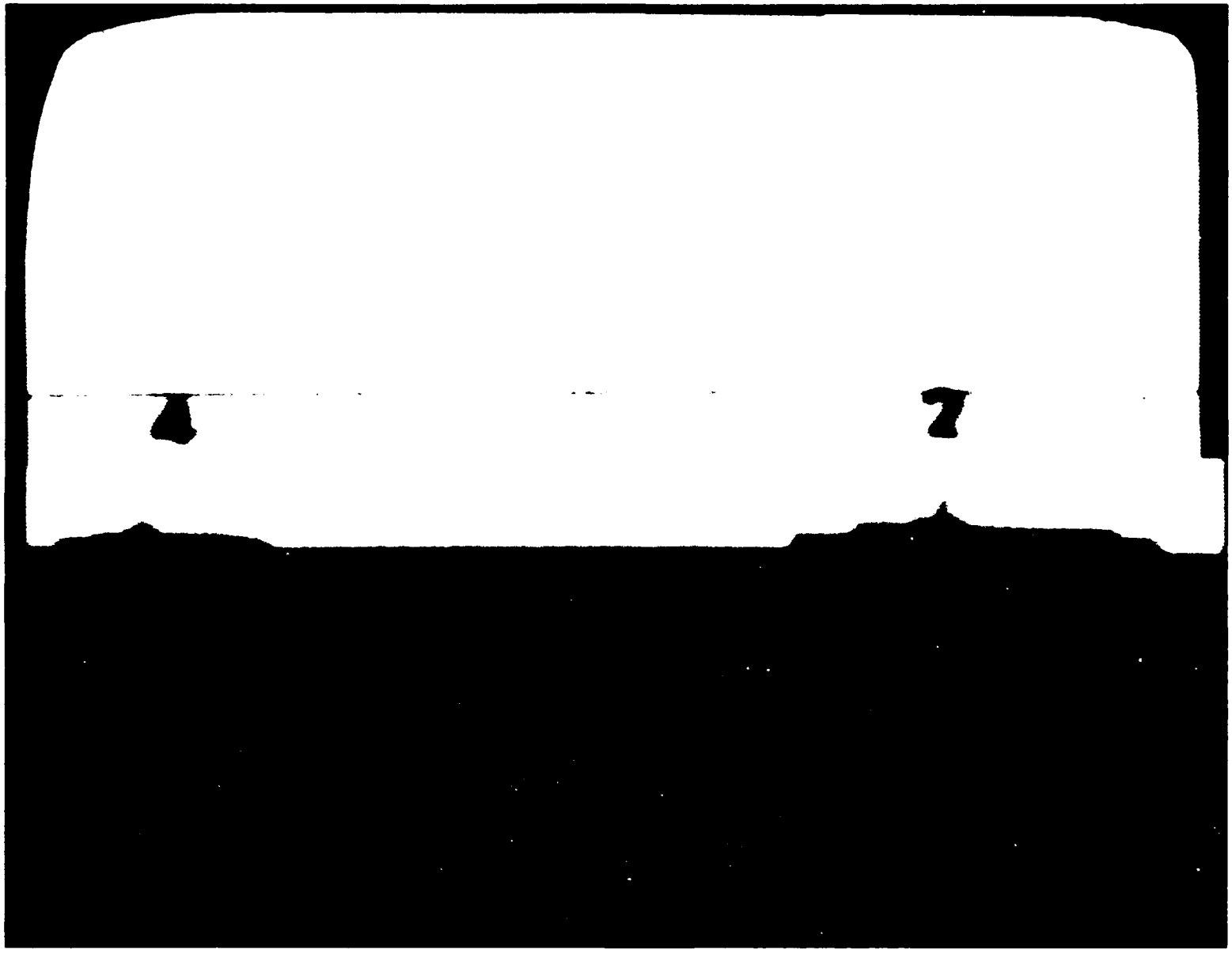

FIGURE 2-6. IMAGERY FROM 2-CHIP HYBRID UNDER 1 4 MOON ILLUMINATION

SECTION III

3.0 THE FEASIBILITY MODEL PANORAMIC SCANNER

The feasibility model panoramic scanner was described briefly in the preceding section; each of the major segments are described in further detail in this section. The major components are a) the CCD sensor arrays (1 x 1728, 128 x 128, and the dual hybridized 128 x 128 configuration) b) the rotary stage and table control electronics, c) the optics, light source, and scene simulation, d) the array control/video processing/scan interface electronics and e) the display subsystem consisting of the "frame freeze", X, Y, Z, and falling raster display modes.

3.1 CCD SENSOR ARRAYS

The high resolution scanning tests referred to in Section 2 were conducted with a 1 x 1728 linear CCD array described below. The device is also referred to as the CCD 121.

3.1.1 CCD Linear Image Sensor (1 x 1728)

The CCD 121 is a monolithic self-scanned 1728 Element Image Sensor designed for scanning. The device is intended to be used for imaging applications that require high resolution, high sensitivity and high speed.

In addition to a row of 1728 sensing elements, the CCD 121 chip includes: two charge transfer gates, two 2-phase analog shift registers, an output charge detector/preamplifier, and a compensation output amplifier. The 2-phase analog shift registers both feed the input of the charge detector resulting in sequential reading of the 1728 imaging elements.

The cell size is 13μ (.51 mils) by 17μ (.67 mils) on 13μ (.51 mils) centers.

The device is packaged in an 24-lead Dual In-Line package with a glass window and with a low reflectance optical cavity.

Figure 3-1 shows a block diagram of the 1 x 1728 device; operating characteristics for the device are shown in Table 3-1.

3.1.2 TDI CCD Image Sensor (128 x 128)

The CCAID-128 was designed as a high performance, low-light-level, integrating-mode, imaging device. The specifications for the device are given in Table 3-2.

The device is composed of an area-imaging array, an output register, and an amplifier section that incorporates two amplifiers. In addition, an electronic input register to facilitate testing and optional gate protection devices are included on the chip. Process control test elements are included on each die to monitor the various steps in fabrication. An electrical schematic diagram of the device is shown in Figure 3-2; a photograph of the device is shown in Figure 3-3. Design details for this device are given in Table 3-3.

The central feature of the CCAID-128 is the area-imaging array, which consists of 16,384 individual photosensor elements arranged in a 128 x 128 element format. The photosensor elements are also the unit cells of 128 vertical, 128-bit CCD registers as shown in Figure 3-4. Each 20 μm x 20 μm photosensor element (or unit cell) is composed of two charge storage areas, two barriers, and a channel stop region. A top view of one photosensor site is also shown in Figure 3-4. The size of each charge storage region is

BLOCK DIAGRAM

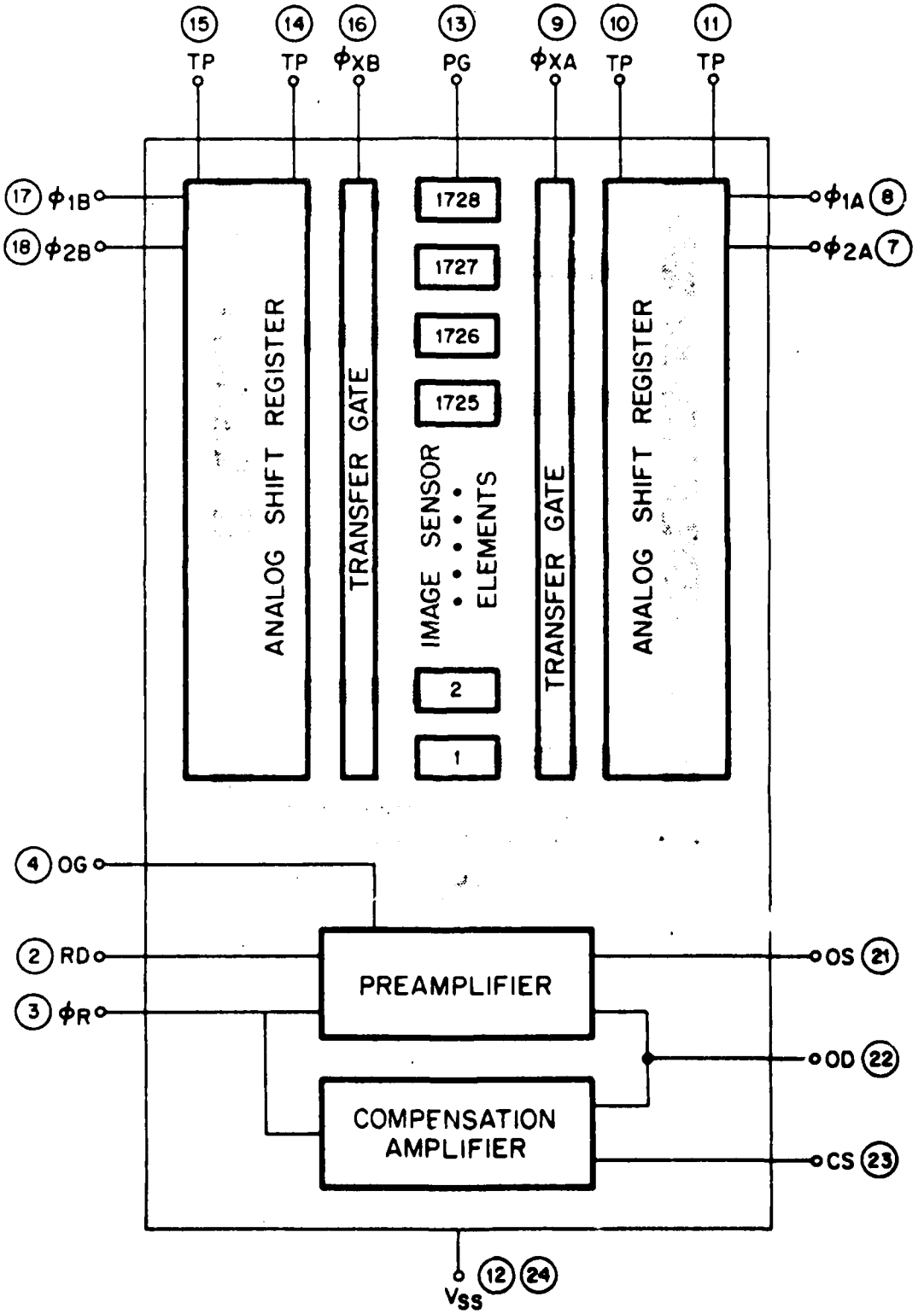

FIGURE 3-1 BLOCK DIAGRAM OF THE 1 X 1728 DEVICE

TABLE 3-1 OPERATING CHARACTERISTICS

$T_A = 25°C$, $f_{\phi_1} = f_{\phi_2} = .5\ MHz$

PARAMETER	MIN.	LIMITS TYP.	MAX.	UNITS	CONDITIONS
Dynamic Range		170			Notes 1 & 2
Noise Equivalent Exposure		3×10^{-3}		$\mu J/cm^2$	Notes 3 & 7
Saturation Exposure		0.5		$\mu J/cm^2$	Note 3
Spectral Response Range Limits	0.45		1.05	μm	
Responsivity		0.4		V per $\mu J/cm^2$	Notes 3 & 7
Photoresponse Non-Uniformity			$\pm$ 10	%	Note 4
Average Dark Signal		2		% of V_{sat}	Note 2
Dark Signal Non-Uniformity		3		% of V_{sat}	Note 2
Saturation Output Voltage, V_{sat}	150	200		mV	Note 8
Power Dissipation		100		mW	V_{OD} = 15V
Output Impedance		1000		Ω	

TABLE 3-2

SPECIFICATIONS FOR THE CCAID-128

No. of columns	128
No. of rows	128
Photocell size	20 μm x 20 μm
Responsivity, internal (2854°K illum)	>65 mA/watt
Non-uniformity of response, col. to col.	≤ 2% RMS
Dark current density, average, 25°C	≤ 10 nA/cm^2
Non-uniformity of dark signal	≤ 2% RMS
Charge-transfer efficiency at 5% of saturation and 1 MHz	≥ 0.9999
NES (Noise Equivalent Signal) at 1 MHz	≤ 40 electrons/pixel
MTF, square wave, 0.8 f_N in-phase (4800°K illum.)	≥ 0.6

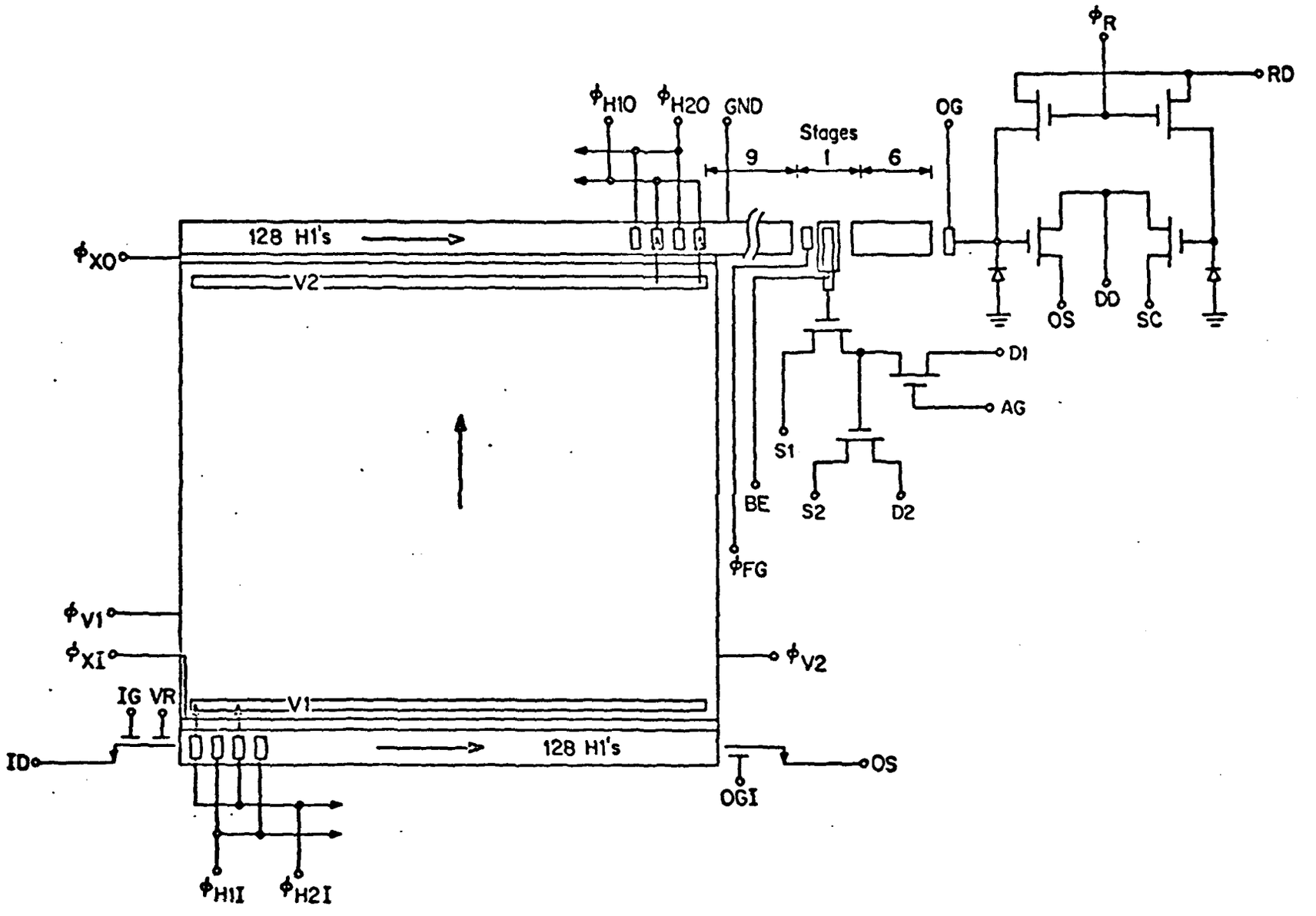

FIGURE 3-2 DETAILED SCHEMATIC OF THE CCAID-128

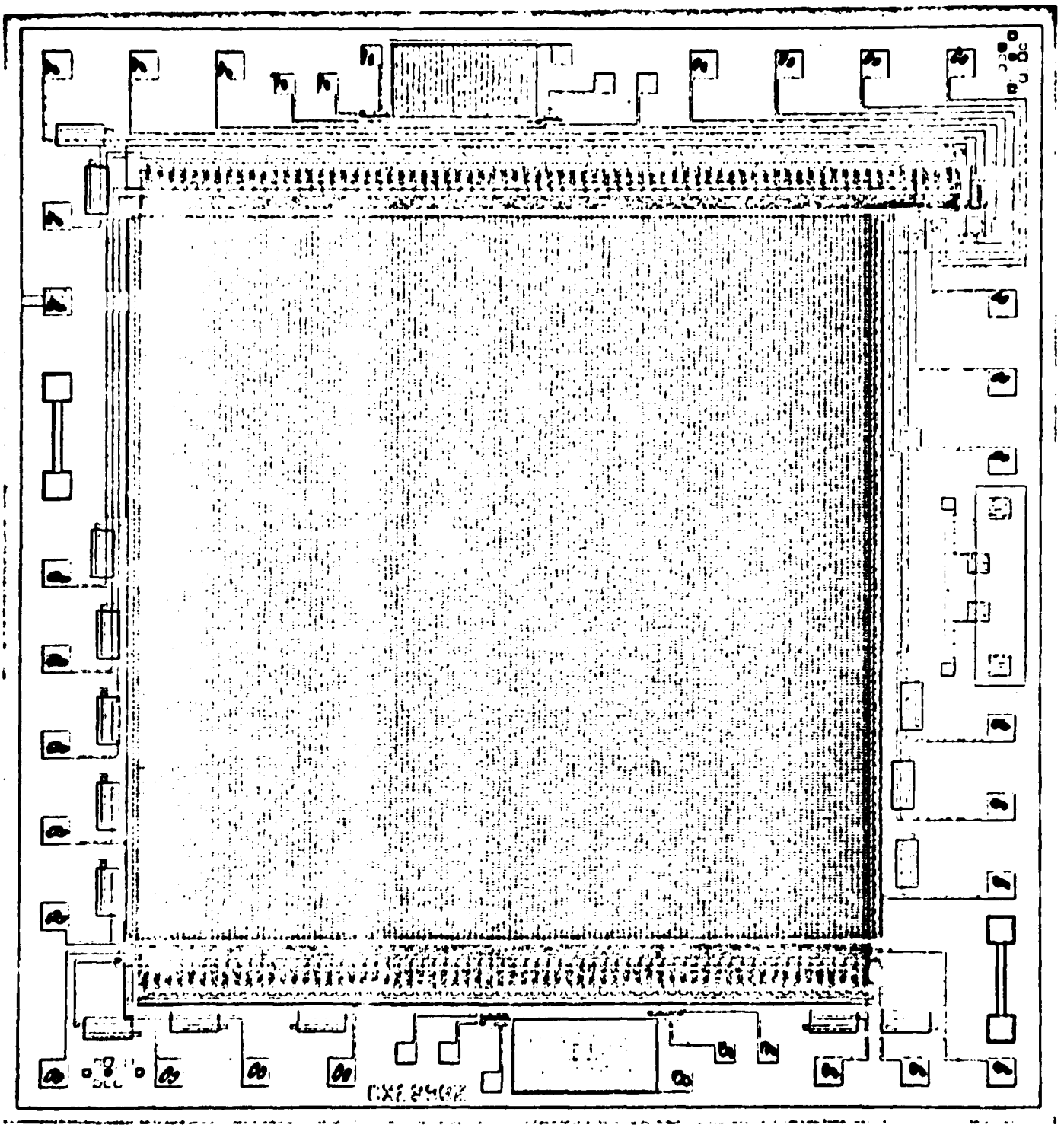

FIGURE 3-3 THE CCAID-128 CHIP

TABLE 3-3

DESIGN DETAILS FOR CCAID-128

CHIP SIZE	146 mils x 154 mils
NUMBER OF CELLS	128 x 128
CELL SIZE	20 μm x 20 μm
ALL REGISTERS	2Ø, gapless, self-aligned
PHOTOSENSOR STORAGE AREA	7 μm x 15 μm = 105 μm^2
FRACTION OF CELL AREA COVERED BY SINGLE LEVEL POLY	60% - neglecting typical geometry changes in processing
SATURATION CHARGE	3.5×10^5 el/px
SATURATION OUTPUT VOLTAGE	100 mV
DYNAMIC RANGE	2000:1 minimum
MINIMUM GEOMETRY	3 μm
MINIMUM MASK DESIGN ALIGNMENT TOLERANCE	2 μm
AMPLIFIERS	FGA and gated charge integrator (GCI)
TOTAL BOND PADS	27
INPUT REGISTER	Included
PROCESS CONTROL TEST ELEMENTS	MOST's, gated diodes, poly-Si resistors

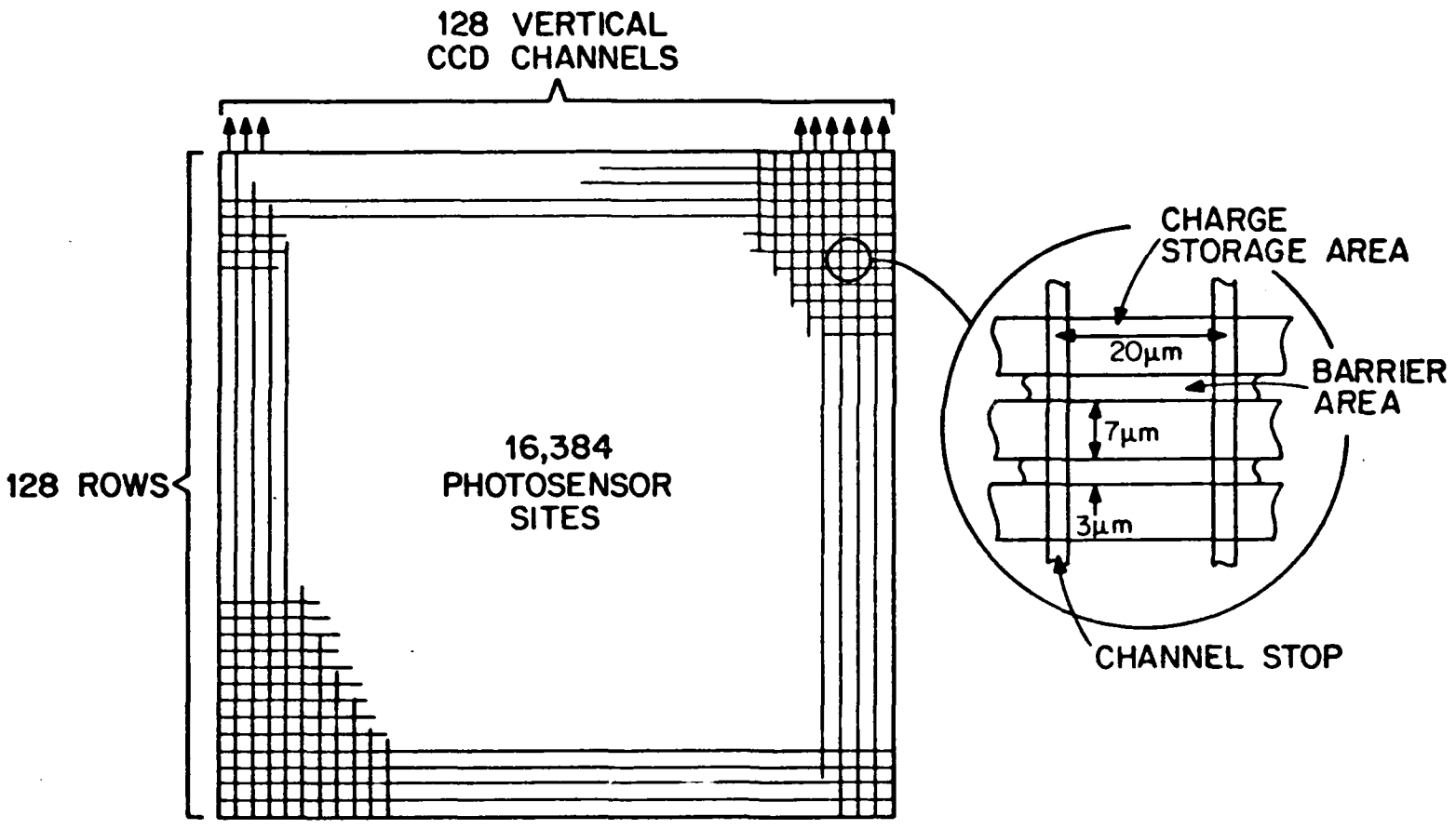

FIGURE 3-4 PLAN VIEW OF THE PHOTOSENSOR AREA OF THE CCAID-128

15 μm x 7 μm; the width of each barrier is 3 μm. The 15 μm dimension takes into account the diffusion of the channel stop dopant.

The unit cell employs a two-phase, overlapping polysilicon gate technology. A longitudinal cross-section through the center of one of the vertical registers is shown in Figure 3-5. The particular thicknesses of the dielectric layers and the polysilicon in the area array are chosen to provide an optimum breadboard optical response over the wavelength range from 0.5 μm to 0.9 μm.

The output register receives charge from the area array via an output transfer gate. The output register cells are 20 μm x 40 μm. The cross-section of the output register in the direction of charge flow is the same as that of the area array, except for the replacement of the upper level nitride vapox combination by thermal oxide.

The two amplifiers, a gated charge integrator (GCI) and a floating-gate amplifier (FGA), are located at the end of an extension of the output register. The FGA provides a capability for low noise charge detection down to extremely low signal level; the GCI serves as a highly linear charge detector suitable for higher signal levels.

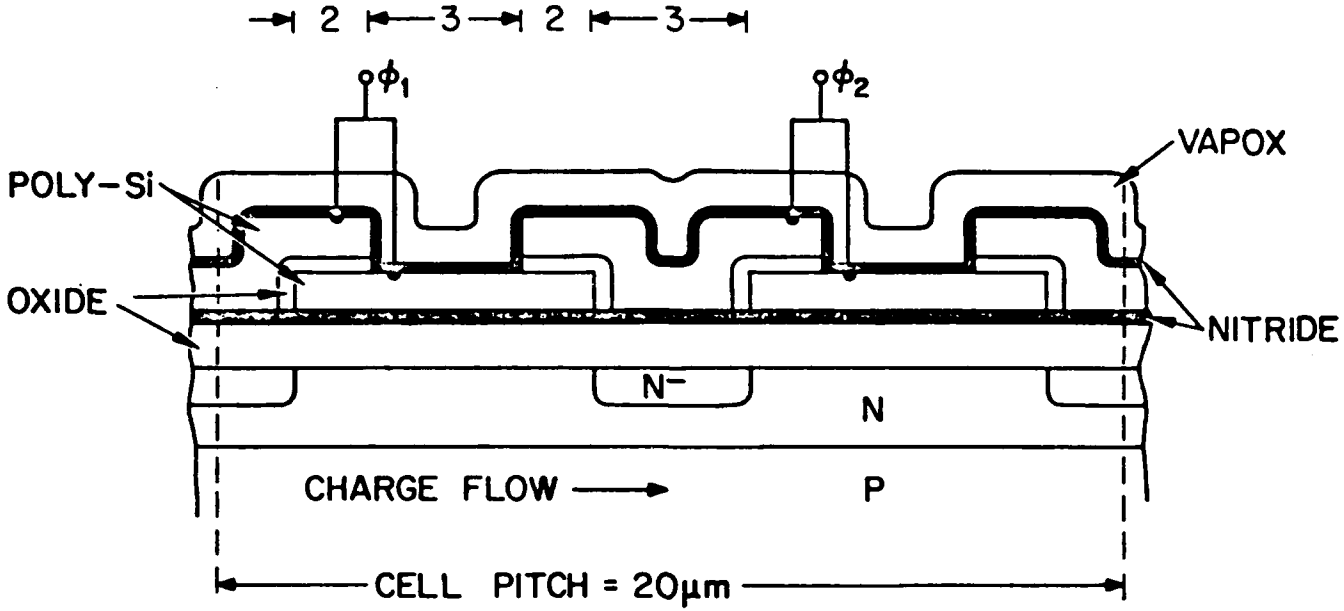

FIGURE 3-5 CROSS-SECTIONAL VIEW OF PHOTOSENSOR CELL OF THE CCAID-128. DIMENSIONS ARE GIVEN IN MICROMETERS.

3.1.3 2-Chip Hybrid (Dual 128 x 128)

The 2-chip hybrid configuration was designed to demonstrate the feasibility of combining multiple CCD chips into one sensor, operated in the time delay and integration (TDI) mode, thus achieving both high resolution and low light level operation with the same sensor. Since this hybridizing work was completed, the state-of-the-art, in terms of making larger TDI sensor configurations, has improved. A newer TDI configuration currently under fabrication is a 1024 x 64 element device being made for the Air Force LOREORS Program. Also, a recent Fairchild proposal (1) submitted to the Navy for further work in the low light level scanning area proposes to use a 1024 x 128 single-chip TDI configuration.

The two-chip hybrid assembly consists of two CCD-128 chips mounted in a bilinear fashion on a ceramic substrate and packaged in a specially designed assembly. The chips in the bilinear assembly are separated by a space equal to 256 array elements, and the end of column #128 of the advanced chip are aligned with the beginning of column #1 of the delayed chip to within $\pm$ half an element. The two chips are parallel to within $\pm$ half an element, and the assembly is flat to within $\pm$0.001".

The photograph of Figure 3-6 shows the linear layout of the 2 devices; Figure 3-7 shows the carrier mounting arrangement of a single chip prior to bonding in the hybrid assembly.

---

(1) "Low Light Level Panoramic TDI CCD Imaging System (LOPATCH)" Fairchild Proposal No. ED-CX-134, dated 18 April 1977.

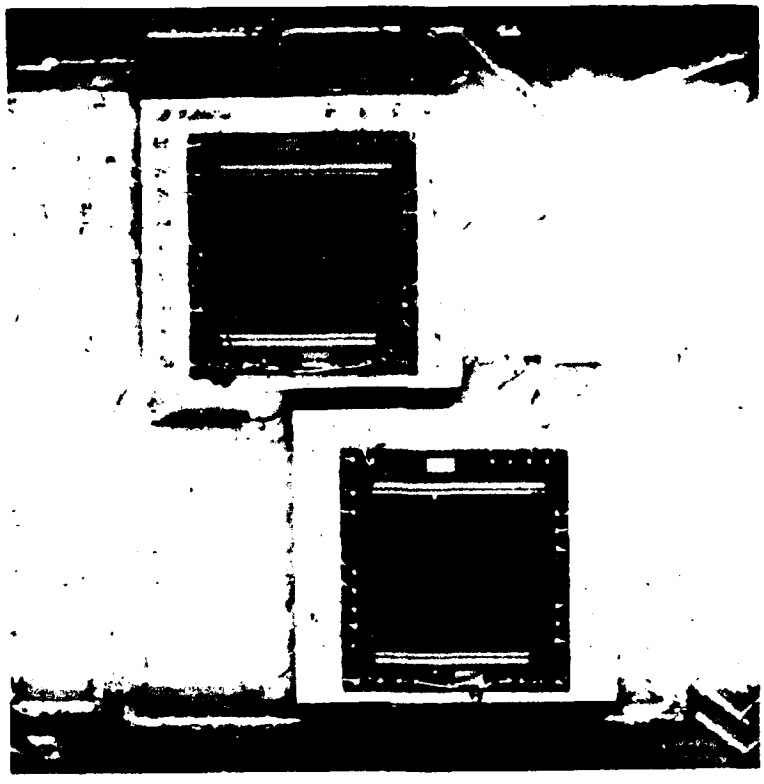

FIGURE 3-6. 2-CHIP HYBRID ASSEMBLY OF 128 x 128 CCD'S (BI-LINEAR CONFIGURATION)

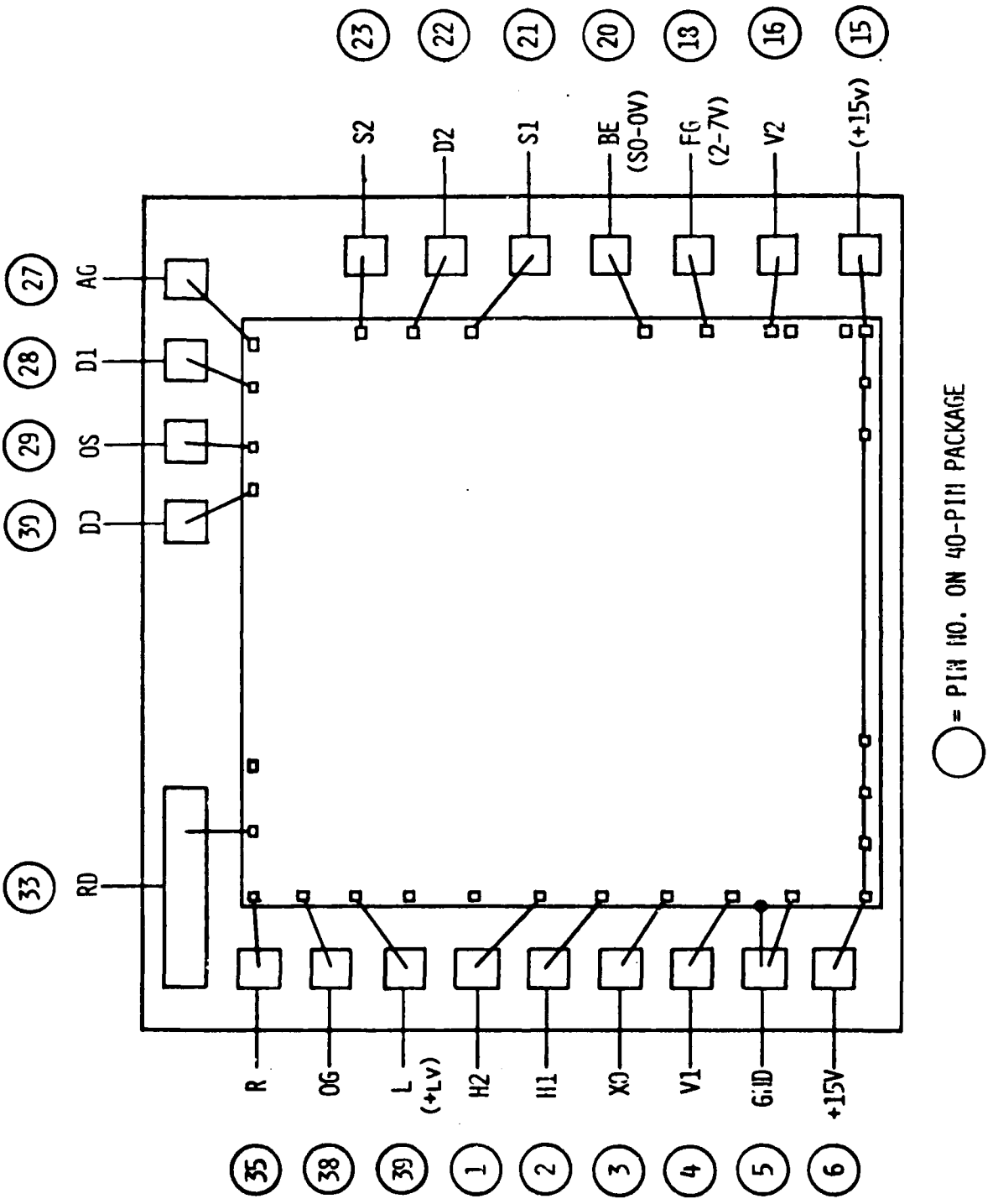

FIGURE 3-7 SINGLE CHIP CARRIER MOUNTING

3.2 ROTARY STAGE/TABLE CONTROL ELECTRONICS

The rotary stage is a highly accurate platform designed to simulate rotary periscope motion about a vertical axis. An X-Y table is supported above a highly rigid rotating stage which is motor driven through a high precision worm and wheel drive. A DC motor with tachometer feedback provides automatic positioning. A rotary encoder senses rotation through the worm drive providing a high resolution. The motion supplied exceeds 180°.

The system used is a modified version of Anorad's standard stage shown in Figure 3-8. A large plate was designed to fit over the assembly and mount the optical components as shown in Figure 3-9. A list of specifications below defines the rotary table in detail.

a) The rotary table is capable of carrying a weight of up to 100 pounds.
b) A D.C. motor-tachometer is provided to allow driving the table at speeds of one-half revolution per 5 to 20 seconds.
c) A velocity control system is supplied to allow adjusting of speed from a minimum to a maximum value as specified above. A precision potentiometer and dial is supplied on the front panel to achieve speed variation from one revolution per 10 seconds to one revolution per 40 seconds. The speed can be adjusted beyond these limits by internal potentiometers in the motor driver.
d) A rotary encoder is provided which is directly coupled to the wheel of the 90:1 worm and wheel drive. The encoder resolution provides up to 2,000 pulses per revolution, resulting in up to 180,000 pulses per revolution.

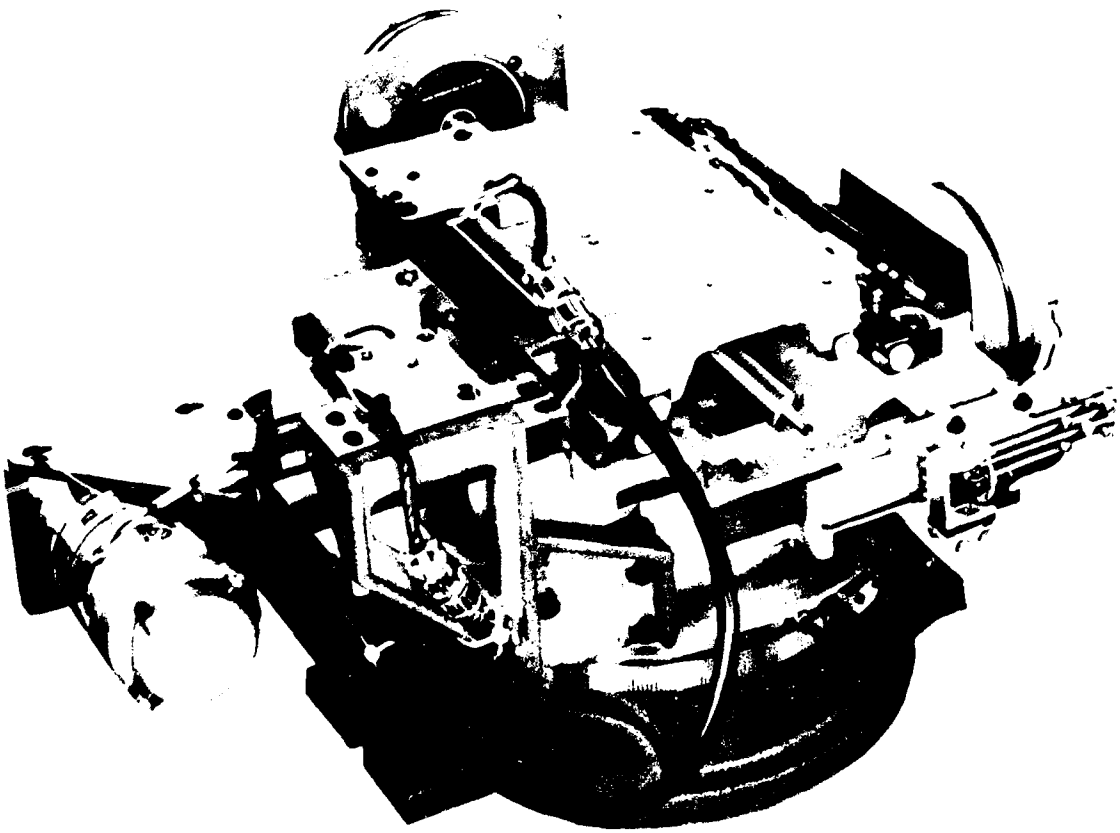

FIGURE 3-8. ANORAD ROTATING TABLE ASSEMBLY

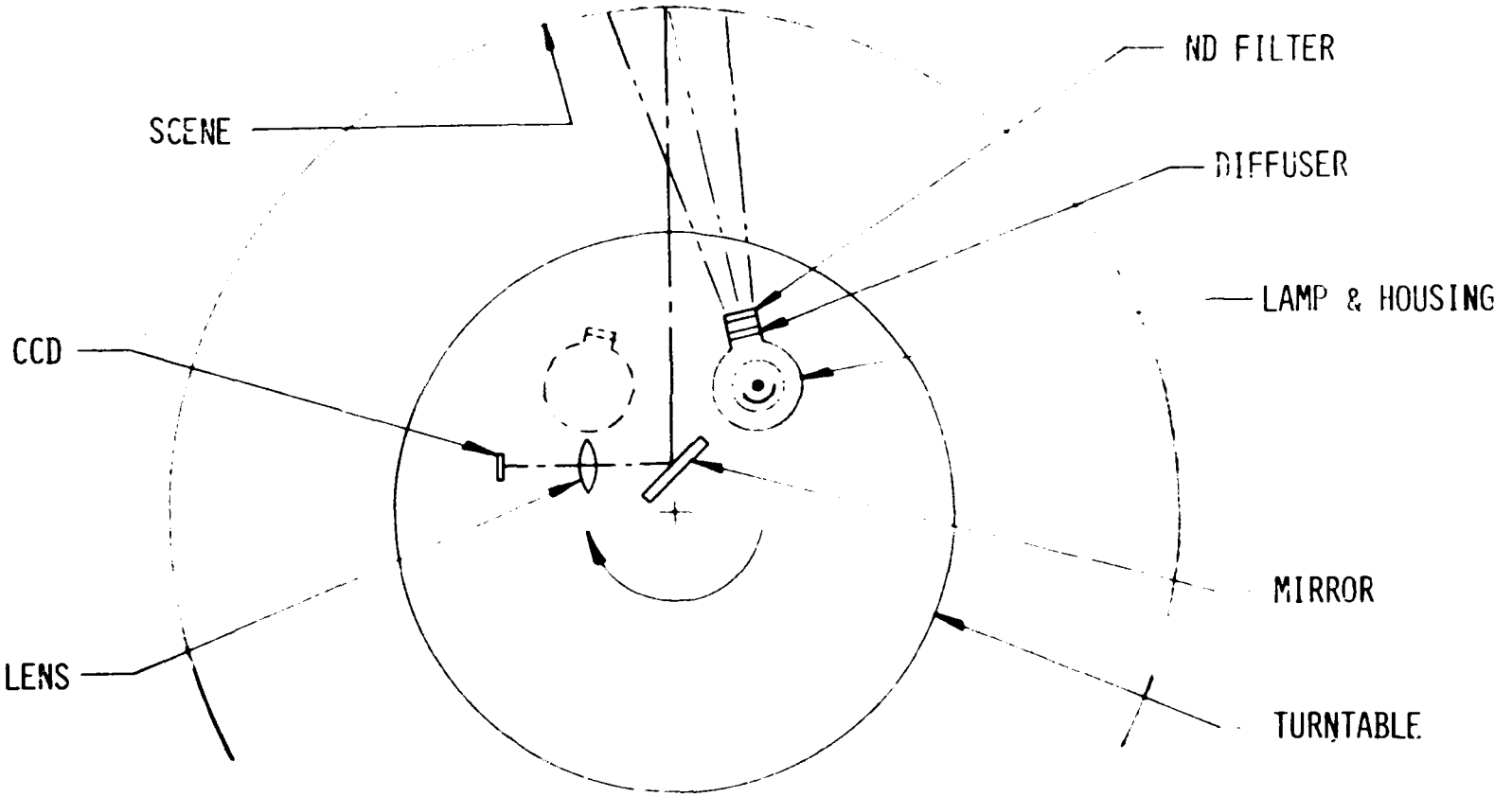

FIGURE 3-9 ARRANGEMENT OF SCENE & LAMP ON ROTARY TABLE

e) A reference pulse is provided to establish a starting location.
f) A digiswitch is supplied to allow counting the number of pulses and provide a square wave output of adjustable width. The duration of the square wave is nominally 20 counts (10 counts high and 10 counts low). The digiswitch is settable with four digits. In this manner, the accumulated inaccuracy cannot exceed one count (1/20 of a cycle) in 128 square waves.
g) Accuracy of the table is $\pm$ one half a minute of arc in any 30° angle.
h) Working surface: square with table axis within .0005".
i) Center running true to .0005".
j) Working surface parallel to base within .0006".
k) Mechanical table accuracy, using a mechanical dial on the table: $\pm$1/2 minute of arc.
l) System accuracy using electronics $\pm$1/10 of a CCD line non-accumulative over the full CCD.
m) The rotary table has an upper surface of 12" diameter.

The panel controls and display for the table control box are shown in Figure 3-10.

3.3 ARRAY ELECTRONICS

The array electronics subsystem constructed for the panoramic scanner consisted of video processing circuits, digital control electronics, array drive circuitry and video tailoring for the various display systems. All hardware was designed to control either one or two arrays, i.e., to accommodate the single chip or the two-chip hybrid testing.

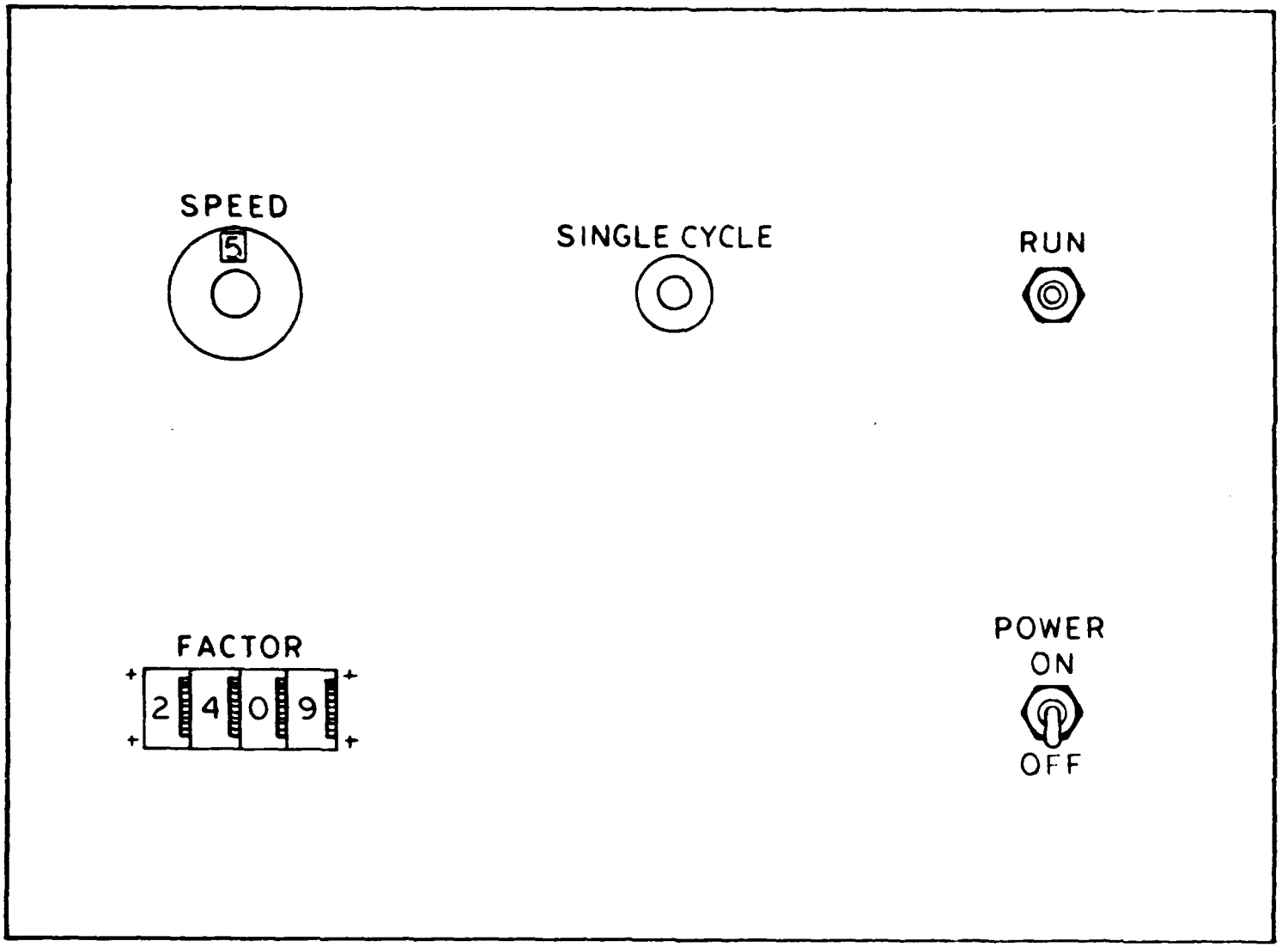

FIGURE 3-10 TABLE FRONT PANEL CONTROLS

3.3.1 Video Processing and Tailoring

Dual video chains were provided in the periscope hardware, in order to service the two-chip hybrid. The diagram shown in Figure 3-11 presents the beginning of the video chain. The circuitry shown in this diagram is all contained on a printed circuit board which also supports the array socket and cooling chamber in the optical path of this scanner simulator system. Two array boards were provided in the hardware, each capable of driving a single array. When the two-chip hybrid assembly was incorporated into the system, an interface board was provided that made connections from the dual chip hybrid array socket to each of the respective array driver boards.

The driver boards shown in Figure 3-11 contain circuitry for biasing the array; buffering, shaping, and driving digital waveforms to the array; and preamplifying the output video from the array. This minimal amount of circuitry is best kept close to the array, both to enable accurate clocking and to minimize noise in the video chain. The low noise, gain-of-ten, amplifier and the coax line drivers begin the video chain. The CCAID-128 arrays have a two-stage floating gate output amplifier.

Figure 3-12 shows the array output processing provided for each chip. Amplified, raw array video is routed through a matched filter. This filter was designed to process raw array video, which resembles a modulated square wave at the 1 megahertz clocking frequency, and reduce the noise content while preparing the video for clamping and sampling. If white noise is present on this "modulated square wave" video, then the ideal matched filter response takes on the very simple form of being the time reverse of the signal waveform. Since the expected signal waveform is a

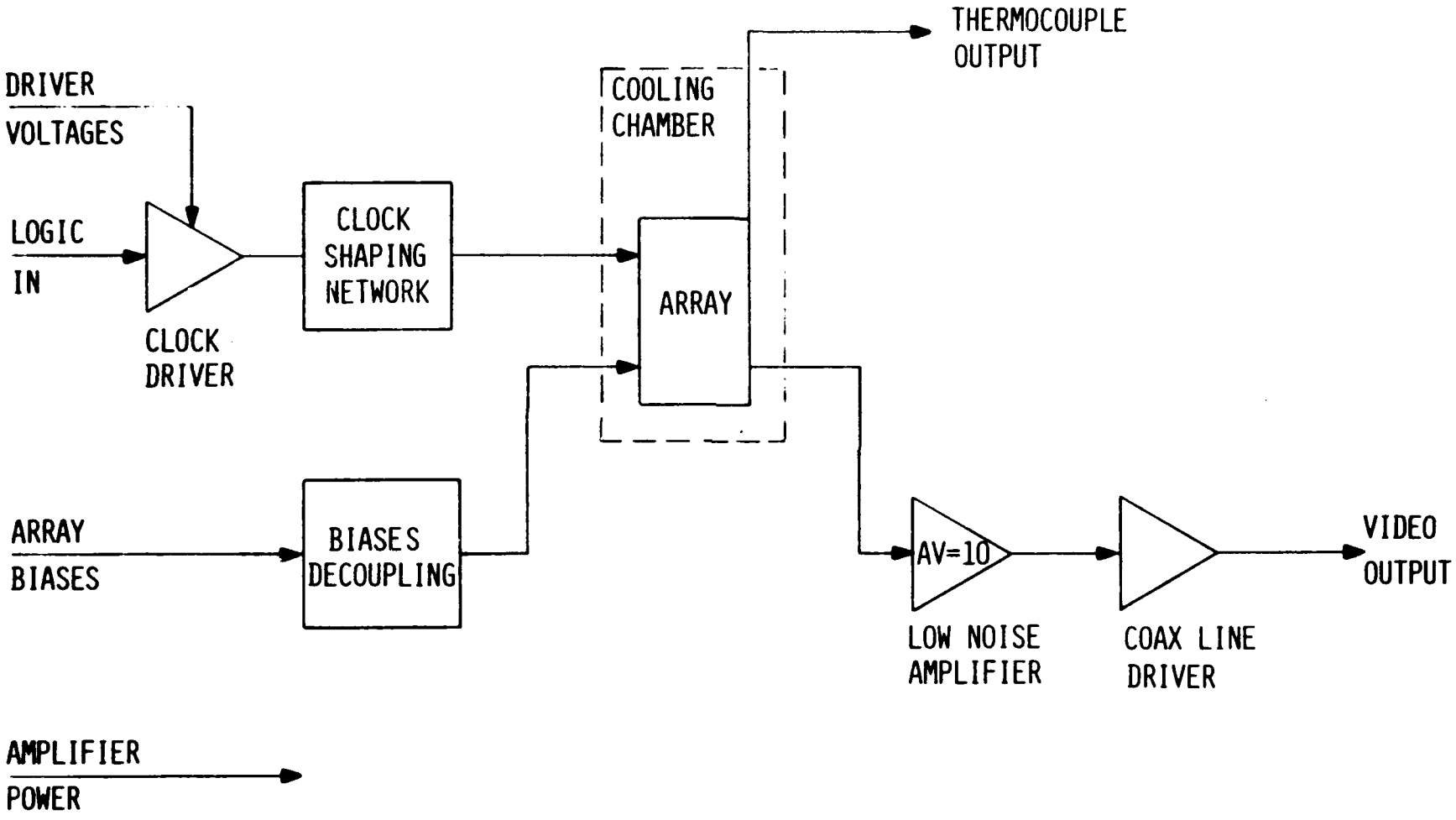

FIGURE 3-11 VIDEO PRE-AMP AND CLOCK DRIVERS

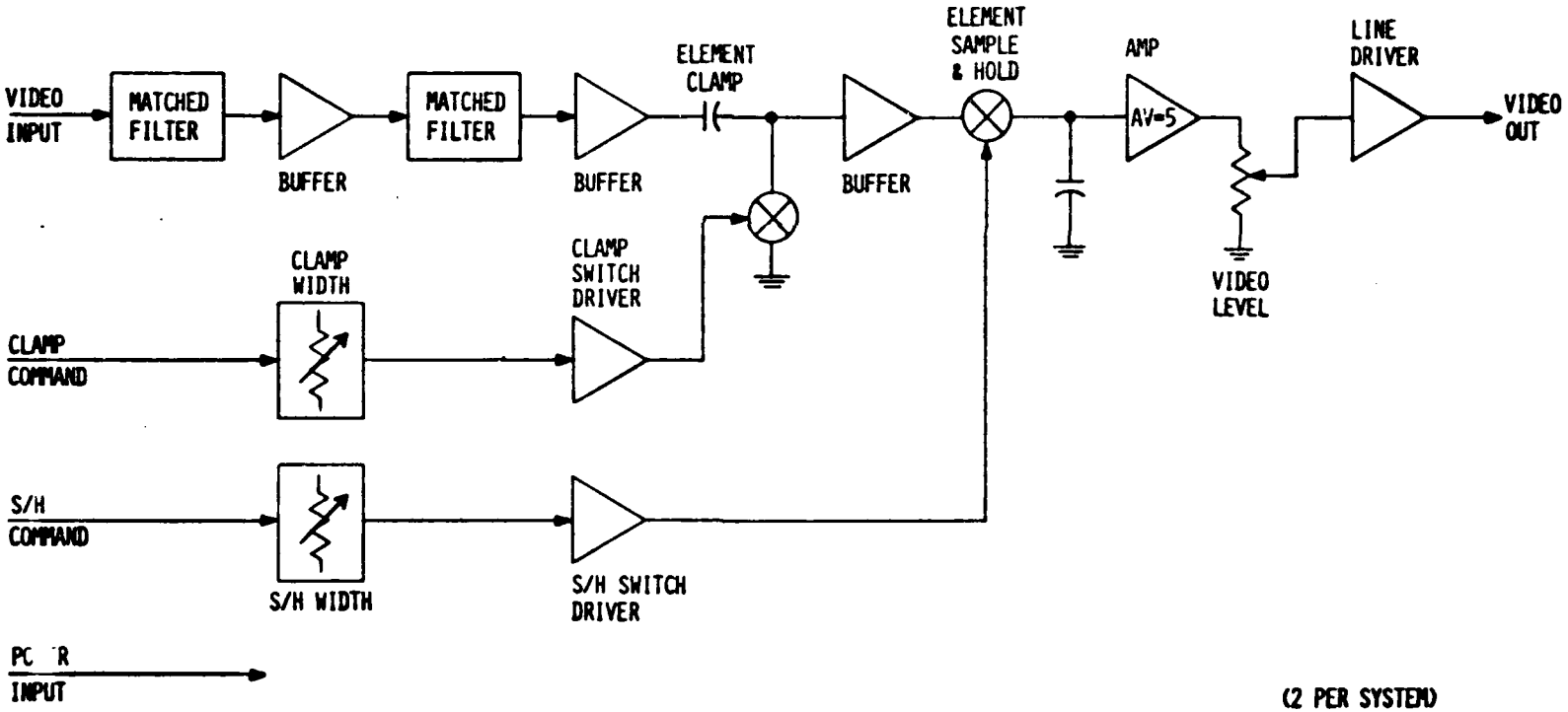

FIGURE 3-12 CAMERA SIGNAL PROCESSING

half square wave of 0.5 microseconds duration, the filter was designed so that, when presented with a very short impulse, it produces a step of voltage which suddenly "dies" after 0.5 microseconds. When passing the rectangular video pulses through the filter, a triangular shaped output pulse whose base is twice as long as the input, signal is produced but the apex of the pulse is just as high as the input square wave. Meanwhile, however, all high frequency noise has been removed and the triangular pulse may still be sampled at the apex with high accuracy. This occurs in the clamp and sampling circuitry depicted by the next several boxes in Figure 3-12. Since each pixel of information is shifted out of the CCD array using two buckets, this is an ideal opportunity to provide a D.C. reference to the video on a pixel by-pixel basis. This procedure effectively removes the low frequency, 1/f noise from the array video. In practice, as a pixel of information is shifted past the floating gate amplifier, one cell is full of charge and its neighbor is empty. The video processing circuitry has been designed to clamp the empty location to ground and then sample the full bucket video. The sampled value is held until the next pixel is clamped and then sampled. The resultant array video has one video "value" per 1 megahertz cycle (1 μs), and the array video has a maximum frequency of 500 kHz. As shown on Figure 3-12, this video is further amplified by five and driven off the video processor board to the interface box signal processor.

Figure 3-13 is a block diagram of the interface box signal processing. This box was designed to process video for each of the three display systems built for the periscope simulator system. Again most of the circuitry is duplicated for the two array chains.

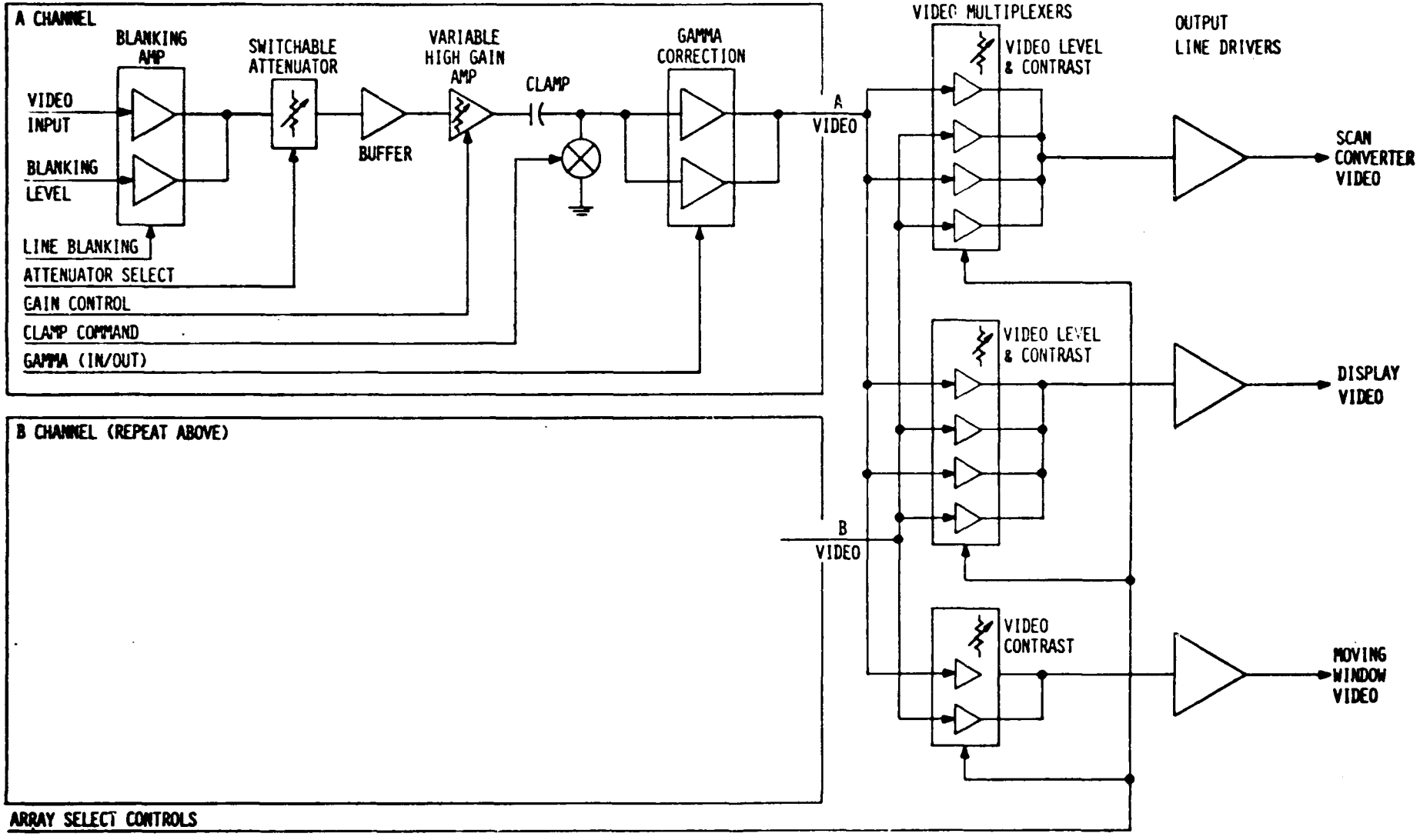

FIGURE 3-13 INTERFACE BOX SIGNAL PROCESSING

Input video, is first routed to a blanking amplifier. This amplifier inserts a blank area into each video chain during all inactive portions of the video line. The next block is a remotely controlled attenuator to reduce video amplitude when high levels are very high. The following amplifier is a high gain video amp which is remotely programmed from the front panel of the interface box along with the attenuator. When starlight testing was accomplished, the attenuator was switched out of the circuit and the high-gain amplifier gain turned up. In this way, signals approaching one volt could be provided for the display systems. After the high-gain amplification, array video was clamped to ground during the blanked line intervals. A selectable gamma correction amplifier was also provided in the processing electronics to compensate for T.V. monitor nonlinearity.

The final stage of video processing is a set of video multiplexers. These multiplexers enable the selection of video from either array for delivery to the three displays. Final video level and bias is also set for each display in these output stages.

3.3.2 Digital Control Electronics

The digital control logic constructed for the periscope scanner system is designed to generate all the clock waveforms necessary for operation of two 128-A CCD arrays. It is represented very simply in Figure 3-14.

The primary logic function is synchronization between the rotating table clocks, which are generated to trigger each line transfer in the integrating mode array, and the one megahertz master array clock. Table clocks are generated as the table rotates an angular distance equal to one element width as projected by the system lens.

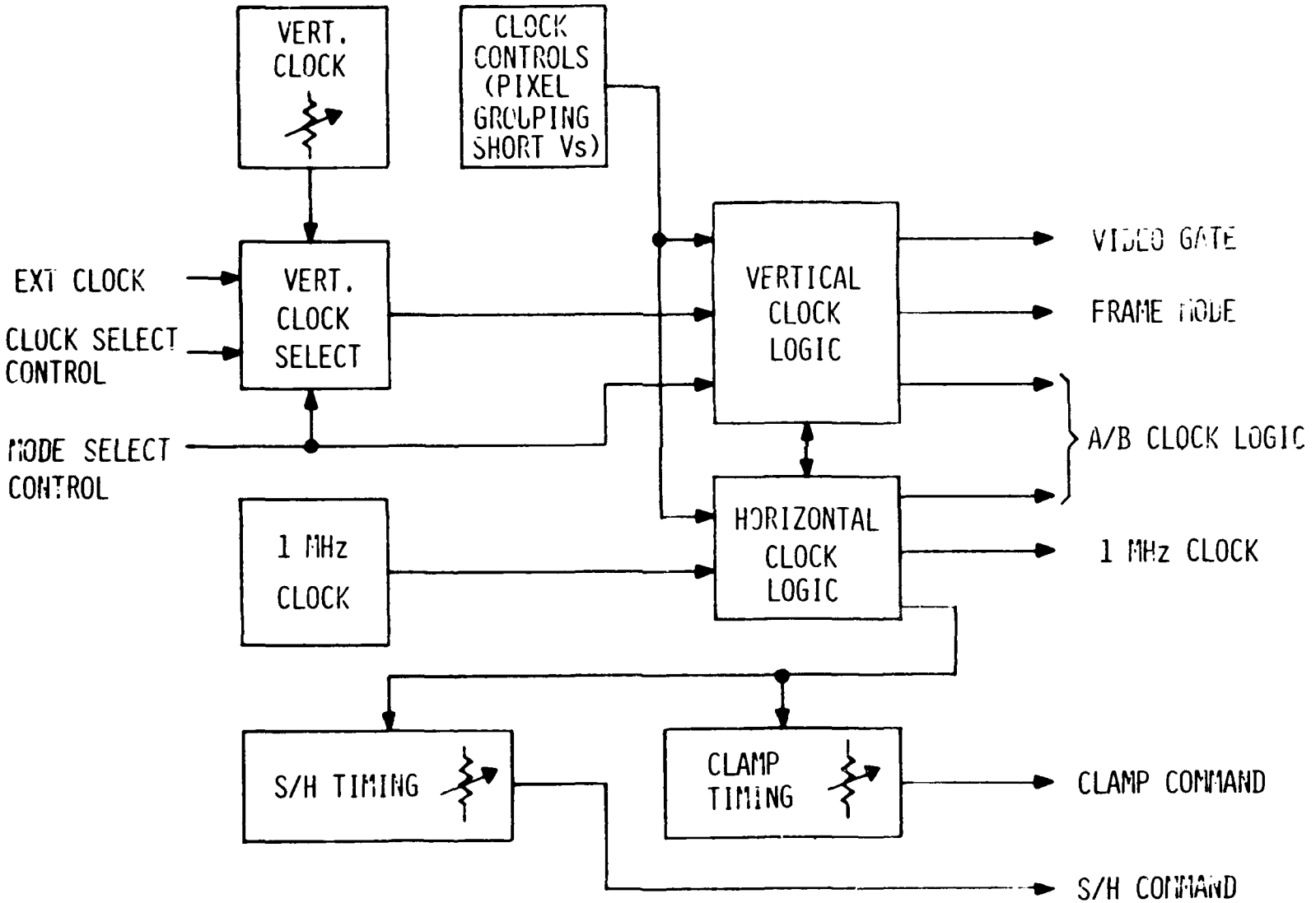

FIGURE 3-14 BLOCK DIAGRAM OF CAMERA LOGIC

As each clock pulse from the table arrives, the two phase horizontal clocks are triggered starting from the next available 1 MHz master clock cycle. This automatically synchronizes the array logic to the table clocks. In addition to the horizontal clocks, two phase vertical clocks,floating gate clocks, clamp pulses, sample pulses, video gate and frame gate pulses are also generated by the camera logic. Figure 3-15 illustrates some of the waveforms generated by the camera logic circuitry and indicates their phasing. Once a line readout cycle has been "kicked off" by the table clocks all array waveform edges are synchronized to the 1 MHz master clock. Counting circuitry is also provided in the array logic to control the frame widths in the displays. Counts of 128 and 256 lines are provided.

Figure 3-16 depicts the logical flow of the interface box control logic. This logic provides drive waveforms for the various display systems. Inputs are accepted from the scan converter, the various front panel controls, the ANORAD rotating table signals the camera logic signals and the frame pointers (preset frame grab positions). After appropriate processing, timing and control signals are sent to each display system.

Sweep waveforms are generated for the scan converters frame freeze display and the XYZ display in the circuitry shown in Figure 3-17. Sweep waveforms are generated from the sync pulses provided by the interface logic using miller run up integrator circuits. Sawtooth waveforms for horizontal (line) and vertical (frame) sweeps on both the XYZ display and the scan converter are generated. Separate amplitude control for each sweep is possible to adjust pictures size on each monitor.

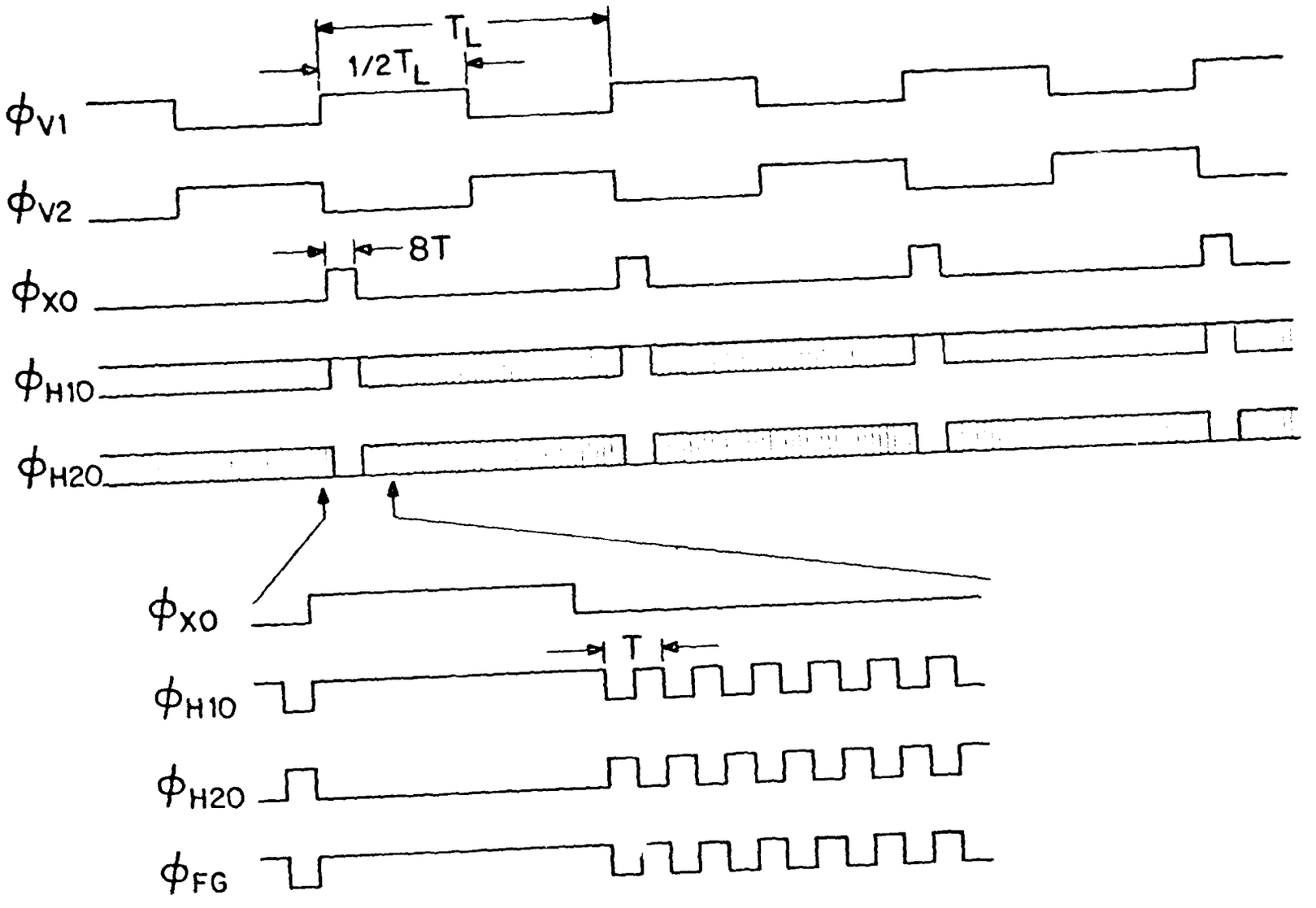

FIGURE 3-15 CLOCK WAVEFORMS REQUIRED TO OPERATE THE CCAID-128 IN THE MII MODE

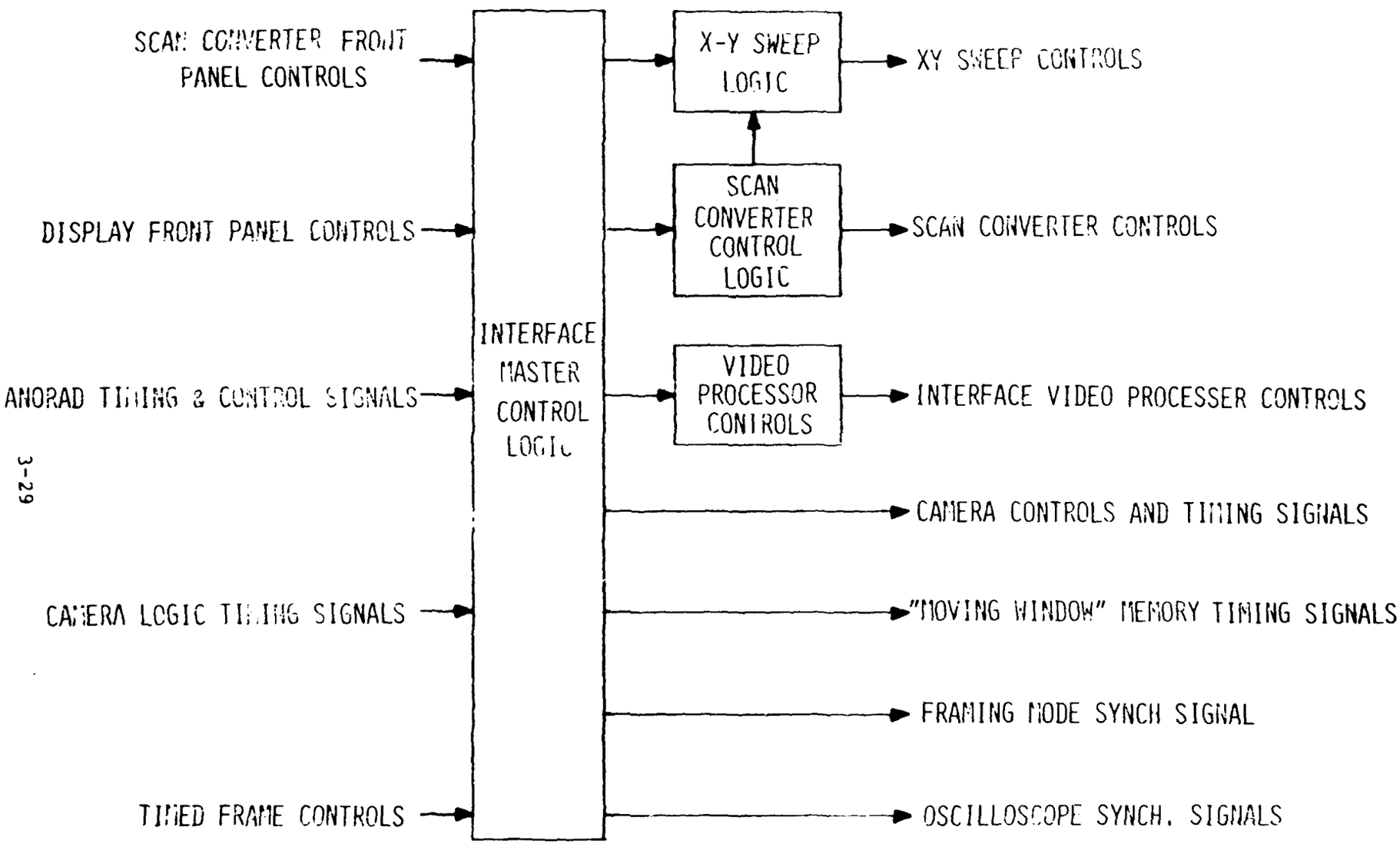

FIGURE 3-16 INTERFACE LOGIC

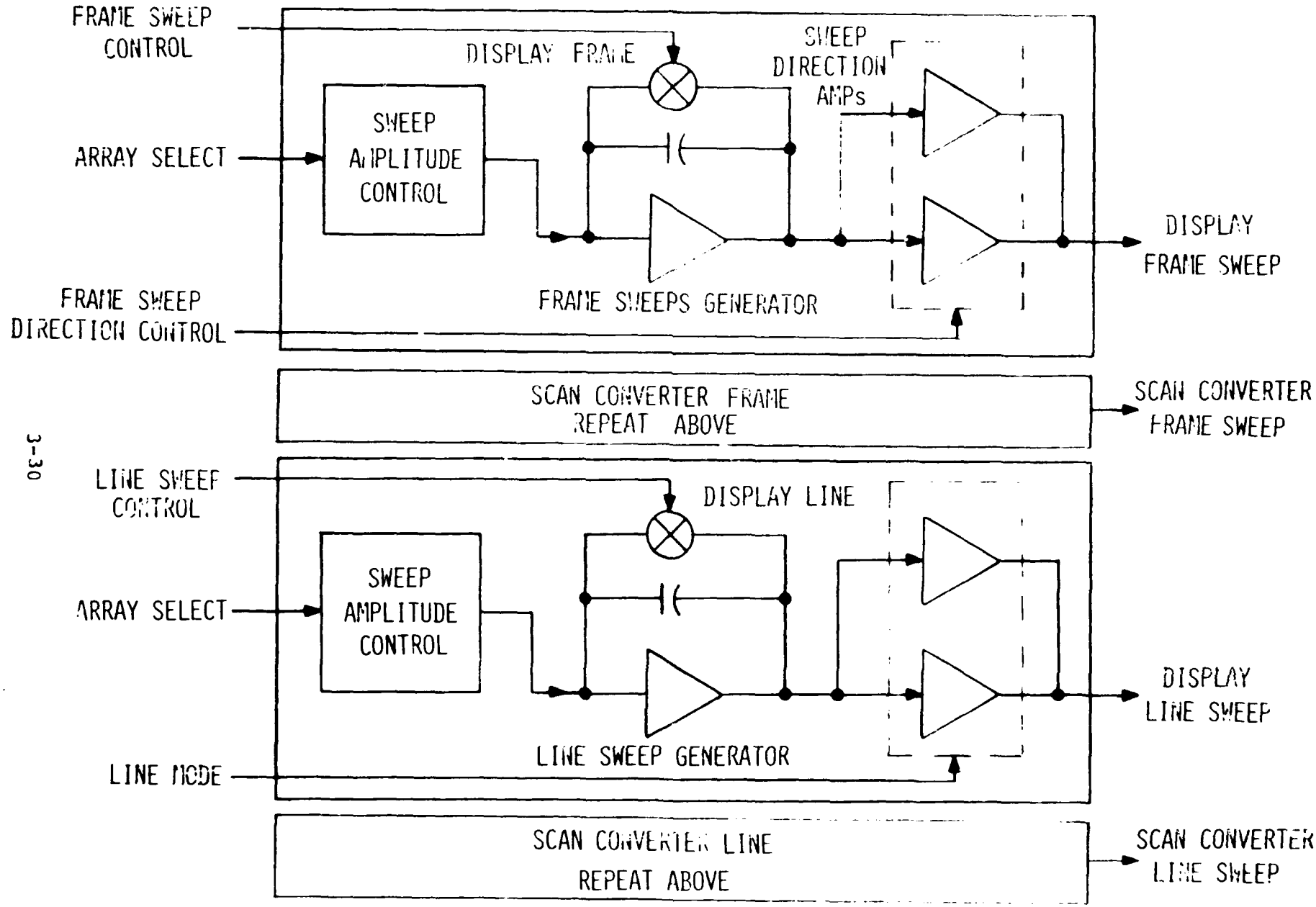

FIGURE 3-17 BLOCK DIAGRAM OF X-Y SWEEP GENERATORS

3.4 DISPLAY SUBSYSTEM

The CCD Periscope hardware contains three separate display systems. Each was designed to demonstrate a particular display mode appropriate for use in a CCD panoramic scanning system. The particular problems of displaying all or part of a panoramic image with an extremely large length-to-width ratio were addressed. The CCD panoramic scanner system, designed and built for the CCD Periscope program images a panorama, using one array, of 5.7° x 180° containing more than 4000 lines of 128 pixels each. The logic, video processing and display systems were also designed to scale up to a two-chip system, imaging double the previous panorama, i.e. 4000 lines of 256 pixels each. The three display systems were designed to investigate different modes of operation. They included a "frame freeze" display, an X,Y,Z display, and a falling raster display.

3.4.1 Frame Freeze Display

The frame freeze display was designed to demonstrate "relaxed time" utilization of the dynamic panoramic imagery. Since the entire panorama contains more information than can be stored in a simple system the frame freeze system was desgined to store a portion of this imagery. This frame storage was accomplished in a Hughes model 639-H Scan Converter which enabled playback of the stored image on a conventional T.V. monitor for leisurely analysis. This demonstrated a portion of the panoramic scanner operational scenario wherein data gathered at high speed is stored for later analysis. It also allowed the gathering of scientific data on the detectability of ship targets at various light levels. The frame freeze display was designed to store a 128 x 128 element frame, when using one CCD chip, and 256 x 256 element frames when using the two-chip CCD hybrid. The CCD camera

is not inherently a framing system. The panorama is scanned in strip mode fashion with successive CCD video lines oriented vertically. To form a frame, as many lines as there are pixels per line are selected from some designated portion of the panorama and stored.

A block diagram of the frame freeze display system is presented in Figure 3-18. Partially processed array video comes to the box labeled signal processing. This box shapes the array video stream into a form suitable for the Hughes scan converter; video amplitude and D.C. level are adjusted. Clamping circuitry in the electronics keeps the D.C. levels fixed regardless of array video variations.

The scan converter interface controls the prime, erase, write, and read functions of the scan converter as well as providing the horizontal and vertical sweeps, synchronized to array video, for use during the write mode of operation. The interface automatically primes and erases the scan converter when a new image is commanded. The array video is then switched into the scan converter along with appropriate X and Y sweeps to load one frame. With a new frame stored the scan converter is switched to "read mode" and it plays the stored image into a conventional T.V. monitor for continuous video until a new frame is selected.

Inputs to the scan converter interface include array line clocks from the array logic and frame trigger pulses generated from the rotating table control electronics. Four adjustable frame trigger pulses are presetable by the system operator, they are reset when the rotating table begins a 180° panoramic scan. The presettable pulses enable the system operator to select an image from one of four previously designated portions of the scene during any pass. These pulses were adjusted to "grab"

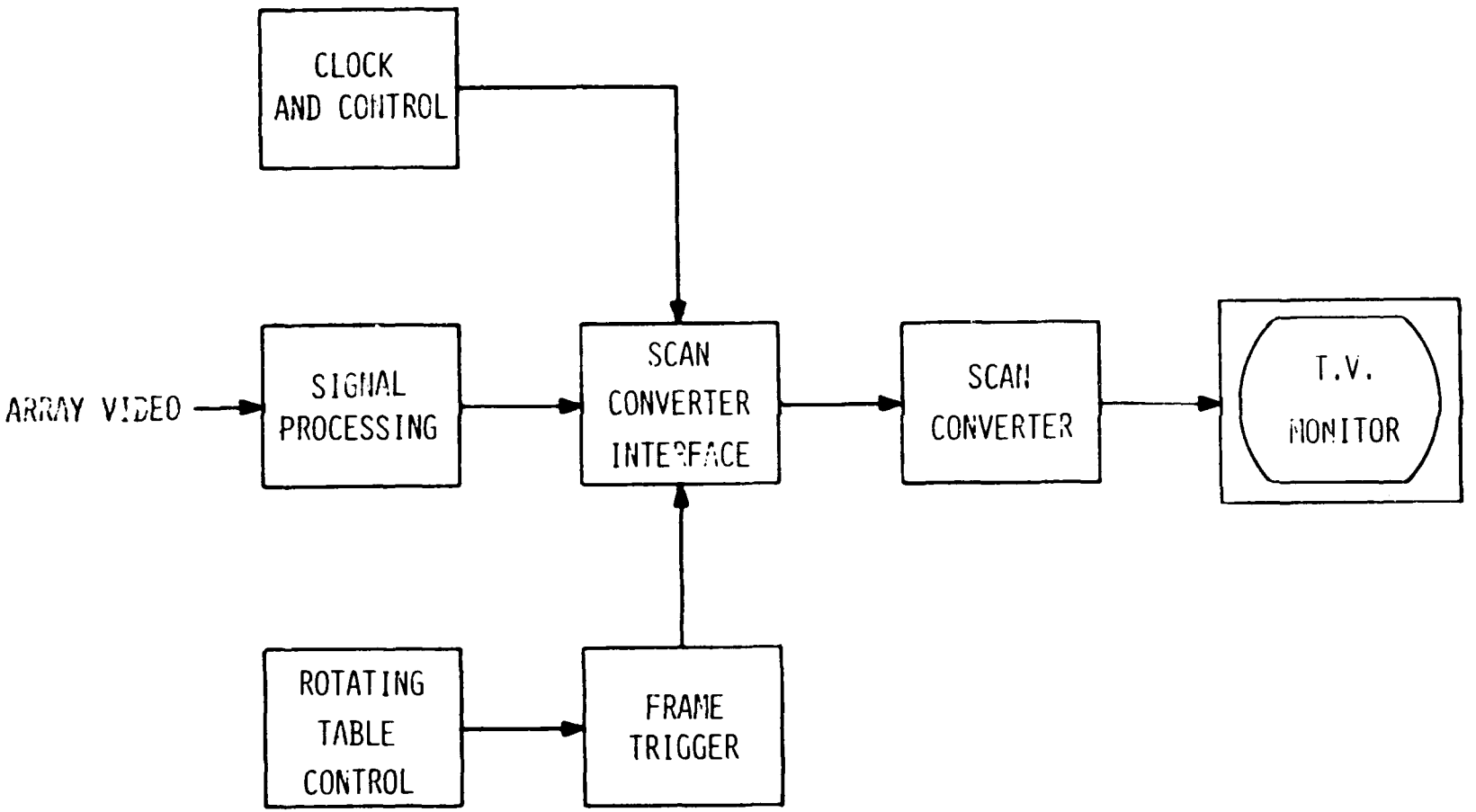

FIGURE 3-18 FRAME FREEZE DISPLAY CONFIGURATION

frames centered around the ship silhouette targets mounted on the periscope installation panorama. When the panoramic scanner is set into continuous operation it pans a 180° scan and retraces. An image is captured by the frame freeze display and held for observation. The low light level target imagery verifying starlight detection using the panoramic scanner was photographed from the monitor of the frame freeze display system.

3.4.2 X,Y,Z Display

The X,Y,Z, display system, designed and constructed for the panoramic scanner, provides the simplest method of line scanned strip mode imagery. The system was implemented for the periscope scanner with a high performance Tektronix model 604, X,Y,Z monitor. Continuous sweep waveforms, representing array video lines, are generated in synchronism with the CCD video and applied to the Y input of the monitor. Array video, processed into proper form of zero to one volt, is applied to the Z axis input of the monitor. The X axis input of the monitor receives a frame sweep waveform identical to that presented to the frame freeze display. This display is intended for use with a polaroid camera for grabbing single shot photos from the high quality display. The polaroid camera shutter is kept open until one frame is triggered across the monitor face. This imagery is captured on high speed polaroid film for quick analysis of system operation.

3.4.3 Falling Raster Display

A falling raster display system, designed to produce information from the panoramic scanner, useful in a tactical, "real time", situation was produced and constructed using internal Fairchild

research and development funds. The falling raster display is essentially a digital, one-frame, memory which can be read at T.V. compatible rates into a standard T.V. monitor. Incoming CCD video lines occur at slower rates than the T.V. compatible video. At the 18° per second panoramic scan rate, used in the periscope scanner, video lines occurred at a rate of 400 lines per second; in one T.V. field time less than seven new CCD video lines are generated. The falling raster display operates by replacing the six oldest CCD lines in the frame memory with the six newest lines during the T.V. vertical retrace. The display observed by the system operator appears as a standard T.V. picture with imagery coming in on the right of the screen and out in the left just as if an area T.V. camera were panned clockwise. In each new field, six new lines are added causing imagery to move from right to left in .7 seconds. This "fall-through" time just gives the observer time to catch and recognize moving objects. The major function of the falling raster has been to convert line scanned, strip mode, imagery into a form useful in a real-time-reaction scenario. An operator watching the T.V. falling raster monitor is able to trigger the frame freeze storage system to save an interesting image for later analysis. The falling raster system only has a transient, one frame, memory which moves along the panorama. Only the last frame is saved when the scanning action is halted.

The falling raster system was designed to store a 256 x 256 element frame in 6-bit digitized form. This design size was large enough to accommodate the two-chip hybrid output when it was used. The same design also accommodated the single chip mode. A description of the falling raster hardware follows.

The Falling Raster Display is a special purpose image memory processor that presents a dynamic "strip chart," "moving window", "waterfall," or "falling raster" on a standard TV monitor.

Because the periscope image is produced by two dual-in-line Charge Coupled Devices (CCD) that are physically offset, a SLACK memory is required to delay the one half of the sensor video that first sees the object. Because the sensor or slow-scan camera is unlike standard TV cameras, additional DISPLAY memory is required to refresh the full TV display. Because "simultaneous" read-write (I/O) is necessary for the dyanmic display a FALLING RASTER BUFFER (FRB) memory is required to temporarily store the input video until the DISPLAY memory is not busy refreshing the TV readout, i.e., until vertical blanking. Finally a static INPUT BUFFER is used for the asynchronous input, since all the other memories (SLACK, DISPLAY, FRB) are dynamic CCD's which require time consuming refresh.

The complete processor consists of approximately 150 integrated circuits (SSI & MSI) which provide the I/O, timing, arithmetic, and control of the 52 CCD memories. Expansion of the image and display resolution will require more CCD's but not many more processing IC's. The present CCD 460 organization of the Line Addressable Random Access Memory (LARAM), which consists of 32 groups of four shift registers 123 elements/line, is not optimum for this 6-bit, 64 gray level image. However, the 16,384 bits per DIP is the densest available. Maximum utilization of the LARAM generates familiarity and problem solutions for further applications. A printed circuit LARAM PCB has been designed and produced for versatile use of 16 CCD's, or 262,144 bits of memory with numerous partition options.

Referring to the block diagrams of Figure 3-19: Video #1 consists of 128 integrated lines of 128 elements physically spaced 128 elements ahead of Video #2 in the direction of motion. The last two elements of #1 and first two of #2 are degraded by edge effects and will be skipped in order to improve the electronic butting. The camera processor mixes the video so that only one A/D is required for reduced quantization errors and cost. A synchronous 1 Megahertz clock and Video Gate (800 per second maximum rate) tell when to sample the video.

The A/D output is alternately steered between INPUT BUFFER A & B. Twelve static 256 x 1 RAM's are used to simplify the skip function and to interface to the LARAM's. Separate Write/Read (I/O) counters address the RAM such that IB-A can READ while IB-B writes and vice versa. The RAM chip select is not used because of the overlap at the end of write enable.

A digital multiplex (MUX) selects either IB-A or IB-B and its output feeds the FALLING RASTER BUFFER (FRB) thru another MUX directly or via the SLACK memory. Only a two line input buffer is required because the FRB and SLACK can be refreshed in less than 2 milliseconds and the maximum input rate is 800 lines per second (1.25 milliseconds).

The SLACK read address is advanced after the next line is written into the same address. Thus the 256 line memory provides 256 line delay before the written line is read out. (An adder IC can reduce the delay by R = W + N). To transfer the two full lines (2 x 256) from the Input Buffer into the FRB the following sequence occurs. After 4096 (32 x 128) refresh clocks (.4µsec or 2.4MHz), 128 clocks READ out the SLACK and WRITE into the FRB: the next two phase 128 clocks (effectively 4.8MHz) Read out of one

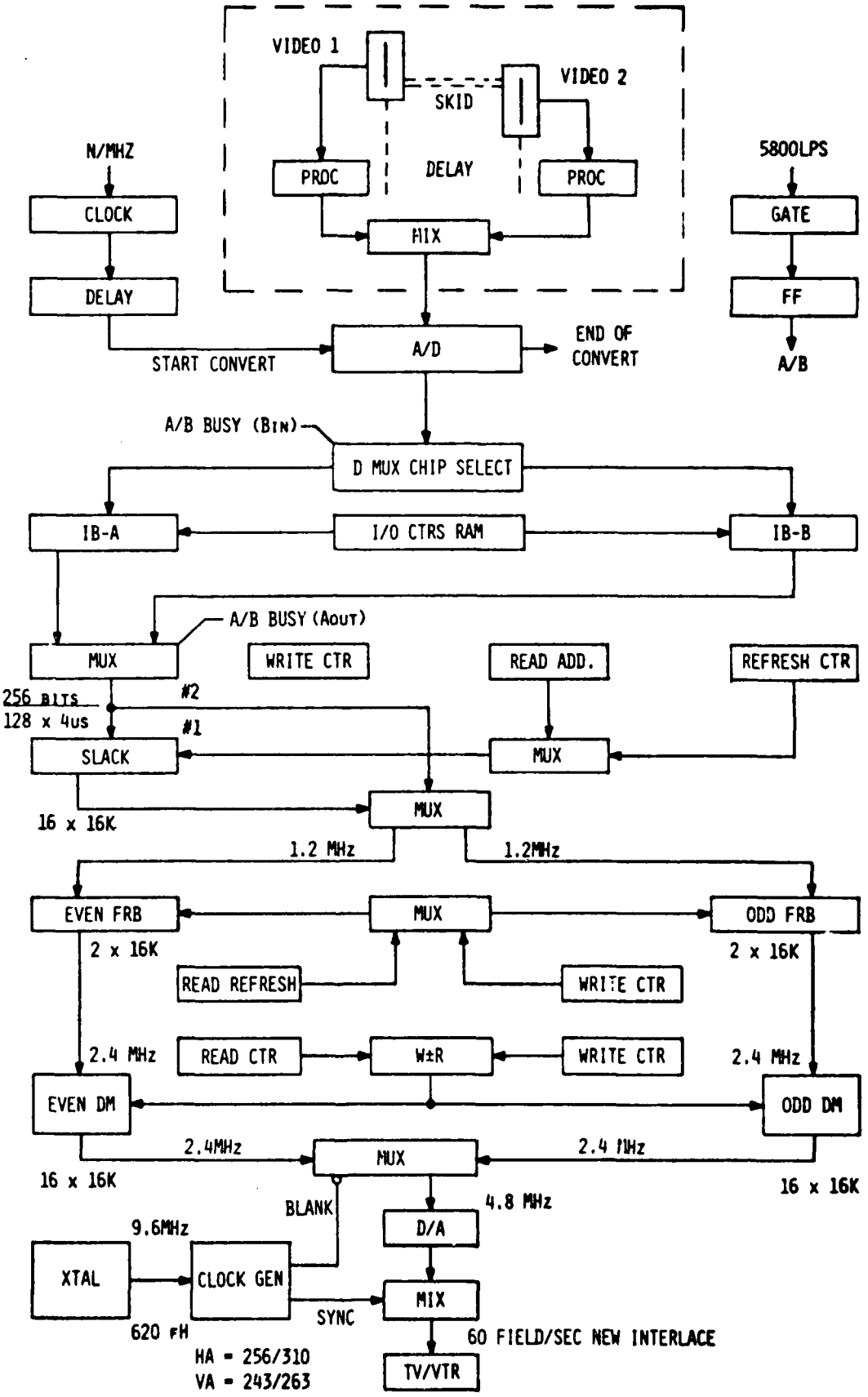

FIGURE 3-19 FALLING RASTER DISPLAY BLOCK DIAGRAM

IB both to Write into Slack and Write into FRB directly; the third interval of 128 clocks Readout the second line of Slack and Write into FRB; and the fourth interval (again two phase) readout the other IB both into SLACK and into FRB. To display the 256 elements during one active TV line (52 μsec) requires a 4.8 MHz clock but the prototype LARAM's can't exceed 2.5 MHz. The FRB and DISPLAY are multiplexed to double the frequency.

The 9.6 Megahertz crystal oscillator (620 x f_h) and clock generator circuits produce eight phases of 2.4 MHz (A,B,C,D) for the various timing functions and LARAM clock drives.

The FRB stores upto 16 full lines and reads them into the Display Memory during TV vertical blanking. Actually the FRB has 32 line capacity because of its multiplexing. The Display Read Counter produces 263 TV lines, of which 20 are blanked, including 13 of the 256 Written lines. Each field falls by the number of lines transferred from the FRB to Display, because the DISPLAY address equals the Write count minus the Read count for falling raster, and Write count plus the Read count for rising raster. A falling raster is thus produced by the "Write plus or minus Read" function, without the carry, such that the top of the monitor begins with the state of the Write counter that is only updated during vertical blanking by the FRB transfers.

3.5 TEST CALIBRATION AND RESULTS

The testing of the three feasibility test configurations, i.e., the high resolution scanner, the integrating mode panoramic scanner, and the two-chip integrating mode hybrid modification were conducted at Fairchild and witnessed by Navy review personnel on three different occasions.

3.5.1 High Resolution Scanner

The high resolution scanner was completed first of the three configurations and subjected to the test conditions cited in the contract specifications and in Table 3-4. The rotating scanning drum shown in Figure 2-3 of Section II carried a calibrated spatial frequency target (IEEE Facsimile Test Target) that was illuminated by a 2854° light source. The light level was adjusted with optical filtering until a 100 ft. lambert brightness value from the highlights of the scene target existed. The photometric level specified was measured with a Pritchard Spectra brightness spot meter.

The video derived from the CCD camera was displayed as 2-dimensional imagery on a TV monitor in both a real time mode and in near real-time via a scan converter (30 frames/sec.) The recorded limiting resolution, as witnessed by several observers (Navy and Fairchild) was clearly at the Nyquist limit of 38 lp/mm for a 100 ft. lambert brightness level in the highlights of the scene.

This excellent result established that high resolution performance can be maintained in small cell devices (17 x 13 μ) even at moderately low light levels and high speed video data rates.

TABLE 3-4

TEST INSTRUMENTATION PARAMETERS
HIGH RESOLUTION ARRAY

Array Type	CCLID 1728
Number of Elements	1728
Element Pitch	13 μm (.00051")
Focal Length	3"
Vertical Angle	16.77°
Scan Rate	37.3°/sec
Exposure Time	260 μs
Lines per 180° Scan	18547
Data Rate	6.9×10^6 elements/sec.
Scene Brightness	100 ft. lamberts

3.5.2 Low Light Level Integrating Mode Operation

The integrating low light level panoramic scanner configuration was operated under the specified contract conditions shown in Table 3-5 and the equipment shown in Figure 2-2 of Section II. The calibration of the light levels for this low light sensor configuration was conducted with spectroradiometric equipment (EGG 545) to establish an accurate simulation of starlight conditions for test. The calibration of the scene irradiance converted to photometric units is shown in Table 3-6. The target ships for the experiment were designed to simulate a horizon silhouette model ship at various ranges. Neutral density filters were used to vary the 2854°K calibrated light source.

The lowest scene irradiance demonstrated to Navy review personnel with all three display systems, i.e., frame freeze, X, Y, Z, and falling raster, and using the referenced ship targets (ship reflectance = 36%) was 9.7×10^{-9} watts/cm^2 (1.5×10^{-4} ft. lamberts). This value corresponds to a clear sky, starlight condition.

The results of the low light level sensor, using one exposure time of 0.325 seconds can be expressed as:

$$9.7 \times 10^{-7}\ w/cm^2 \times 0.325\ sec = 3.15 \times 10^{-9}\ \frac{w\text{-}s}{cm^2} = 31.5\ \mu J/M^2$$

The measured noise equivalent exposure (NEE) of the TDI sensor used was measured as 0.425 $\mu J/M^2$ as shown in Table 3-7. This value would produce a signal-to-noise ratio of 1. Therefore, the signal-to-noise ratio related to the measured scene irradiance of 9.7×10^{-7} w/m^2 can be expressed as the ratio of the energy density at the array compared to the noise equivalent exposure value. Taking into account the T number of the lens, i.e., 1.08, the signal-to-noise ratio that existed for the measured scene irradiance level can be stated as:

$$S/N = 31.5/4(1.08)^2/.425 = 16:1$$

TABLE 3-5

TEST INSTRUMENTATION PARAMETERS
TDI ARRAYS

Array Type	CCAID 128
Number of Elements	128
Element Pitch	20 μm (.00079")
Numbers of Integrations/line	128
Focal Length	1"
Vertical Angle	5.86°
Scan Rate	18°/sec.
Exposure Time	325 ms
Lines per 180° scan	3932
Vertical Clock Frequency	393 Hz
Data Rate	1 MHz (with overscan)
Scene Illumination	3×10^{-9} W/cm^2

TABLE 3-6 CALIBRATION OF SCENE

FILTER (S) SET A	SCENE HORIZON LUMINANCE[1] (FT-LAMBERTS)	APPROXIMATE HORIZON SKY LUMINANCES[3] (FT-LAMBERTS)
		15 HEAVILY OVERCAST DAY
NONE	12.14	
ND 0.3	6.44	
ND 1.0	1.54	
		1.5 SUNSET-OVERCAST
ND 2.0	0.267	
		0.15 QUARTER HOUR AFTER SUNSET - CLEAR
ND 3.0	2.04×10^{-2}	
		1.5×10^{-2} HALF HOUR AFTER SUNSET - CLEAR
ND 4.0	1.63×10^{-3}	
		1.5×10^{-3} BRIGHT MOON, CLEAR
ND 4.0 + ND 0.3	8.02×10^{-4}	
ND 3.0 + ND 2.0 + ND 0.3	1.94×10^{-4}	
		1.5×10^{-4} STARLIGHT[2] CLEAR SKY

(1) LAMP CALIBRATION AT 2854°K
(2) FROM CAMPANA
(3) RELATIVE SKY LUMINANCE FROM MIDDLETON W.E.K. VISION THROUGH THE ATMOSPHERE 1952

TABLE 3-7 TEST DATA SUMMARY FOR THE SCAMD-128A

PARAMETER	5W2 #19
A. CHARACTERIZATION	
Vsat (volts) *	2.1
Dynamic Range	2800
Linearity (r)	1
NES (electrons/cell)	72
NEE ($\mu J/m^2$)	.435
Responsivity, 2854°K (mA/watt)	66.6
B. IMAGING TRI-BAR TARGETS	
Fraction of Saturation	1/2,1/186 1/374 1/748
C. SQUARE WAVE RESPONSE	
Wide Band CTF**at 0.9NL	
Horizontal, 1/2 Sat.	.49
Horizontal, 1/20 Sat.	.35
Vertical, 1/2 Sat.	.37
Vertical, 1/20 Sat.	.36
Narrow Band CTF**at 0.9NL	
Horizontal, 1/2 Sat., .6-.7 μm	.85
Horizontal, 1/2 Sat., .7-.8 μm	.58
Horizontal, 1/2 Sat., .8-1.1 μm	.25
D. NARROW BAND UNIFORMITY	
Full 2854°K	3.5%
.8-1.1 μm	4%
.7-.8 μm	1.8%
.6-.7 μm	1.5%

It is clear, therefore, that a reduction of the scene irradiance from the measured value of 9.7×10^{-9} w/cm^2 to the goal value of 3×10^{-9} w/cm^2 will still provide conditions for adequate detection, i.e., a signal-to-noise ratio of 16/9.7/3 5:1.

3.5.3 2-Chip Hybrid Integrating Mode Operation

The 2-chip hybrid configuration, described in paragraph 3.1.3, is a dual 128 x 128 TDI bilinear arrangement designed to achieve a greater number of picture elements in the sensor format. The bilinear arrangement, or offset, "butting" arrangement is used to achieve the alignment of the end picture element of one array to the beginning picture element of the second array. The offset is compensated for in the processing and display electronics.

Four assemblies of dual 128 hybrid assemblies were fabricated in the program; one mechanical mockup to verify the alignment procedure and three operational units. The first operation hybrid assembly utilized the two best performing devices. Unfortunately, this assembly was irreversibly damaged by a probe scratch on the edge of one device and it had to be set aside. The second assembly was also set aside because of a crack that developed on one of the carrier substrates. The third and final hybrid was used to produce the 256 x 256 imagery shown in Figure 2-6.

The scene illumination level for the test was in the range of 1/4 moon conditions. The two 128 x 128 devices used in the final assembly were poorer than the earlier assemblies but results show reasonable matching of the upper and lower sensors in the referenced photograph. The faint horizontal white line in the center of the photograph represents the butting interface. The dark horizontal line above this point is caused by a defective pixel in the upper sensor. The chips were mounted to provide a two pixel overlap

between vertical lines. When butted in the displays, the last pixel of chip number one and the first pixel of chip number two were electronically removed from the video chain. Electronic removal is valid since they cover redundant information in the panorama. This was done to eliminate imperfect pixels, which might occur at the end of the array, from the butt joint.

Referring to Figure 2-6, the apparent horizontal misalignment between the upper and lower halves of the picture, seen on the right side, results from the fact that several lines have been blanked from the upper half picture in order to retrace the scan converter and print the lower band. Vertical lines spanning the two chips (none are shown in this scene), have been shown to be aligned within 1/2 pixel.

3.6 Periscope Motion Simulation Testing

A simple, cost effective scheme for simulating periscope motion was designed, constructed and incorporated into the existing CCD parnoramic system. The periscope motion studies, described in Section IV of this report, indicate that all vibration induced image motion in an operational panoramic system, with targets effectively at infinity, reduce to a) components of vertical image translation of all points in the scene plus b) image rotation around the center of the array. When looking ahead (or behind) along the direction of travel the periscope tip oscillation reduces to a pure rotational image smear with a sinusoidal period. When looking at 90° to the direction of travel, the image smear is purely translational across the axis of CCD integration and again is characterized by a sinusoidal period. At all other orientations between 0° and 90° the vibration is a combination of the two effects, i.e., in perfect phase with each other, and shifting in peak-to-peak amplitude from one form to the other as the sine of the pointing angle. The objective of the motion simulation testing was to evaluate the image degradation resulting from the set of motions found to be typical for a Type 16 periscope as described in Section IV. A further objective was to provide data useful for the evaluation of system performance of future camera designs and determine the level of stabilization required for the desired performance.

3.6.1 Target Motion Simulation

A block diagram of the motion simulator is shown in Figure 3-20. A significant aspect of the motion simulator is that the test targets were moved and not the CCD array with its associated mount plus electronics; this arrangement simplified implementation of the technique. Image smear was achieved by operating the TDI array in its "framing mode" while imaging a vibrating target.

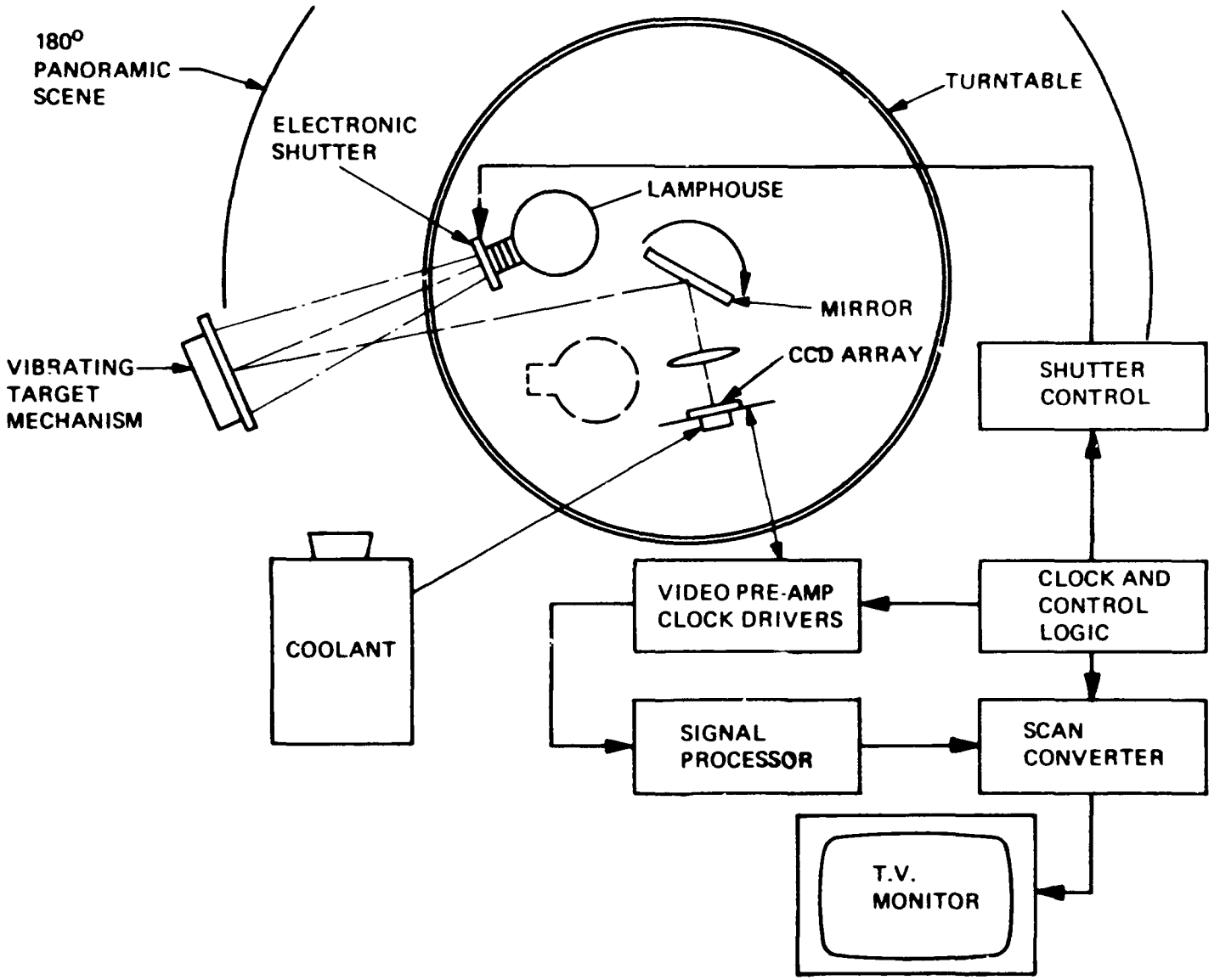

FIGURE 3-20. ARRANGEMENT OF MOTION SIMULATOR ON ROTARY TABLE

The framing mode is a method of operating the time delay and integration device. To implement it, a target scene is imaged on the array (which is a 128 x 128 element sensor) while the charge transfer clocks are stopped. An electronic shutter on the light source of the panoramic scanner controls the integration time. When the shutter closes, the clocks start and transfer the single stored charge image into the scan converter "frame freeze" system. The image is then made available on a CRT monitor for analysis. Target motion is provided by a motor driven stage which oscillates the target in vertical translation and axial rotation with adjustable amplitude, phasing and frequency. The relative phasing of the two motions can be adjusted continuously through 360°. The amplitudes of motion are independently adjustable from zero to ±.25" and ±.5° respectively for translation and rotary motion. The frequency of vibration is variable from 0 to 25 Hz with both motions being belt driven from one motor at the same frequency. Figure 3-21 shows the target motion simulator. Figure 3-22 shows an expanded view of the adjustment mechanism.

3.6.1.1 Adjustment of Amplitude of Vibration

There are two independent eccentrics; one for rotation, and the other for up-down motion.

To adjust the amplitude, loosen set screw and bolt head as shown in Figure 3-22.

To adjust amplitude to zero, align two marks as shown in Figure 3-22.

At 180° where the marks are opposite each other, the amplitude in the Y motion is ±.25" (for a total motion of .5").

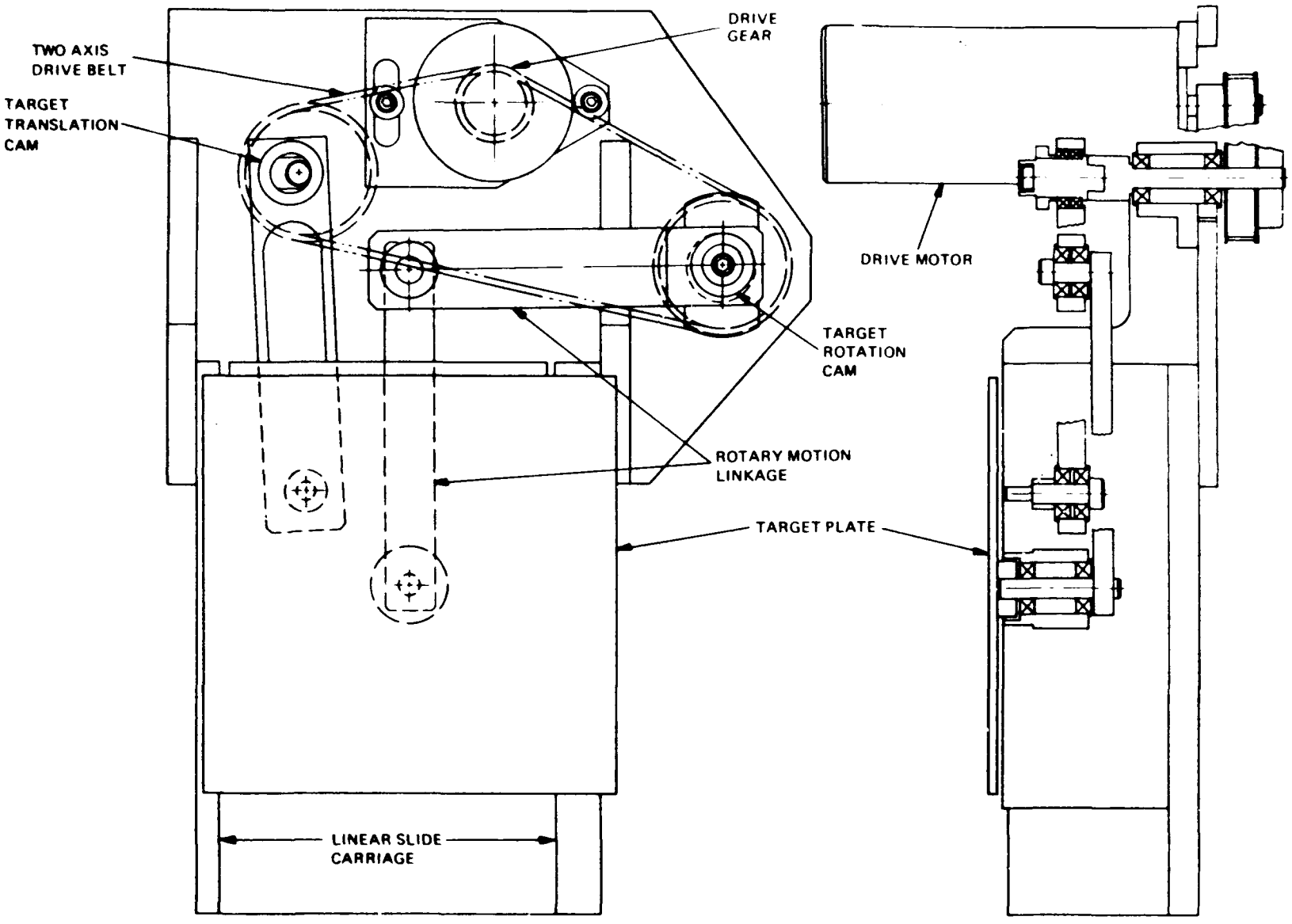

FIGURE 3-21. TARGET MOTION SIMULATOR

The maximum amplitude at 180° in Θ is ± 1/2° for a total angle of 1° peak-to-peak.

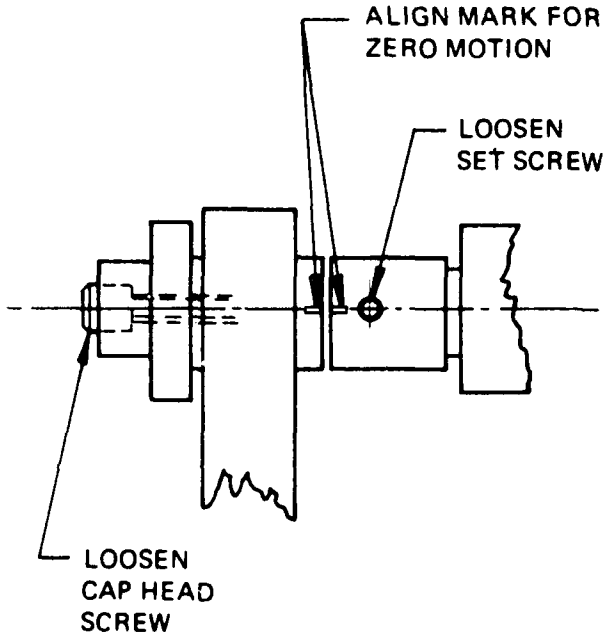

FIGURE 3-22 MOTION ADJUSTMENT MECHANISM

3.6.1.2 Adjustment of Frequency of Vibration

There is a gear reduction between motor and eccentric drive. Consequently the frequency of the motor is double the frequency of vibration.

For example, if the desired frequency is 5 hertz, then the frequency of vibration is 5 hertz x 60 = 300 RPM. The speed of the motor must then be 600 RPM.

Consequently, to convert hertz to RPM of motor, multiply by 120.

2 Hertz = 240 RPM
5 Hertz = 600 RPM
10 Hertz = 1200 RPM
12.5 Hertz = 1500 RPM = 1 cycle per array integration time.
15 Hertz = 1800 RPM
20 Hertz = 2400 RPM
25 Hertz = 3000 RPM

3.6.1.3 Adjustment of Phasing of Motions

By loosening the set screws on the driven gear for either of the motions, the phase of its motion relative to the other may be shifted. This adjustment allows a full 360° variation in phasing between axes.

3.6.1.4 Calibration

Aside from the reference marks for zero motion, several calibration points were determined for the vibrating stage. With the use of a dial indicator, alignment marks on the eccentrics were provided to allow 1,2,3 & 4 pixels of peak-to-peak, vertical image translation and peak-to-peak rotational angles of .896° and 1.14° which result in peak-to-peak pixel smear at the end of the array of 1 and 1.3 pixels respectively. For the purposes of comparison between array length, lens focal lengths and uncompensated periscope motion, all vibrations have been expressed in terms of peak-to-peak pixels.

3.6.2 Pixel Motion For A Type 16 Periscope

Table 3-8 is based on the analysis of periscope motion, presented in Section IV. Two columns express the image motion resulting from the periscope vibration in terms of peak-to-peak pixels for a full cycle of vibration. A two-inch focal length lens is assumed. For rotation, column four gives the peak-to-peak number of pixels of image smear caused by one complete cycle of mast vibration at the array extreme. The rotational component of vibration (around the array central axis) has different effects depending on how far out from the array center is considered. This effect is independent of lens focal length. Figure 3-23 illustrates the effect of image rotation on the CCD array as a function of image position. The arrows indicate instantaneous image motion. The values in Table 3-8 of peak-to-peak pixel motion are calculated for the array extreme indicated in the figure. For periscope speeds, away from resonance (using the 128 array) this component of image smear is less than 1/4 pixel and, as such, would not be significant. Near a resonance the effect is seen to be much worse and would have to be corrected. In addition, a longer array would experience a more severe image smear at the array extreme. For example, the image smear at the extreme of a 1024 element array would be 1.5 pixels peak-to-peak at a speed of 6 knots as compared to .192 pixels for the 128 element array. Column seven of Table 3-8 gives the number of pixels of peak-to-peak image translation resulting from mast vibration when the sensor is looking 90° to the direction of travel. In this case, every pixel is translated equally in the vertical axis and the magnitude, in pixels, is related to the lens focal length. A two-inch focal length is assumed in the table. The image smear in this case is shown to be quite significant at most periscope speeds. The image motion testing described herein was designed to evaluate the impact of unstabilized components of these motions on output image quality.

TABLE 3-8. PERISCOPE MOTION SUMMARY - TYPE 16
(EXTENSION 14 FEET)

VELOCITY (knots)	DYNAMIC DEFLECTION FREQUENCY (Hz)	PEAK ANGLE (deg.)	P-P ROTARY RUNOUT AT ARRAY EXTREME (pixels)	PEAK ANGULAR VELOCITY (deg/sec)	"Y" PEAK SINGLE AMPLITUDE* (inches)	P-P TRANSLATION (pixels)
1	.54	.006	.0135	.02	.0025	.53
2	1.08	.020	.0447	.14	.0084	1.77
4	2.25	.068	.15	.99	.029	6.03
6	3.73	.086	.192	1.93	.036	7.63
8	5.40	.382	.853	14.3	.160	33.9
8.5	7.00	2.50	5.59	111.0	1.05	220
10	7.56	.236	.527	13.8	.099	20.9
12	9.75	.155	.346	11.8	.065	13.7
14	12.3	.100	.223	9.7	.042	8.87
16	15.6	.105	.234	11.7	.044	9.3
18	19.9	.109	.244	14.3	.046	9.67
20	22.5	.109	.244	14.9	.046	9.67

* for target at 24"

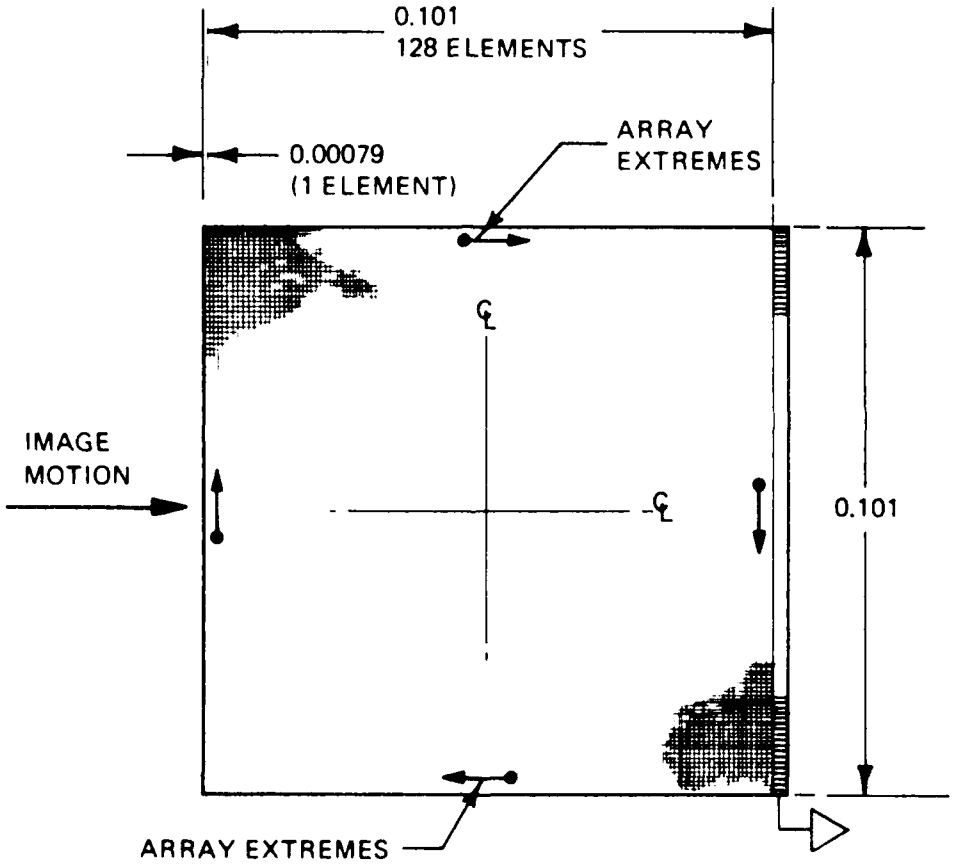

FIGURE 3-23. APPARENT IMAGE MOTION DUE TO ARRAY ROTATION

3.6.3 Test Description

Using the target motion simulator and the frame freeze capability of the CCD sensor a series of images of a special test target were made using varying amounts of vibration on the test target. Figure 3-24 shows the test target used for image degradation testing. The target contains tri-bar patterns at many orientations ranging in spatial frequency from 1 to .56 of the array Nyquist frequency. The central tri-bar pattern is .56 of Nyquist and the eight radial target segments vary from .63 Nyquist near the center to 1.0 Nyquist at the target perimeter. This is calibarated for one-inch lens with the target 25 inches from the array.

A full range of vibration conditions were simulated using the target motion simulator. The values used for vibration amplitude are given in Table 3-9. In order to simplify the testing, a certain set of conditions were assumed. The integration time of the array was set at 80 milliseconds; this is a direct consequence of a panoramic system scanning at 36° per second with a two-inch lens. In order to eliminate the problems of phasing, vibration frequency was set at 12.5Hz to allow one full cycle of motion per integration time. This is equivalent to the mast vibration frequency encountered at 14 knots.

Figure 3-25 to 3-28 illustrate the eight test conditions documented. In each case the image motion photo is compared to a photo of the test target with no motion applied, as it was phased just before introduction of the vibration. As can be seen from the "no vibration photos", it is not possible to adjust the target position in the CCD array such that all bars and spaces of all test patterns are aligned in phase with the array elements. Since these "before" positions vary with each test setup, they are shown for comparison with their corresponding moving image.

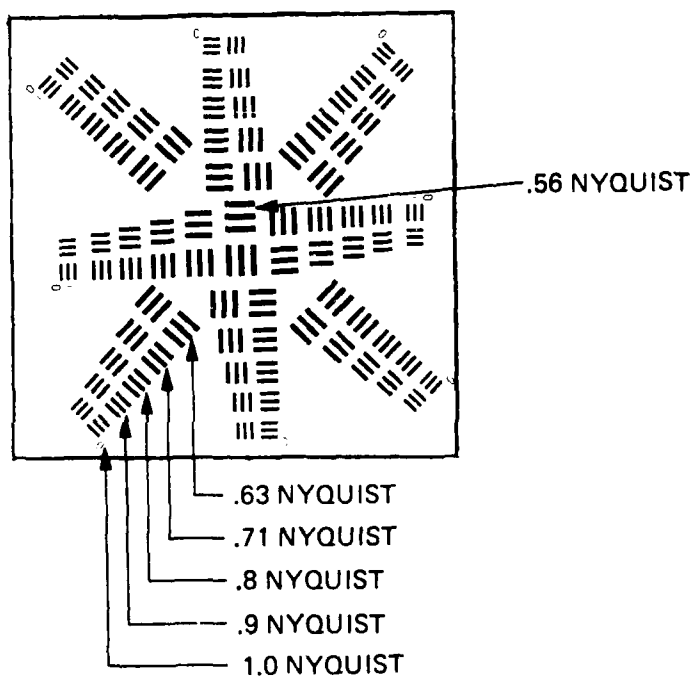

FIGURE 3-24. MOTION ANALYSIS TEST TARGET

TABLE 3-9. IMAGE VIBRATION - TEST PARAMETERS

TEST #	IMAGE TRANSLATION (p-p pixels)	IMAGE ROTATION (p-p pixels)	SIMULATED Heading(deg)	VIBRATION FREQUENCY(HZ)	EQUIVALENT PERISCOPE SPEED(Kn)
1	0	0	N/A	0	0
2	1	0	90	12.5	14
3	2	0	90	12.5	14
4	3	0	90	12.5	14
5	0	1	0	12.5	14
6	0	1.3	0	12.5	14
7	1	1	45	12.5	14
8	2	1.3	45	12.5	14

Figure 3-25 illustrates the image smear resulting from one and two pixels of peak-to-peak sinusoidal image translation. For the top right photo, illustrating one pixel of peak-to-peak motion, very little difference between the before and after photos is noticeable, i.e., some of the Nyquist targets are worse and some are better. Bar patterns aligned parallel to the image motion (vertical bars) suffer no noticeable degradation. The variations in target phasing accounts for Nyquist resolution improvement in some cases. This phenomenon occurs when a bar pattern is initially out-of-phase with the array elements. During image oscillation, however, the target group is actually in-phase for a greater proportion of the sinusoidal period than out-of-phase this results in improved resolution. When the vibration reaches two pixels, peak-to-peak, all Nyquist bars perpendicular to the image motion are lost but the .56 Nyquist bars at the target center are still resolvable. This is in good agreement with the theoretical consideration outlined in the following sections. The upper photos in Figure 3-26 illustrate the resolution loss with three pixels of vibration.

The lower photos of Figure 3-26 illustrate the effects of one pixel of peak-to-peak image rotation. In this case, tri-bars patterns at the Nyquist limit are lost whenever they are perpendicular to the rotational component of image motion. This includes the right hand horizontal tri-bars and the bottom vertical tri-bars. Figure 3-27 illustrates the effect of 1.3 pixels of p-p rotation, the maximum possible with the motion simulator. As anticipated, the effect is not noticeably different from one pixel of motion.

Figure 3-28 illustrates two cases of combined image motion. The top photos show one pixel, peak-to-peak of translation and vibration combined and in proper phase. The combined effects are not severe. The lower photos show combined motions of two pixels,

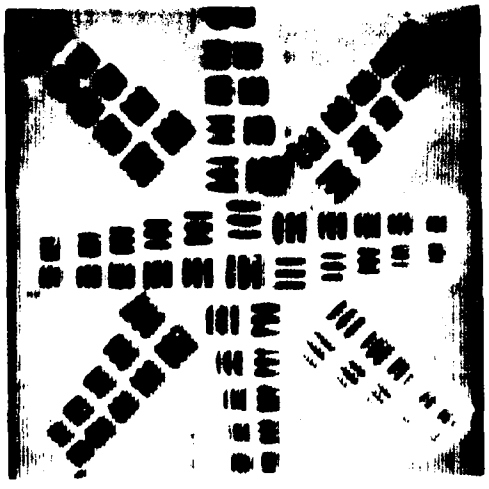

NO IMAGE MOTION

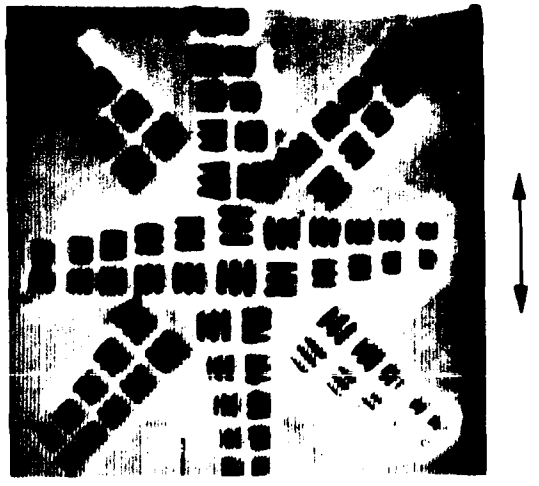

ONE PIXEL OF PEAK TO PEAK
IMAGE TRANSLATION

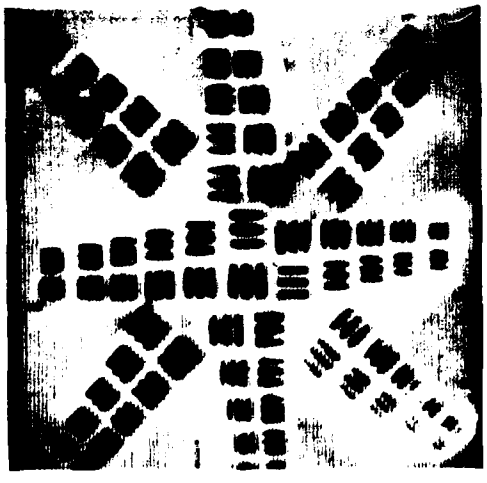

NO IMAGE MOTION

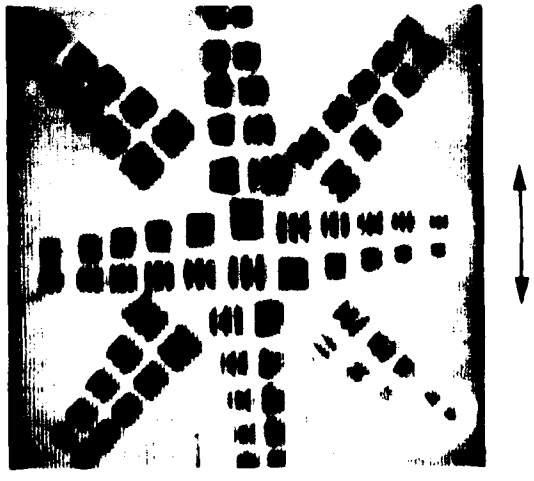

TWO PIXELS OF PEAK TO PEAK
IMAGE TRANSLATION

FIGURE 3-25. IMAGE MOTION RESULTS

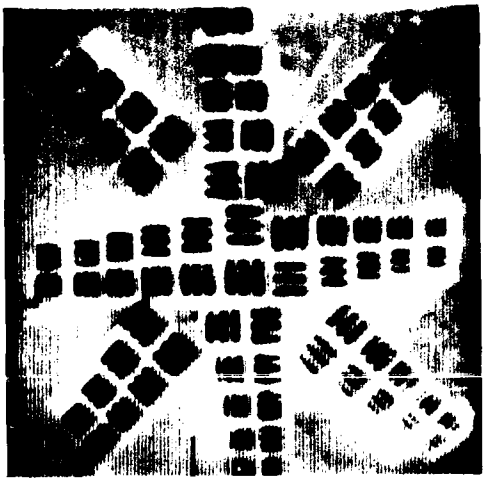

NO IMAGE MOTION

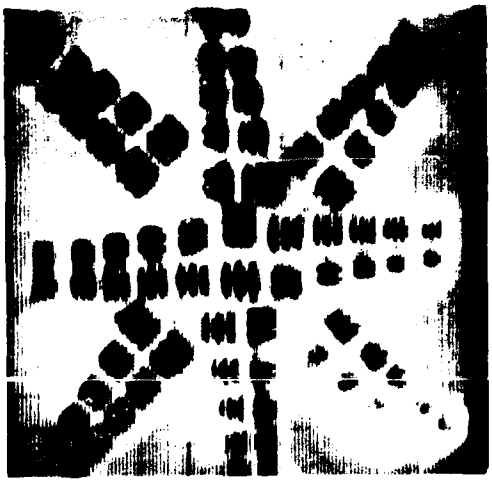

THREE PIXELS OF PEAK TO PEAK
IMAGE TRANSLATION

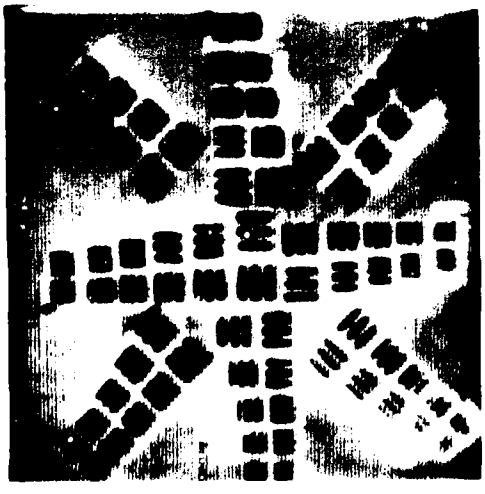

NO IMAGE MOTION

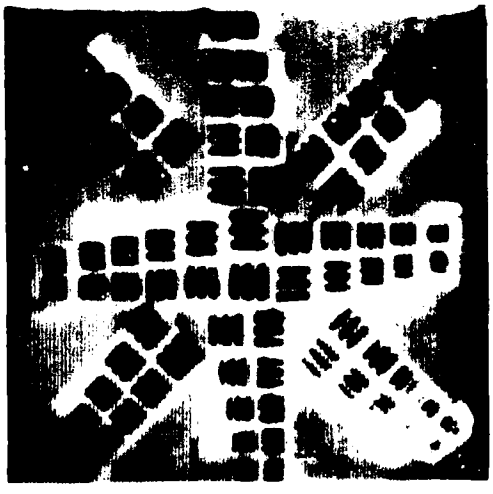

ONE PIXEL OF
PEAK TO PEAK ROTATION

FIGURE 3-26. IMAGE MOTION RESULTS

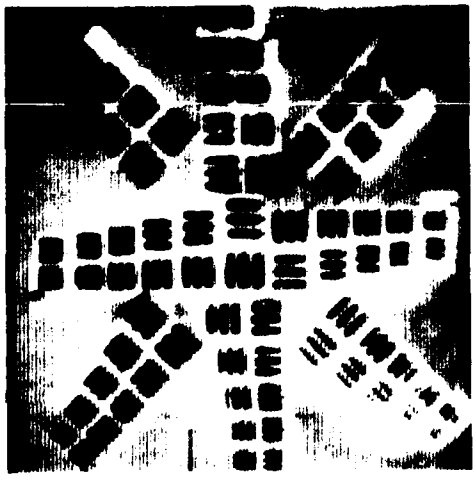

NO IMAGE MOTION

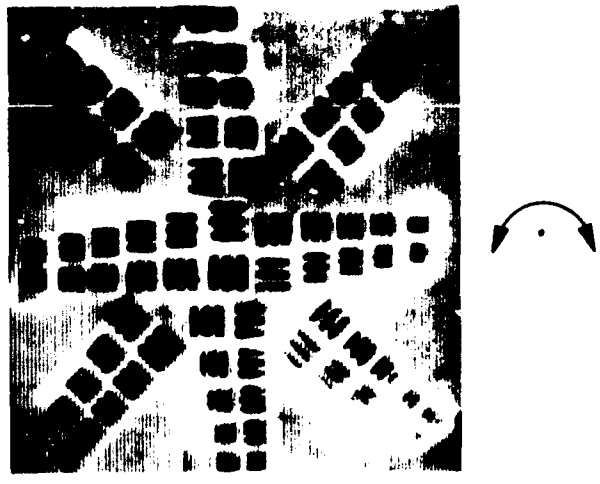

1.3 PIXELS OF PEAK TO
PEAK ROTATION

FIGURE 3-27. IMAGE MOTION RESULTS

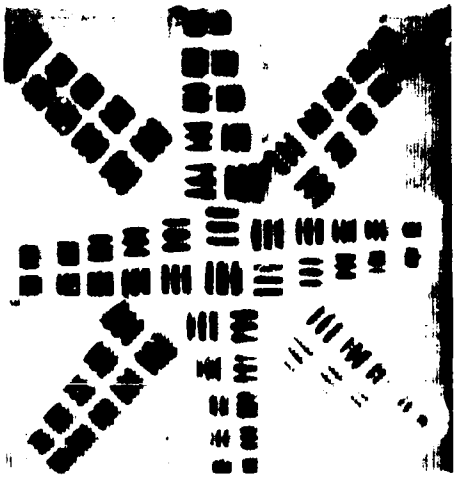

NO IMAGE MOTION

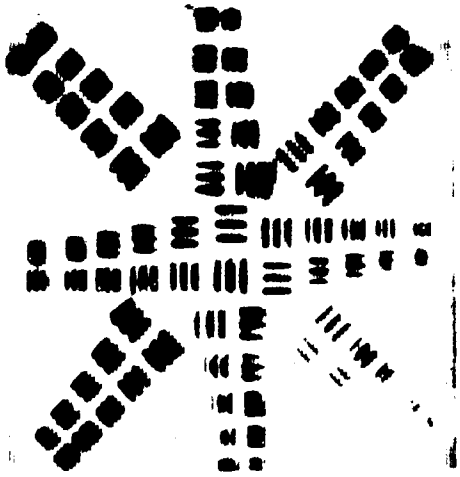

ONE PIXEL PEAK TO PEAK
TRANSLATION AND ROTATION

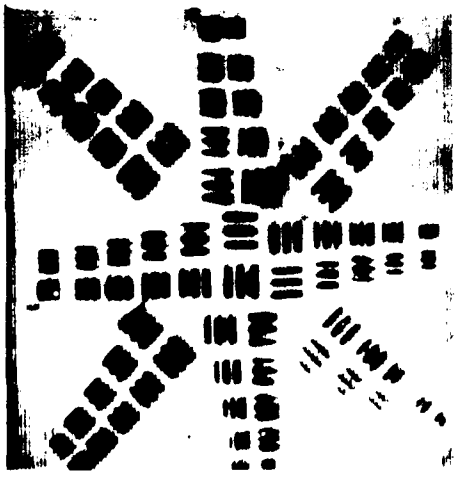

NO IMAGE MOTION

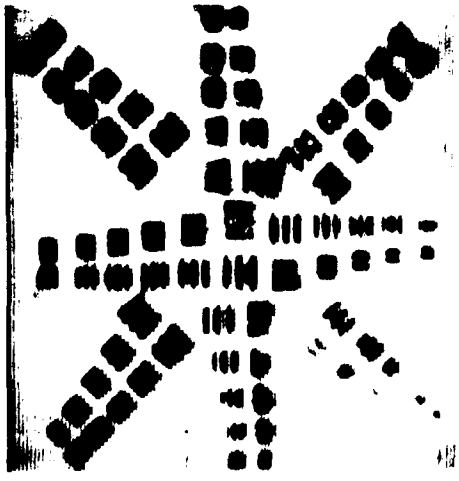

TWO PIXELS OF TRANSLATION
AND 1.3 PIXELS OF ROTATION

FIGURE 3-28. IMAGE MOTION RESULTS

peak-to-peak translation and 1.3 pixels of rotation. The loss of horizontal resolution is primarily caused by the translation motion.

3.6.4 Theoretical Considerations

The most severe component of image motion predicted from the Type 16 studies is in the translation direction. It is clear from the photos that more than one pixel of peak-to-peak uncorrected vibration will seriously degrade image quality. For residual vibrations of less than one pixel, phasing considerations may actually improve resolution in isolated cases, but on the average, image modulation will degrade. The testing aparatus was not designed to provide quantitative measurement of MTF reduction due to vibration, but only limiting resolution data. For simple motion cases however, the effect of these motions has been documented in the literature. Figures 3-29 and 3-30 quantify the theoretical MTF of a perfect system operating in the presence of external vibrations. Figure 3-29 shows the MTF resulting from sinusoidal image vibration of one and two pixels, peak-to-peak amplitude. The MTF, at the Nyquist limit, for one pixel of motion, is down to 46 percent.

Combining this with an array MTF of 45 percent at Nyquist, the resulting system MTF becomes 20 percent. This is easily detectable on a high contrast image as the test photos confirm. For two pixels of motion, the MTF at Nyquist is totally lost. Figure 3-30 shows the effect of peak linear smear of one and two pixels. Although all vibrations encountered in the periscope system are oscillatory and nearly sinusoidal, they vary in frequency. For a fixed array integration time of 80 milliseconds (12.5Hz), many of the periscope vibrations encountered in an operational system will only complete a fraction of a cycle during the integration period, i.e., at boat speeds below 8 knots. This fraction may be such that the image motion is most closely approximated by a linear smear. In such cases, the curve of Figure 3-30 can be used to predict system MTF.

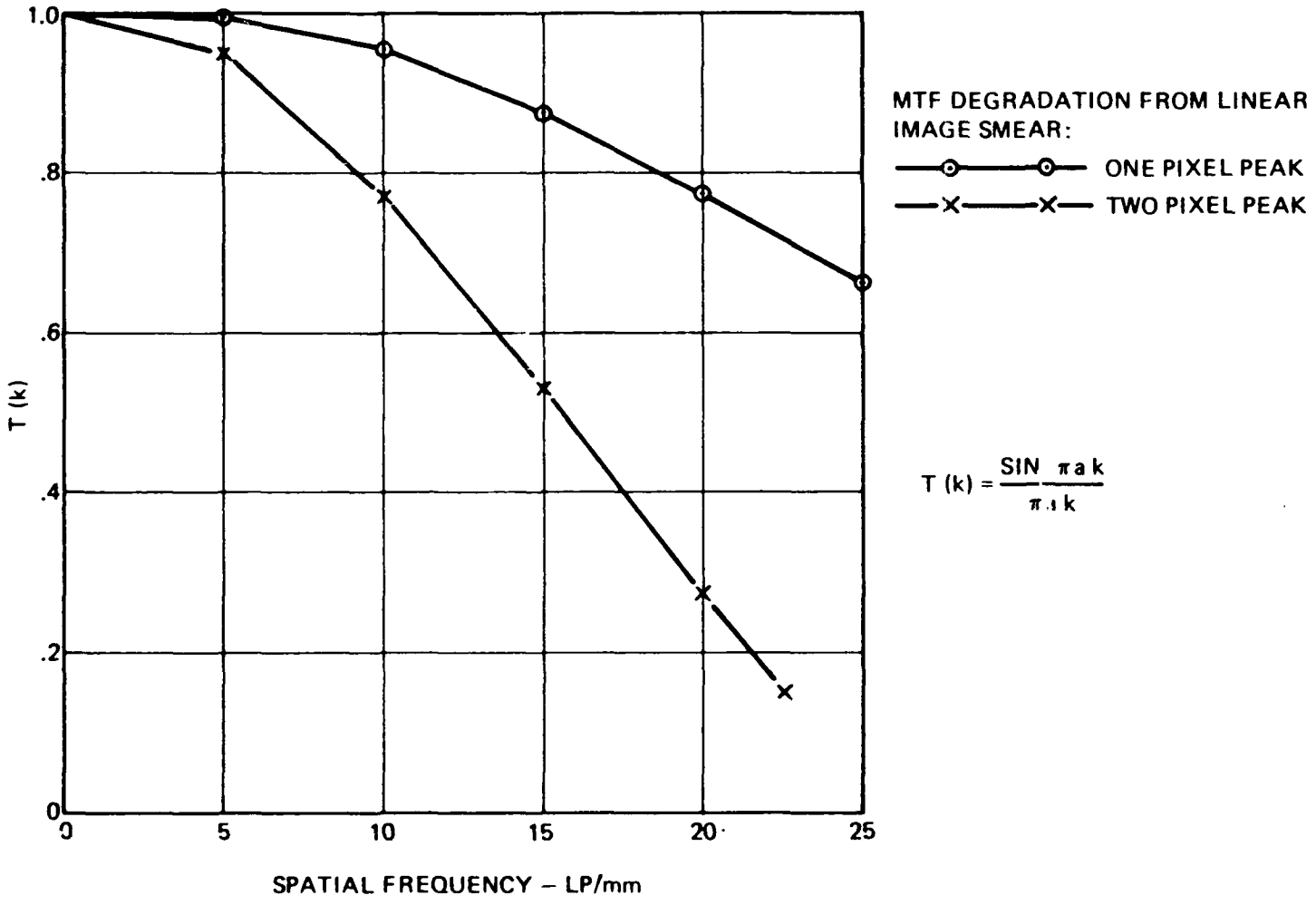

FIGURE 3-29. MTF DEGRADATION DUE TO SINUSOIDAL IMAGE MOTION

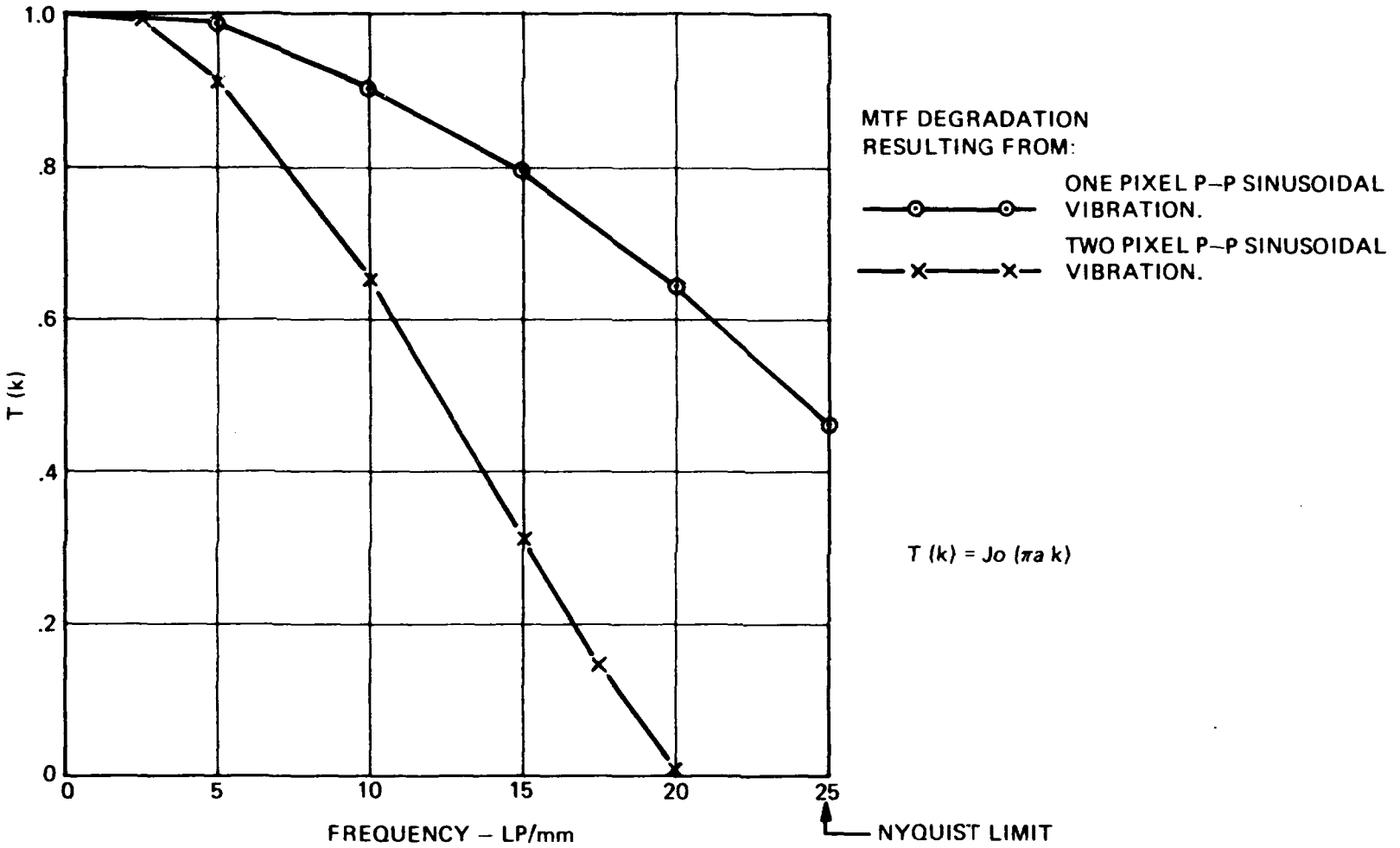

FIGURE 3-30. MTF DEGRADATION DUE TO LINEAR IMAGE MOTION

SECTION IV

STABILIZATION ANALYSES

4.0 STABILIZATION ANALYSES

The stabilization study efforts conducted in this program addressed primarily a) an analysis of Navy-supplied data on submarine periscope motion, b) computations of static and dynamic persicope tip motions using a "model" of a Type 16 periscope configuration, and c) motion sensing design concepts related to CCD Periscope System. The analysis and computation of "worst case" periscope tip motions, not supplied by Navy data but derived from inputs, Navy modeling data, (see references) are important toward establishing a stabilization design configuration for this integrating TDI CCD sensor approach.

Paragraph 4.1 of this section develops the modeling and periscope motion predictions; the design concepts developed are described in Paragraph 4.2; recommendations for further work in this stabilization area are presented in Paragraph 4.3.

4.1 FORCES ON VERTICAL CYCLINDERS MOVING THROUGH A LIQUID HAVING A FREE SURFACE

Forces on a moving cylinder are of two kinds: (1) those resulting from the motion of the cylinder and (2) those generated by surface waves. The former includes

viscous drag forces, periodic lift forces due to vortex shedding and wave-making drag. The latter includes wave induced viscous drag and inertial forces due to the unsteady motion of the fluid. To obtain an estimate of the importance of each of these forces, each will be considered to act independent of the others.

4.1.1 Steady Viscous Drag

With reference to Figure 1, the viscous drag force (Fo) per unit length of cylinder can be represented as

$$Fo = \frac{C_d \rho_w V^2 D}{2}$$

where ρ_w = density of water and C_d = viscous drag coefficient.

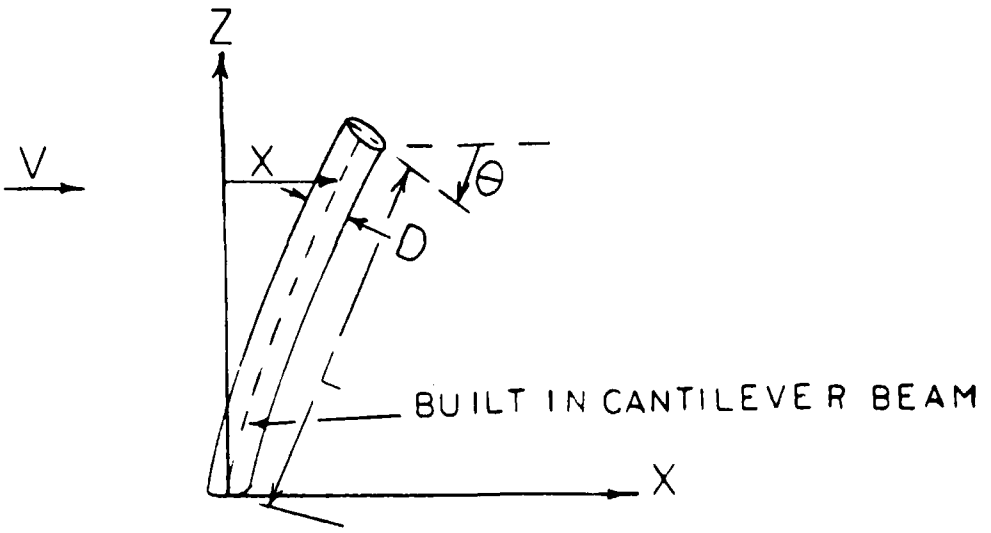

FIGURE 4-1 SYMBOLS FOR BEAM

Values for the drag coefficient (C_d) are plotted in Figure 4-2. As a function of the Reynolds number ($Re = VD/\nu$, ν = Kinematic Viscosity). In the range of interest, C_d has values between 1.2 and .3.

For a cantilever beam of length (L) subject to a uniform force of, Fo, per unit length, the deflection is

$$X(Z) = \frac{F_o}{EI}\left[\frac{L^2Z^2}{4} - \frac{LZ^3}{6} + \frac{Z^4}{24}\right]$$

At the top of the beam, the deflection is a maximum and equals

$$X(L) = \frac{3F_oL^4}{24EI}$$

Where E = Young's modulus

I = Moment of inertia of beam cross section ($I = \frac{\pi D^4}{64}$, for uniform density cylinder)

If only the lower section (L_1) of the beam is subject to the uniform force Fo, the deflection becomes

$$X_1 = \frac{F_o}{EI}\left[\frac{L_1^2Z^2}{4} - \frac{L_1Z^3}{6} + \frac{Z^4}{24}\right]$$

For small deflections, the beam slope at the top (full submerged beam) is

$$\frac{dX}{dZ} = \frac{F_oL^3}{6EI} = TAN\,\theta \approx \theta$$

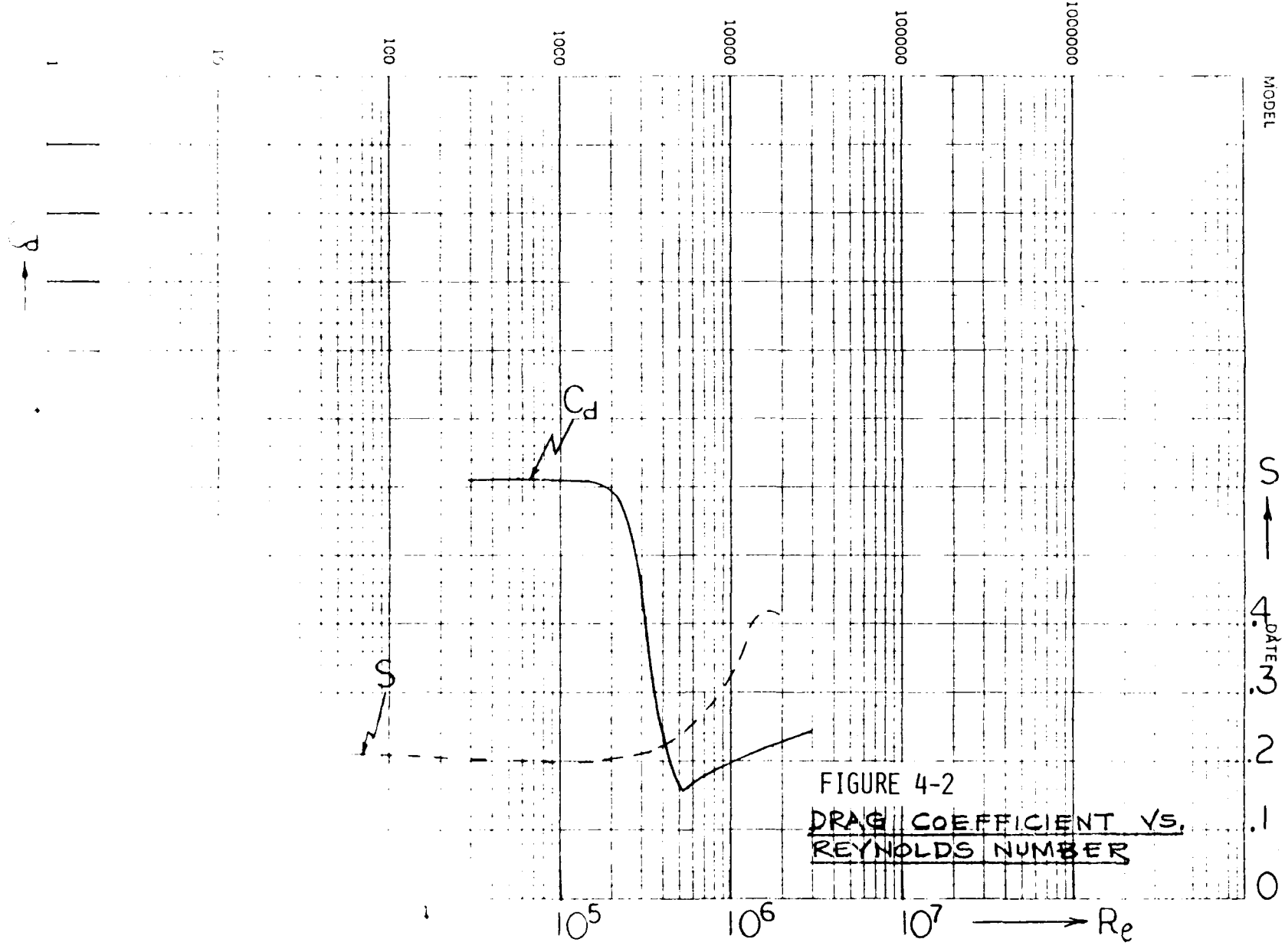

FIGURE 4-2
DRAG COEFFICIENT VS. REYNOLDS NUMBER

Values for both the deflection angle and X(L) at the top of a fully submerged cylinder are tabulated in Table 4-1 and shown in Figure 4-3.

TABLE 4-1 CALCULATED STATIC DEFLECTION VERSUS VELOCITY

Cylinder Length (L)	19 Feet
Cylinder Inner Diam.	6.5 Inches
Cylinder Outer Diam.	7.5 Inches
Young's Modulus (E)	29×10^6 LB /Inch^2

VEL (Knots)	Θ (Degrees)	DEFL (Inches)
1	.011	.032
2	.043	.127
3	.076	.226
4	.079	.237
5	.080	.238
6	.102	.305
7	.143	.428
8.	.204	.610
9	.266	.794
10	.338	1.01
12	.518	1.55
14	.718	2.14
16	.959	2.86
18	1.24	3.70
20	1.56	4.66

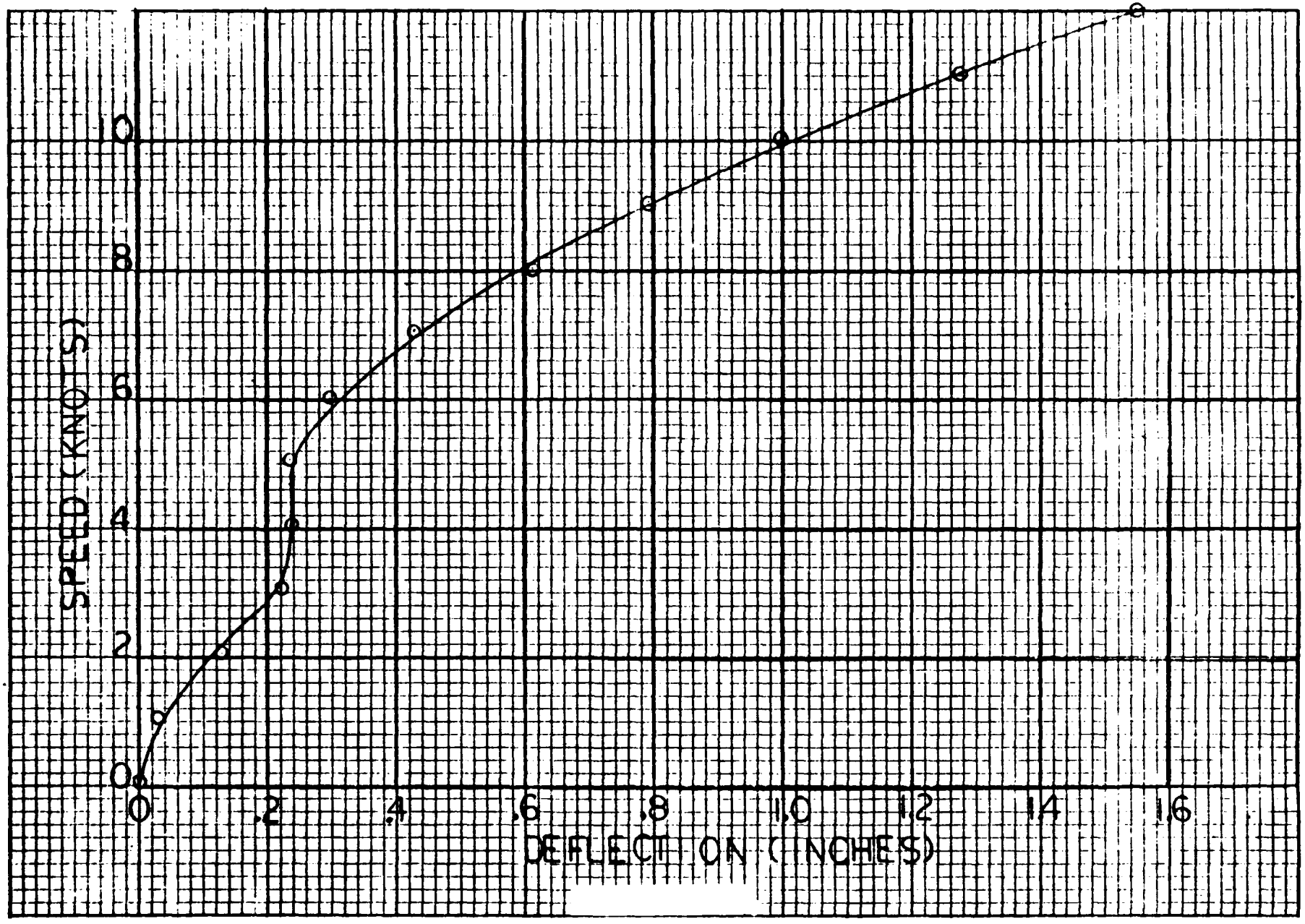

FIGURE 4-3 Speed Vs. Periscope Deflection

Static deflections (X) at the top of a fully submerged cylinder have also been calculated based on data presented by J. S. Pepi (1973). This data approximates closely the type 16 periscope. The results are summarized in Table 4-2.

TABLE 4-2 CALUCLATED STATIC DEFLECTION VERSUS VELOCITY

Cylinder Length (L)	14 Feet
Moment of Inertia (I)	67.7 Inches^4
Young's Modulus (E)	28 x 10^6 LBF/Inch^2

VEL (Knots)	DEFL (Inches)
1	.014
2	.046
4	.14
6	.14
8	.24
10	.39
12	.59
14	.85
16	1.1
18	1.43
20	1.77

4.1.2 Wave Induced Viscous Drag

Due to surface waves, a partly (or fully) submerged cylinder will experience periodic viscous drag forces. In the case of Figure 4-4 the horizontal force (F_w) per unit length of cylinder is for a stationary cylinder given by (Ippen, 1966):

$$F_w = \frac{1}{2}\rho_w U|U| D\, C_w$$

where U is the horizontal wave velocity and C_w is a drag coefficient. Experimental data for C_w show a great deal of scatter (Agerschou, 1966) within the range from .5 to 2.5.

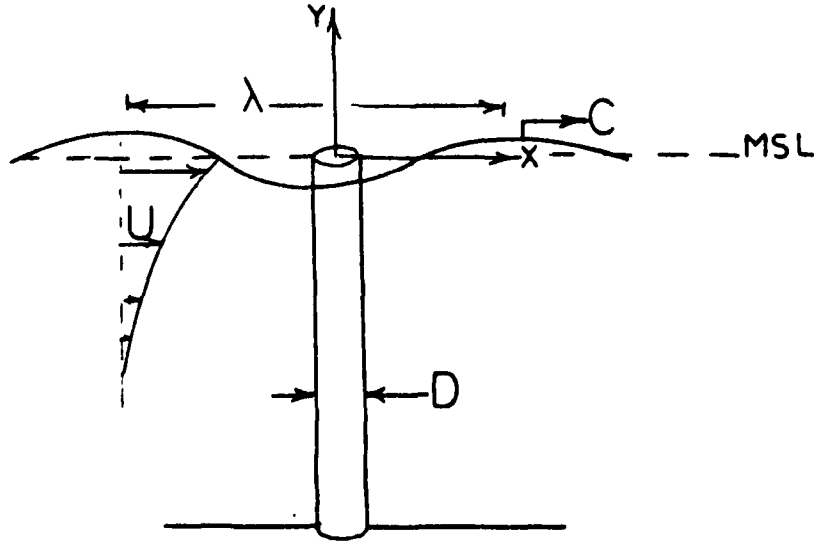

Figure 4-4

Wave Forces on a Cylinder

The wave force (F_w) is periodic and decreases rapidly with depth. To compare F_w with Fo, we note that U is given approximately by

$$U = \frac{ag}{c} EXP(\frac{2\pi}{\lambda}Y) COS(\frac{2\pi}{\lambda}X - \frac{2\pi}{T}t)$$

The maximum value of U is

$$U_{MAX} = \frac{ag}{c}$$

where a = Wave Amplitude

g = 32.2 feet/sec^2

c = Wave Speed

$= \frac{gT}{2\pi}$ (Deep Water)

or $= \sqrt{\frac{g\lambda}{2\pi}}$

In Table 4-3 are tabulated values of U_{max} for different wave lengths (λ) assuming waves of maximum wave steepness ($\frac{2a}{\lambda} = .142$). For representative values of "λ" and "a", U_{max} has values of 2 or 3 knots. F_w is therefore of the same order as Fo at these speeds. The force F_w is periodic and induces vibrations in the direction of propagation.

TABLE 4-3 MAXIMUM HORIZONTAL WAVE VELOCITY

U_{max} (Feet/sec)	Wave Length (λ) Feet	Amplitude (a) Feet
2.3	5	.36
3.2	10	.71
5.1	25	1.78
7.1	50	3.55
10.1	100	7.1
14.3	200	14.2
20.2	400	28.4

However, since the frequency of a wave is much lower than the natural frequency of any cylinder of interest, resonance is not possible. Even when the cylinder moves with a velocity (V) in a direction opposite to the wave propagation, the increased frequency at which the cylinder sees the waves is still not in the range of its natural frequency. This is shown in Table 4-4 where calculated values of the frequency (f) of a wave of length (λ) as measured on a cylinder moving with velocity (V) is listed. The frequencies can be seen to be less than one for wave lengths of interest.

TABLE 4-4 WAVE FREQUENCY ANALYSIS

(Feet)	V (Knots)	f (CPS)	V (Knots)	f (CPS)	V (knots)	f (CPS)
5	2	1.7	5	2.7	10	4.4
10	2	1.05	5	1.6	10	2.4
25	2	.59	5	.79	10	1.1
50	2	.39	5	.50	10	.66
100	2	.26	5	.31	10	.40
200	2	.18	5	.20	10	.24
400	2	.12	5	.13	10	.16

4.1.3 Wave Generated Inertia Forces

Due to the time dependent motion of the fluid particle in a wave a body influenced by waves will experience an inertia (or mass) force (F_m). This mass force per unit length of a cylinder is expressed as (Ippen, 1966):

$$F_m = C_m \frac{\pi D^2 \rho_w \dot{U}}{4}$$

in which C_m is the mass coefficient, and $\dot{U}$ the horizontal water particle acceleration. There is much scatter in the experimental data for C_m with a value of 2 often used. A comparison of the total inertia force and viscous wave induced force acting on a cylinder indicates that the ratio of these forces are of the order

$$\frac{\pi C_m D}{C_d a}$$

where D is the cylinder diameter (7.5 inches) and "a" the wave amplitude. For waves of moderate height, the wave induced viscous and mass forces are of comparable magnitude. Again, as for the viscous drag, there is no possibility of induced resonance due to the inertia force.

4.1.4 Wave-Making Drag

The motion of a partially submerged cylinder through still water creates surface waves. If the motion of the cylinder remains steady, the resulting force on the cylinder is steady. This force acts approximately at the position on the cylinder corresponding to the position of the average horizontal particle velocity in the transverse waves in the wake of the cylinder (McCormick, 1973). The depth at which the force acts is

$$\bar{Y} = -.037\,V^2 \ (\text{SEC}^2/\text{FT})$$

where V is the speed of the cylinder. The wave making force (F_R) can be represented as

$$F_R = C_R \frac{DL_w \rho_w V^2}{2}$$

where L_w represent the wetted length of the cylinder and C_R is a wave making drag coefficient. The parameter C_R depends on $V/\sqrt{gD}$. Data presented by McCormick(1973) for C_R is listed in Table 4-5.

TABLE 4-5 WAVE MAKING DRAG COEFFICIENT

$V/\sqrt{gD}$	C_R
1	.8
1.5	.6
2	.45
2.5	.35
3	.3

Based on the above results the static deflection of the top of a cantilever cylinder has been calculated and are tabulated in Table 4-6. These results are only approximate but indicate an effect of the same order as the static deflection due to viscous drag.

TABLE 4-6 STATIC DEFLECTION DUE TO WAVE MAKING

Cylinder Length (L)	19 Feet
Cylinder Outer Diam.	7.5 Inches
Cylinder Inner Diam.	6.5 Inches
Cylinder Submerged	17 Feet
Young's Modulus (E)	29×10^6 LBF/Inch^2

VEL (Knots)	Wave Force (LBF)	DEFL (Inches)
2	108	.18
4	288	.43
6	432	.51
8	576	.43

4.1.5 Vortex Induced Unsteady Forces

When water flows past a cylinder, a periodic wake is formed by vortices shed from alternate sides of the cylinder. If the cylinder is free to oscillate it will do so in the cross flow direction. Apparently, oscillations in the flow direction are also possible (King, 1974), but at a smaller flow velocity and with a smaller amplitude.

The frequency of vortex shedding is

$$f_s = \frac{SV}{D}$$

where S is the strouhal number.

The strouhal number is plotted in Figure 4-2 for a rigid cylinder. Not much is known about S for a non-rigid cylinder, but Wotten (1969) has presented data indicating that S is generally a factor of 2 smaller for a non-rigid cylinder. For the cylinders under consideration, f_s equals the natural frequency of the cylinder when V is in the range between 4 to 8 knots. Table 4-7 summarizes the natural frequencies of a number of periscopes. These are found to lie in the range from 3 to 7 CPS. When f_s is near the natural cylinder frequency, resonance occurs and large oscillations take place.

Periscope Type	Reference (See Ref. Section)	Natural Frequency (Fundamental)	Young's Modulus (E)	Moment of Inertia (I)	Structural Mass Density (M_s)	Periscope Extension (L)	Faired (F) or Unfaired (UF)	Comments:
Rewson # 16 (without sensor package)	1,7	4.3 CPS*	29.6×10^6 LBS/in^2	OD 7.5" ID 6.5" $I = 67.7 in^4$	8.04×10^{-3} $\frac{LBF-SEC^2}{in^2}$	19 Ft		*Calculated
# 8B	2,3	5 CPS				14 Ft		Tower Test
		3 to 6 CPS					F	Sea Test
# 15B	4	3.5 CPS					F & UF	
# 16	5,6	7 CPS*	28×10^6 LBS/in^2	OD 7.5" $I = 67.7 in^4$	4.74 LBS/in**	14 Ft		*Calculated **Effective W of Peri: per Unit Length

TABLE 4-7 SUMMARY OF REF. DOCUMENT DATA

The transverse force (or lift) caused by vortex shedding can be expressed as

$$F_L = C_L \frac{D\rho_w V^2}{2} SIN(2\pi f_s t)$$

when the vortex shedding is regular.

Usually the lift coefficient C_L is assumed equal to the viscous drag coefficient C_d although they may differ by as much as a factor of 4 or more at times (Laird, 1965).

Table 4-8 summarizes results from Pepi (1973) for the horizontal and angular deflections of a 14 feet long, fully submerged cantilever cylinder. Calculations based on these relationships are shown in Table 4-9 and Figures 4-5 & 4-6.

Under certain conditions (Table 4-4), the fluid velocity, due to surface waves will be sufficient to induce vortex shedding at the natural frequency of the cylinders under consideration. However, little is known about the resulting lift force and therefore, it is not possible to estimate its importance.

TABLE 4-8 VORTEX INDUCED OSCILLATIONS

Cylinder Length	14 Feet
Cylinder Outer Diam.	7.5 Inches
Moment of Inertia (I)	67.7 Inches^4
Structural and Virtual Mass	4.74 LBM/Inch.
Young's Modulus	28×10^6 LBF/Inch^2
Natural Frequency	7.0 CPS

X_s (Inches) = Peak side to side deflection (Top of cylinder) = .077 WT

T = Amplication Factor

W = Viscous Drag Force Per Unit Length (LBF/Inch)

θ = Angular Deflection (Top) = $\theta_s \, SIN(2\pi f_s t)$

θ_s = Peak Angular Deflection = 6.3×10^{-4} WT

$\dot{\theta}$ = Angular Velocity = $\dot{\theta}_s \, COS(2\pi f_s t)$

$\dot{\theta}_s$ = Peak Angular Velocity = $3.96 \times 10^{-3} \, W f_s T$

$\ddot{\theta}$ = Angular Acceleration = $-\ddot{\theta}_s \, SIN(2\pi f_s t)$

$\ddot{\theta}_s$ = Peak Angular Acceleration = $2.49 \times 10^{-2} \, WT f_s^2$

d = Acceleration (Top) = $-(2\pi f_s)^2 X_s \, SIN(2\pi f_s t)$

d_s = Peak Acceleration = $.077 WT(2\pi f_s)^2$

TABLE 4-9 CALCULATIONS OF PERISCOPE MOTION vs. SPEED GPS

Periscope Speed (Knots)	1	2	4	6	8	8.5 (resonance)	10	12	16
Peak Deflection X_s (Inches)	.014	.048	.152	.187	.812	5.39	.520	.334	.226
Peak Angular Amplitude θ_s (Degrees)	.0065	.0223	.0754	.0877	.380	2.53	.244	.156	.106
Peak Angular Velocity $\dot{\theta}_s$ (Deg./Sec)	.02	.14	.996	1.93	14.4	111	13.8	11.8	11.7
Peak Acceleration $\ddot{\theta}_s$ (Inches/Sec^2)	.138	11.9	26.5	90.4	1154	10430	1660	1900	2730
Peak Acceleration a_s (G's)	.00036	.0308	.0685	.234	2.99	27.0	4.3	4.91	7.07

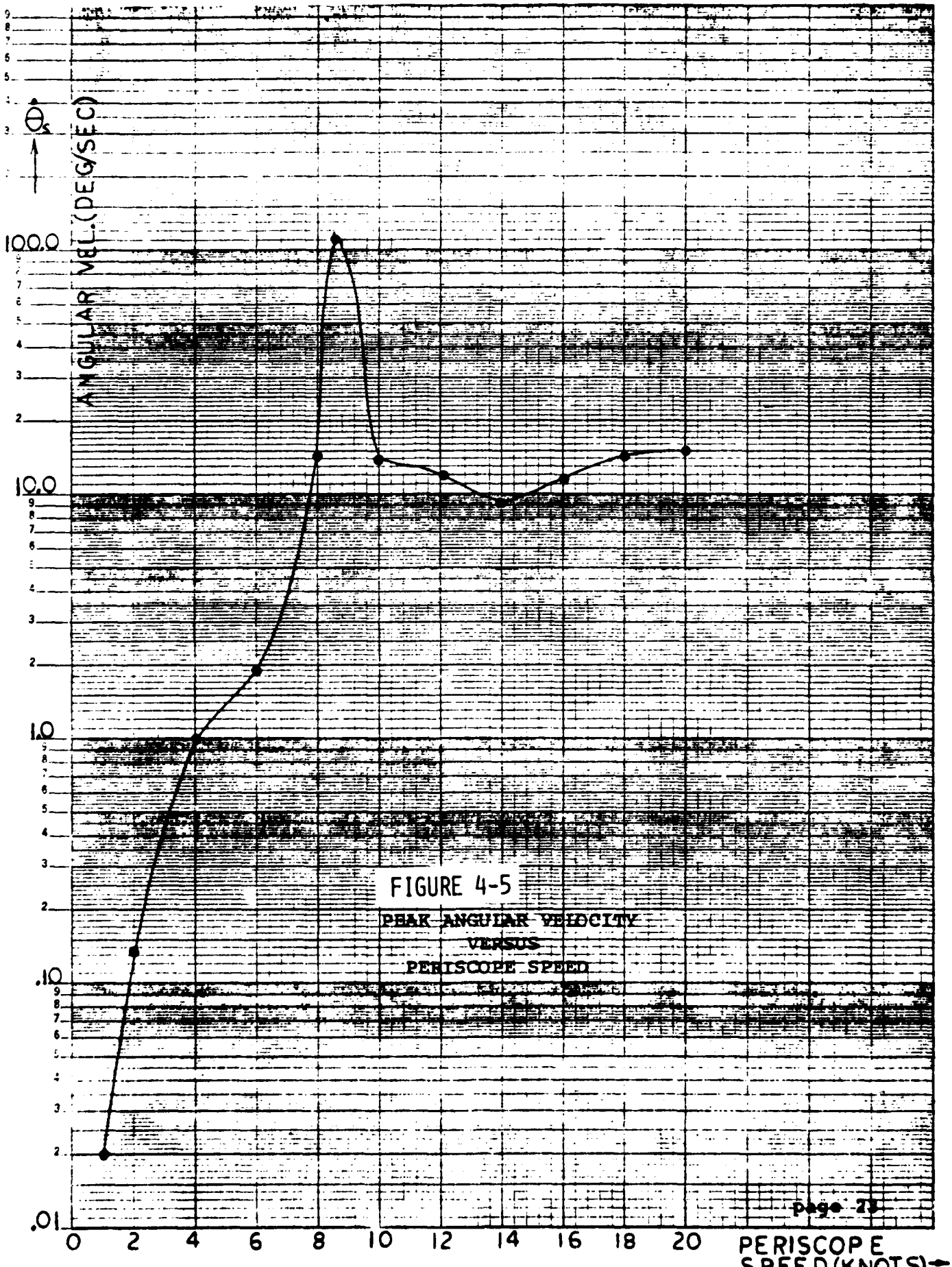

FIGURE 4-5

PEAK ANGULAR VELOCITY VERSUS PERISCOPE SPEED

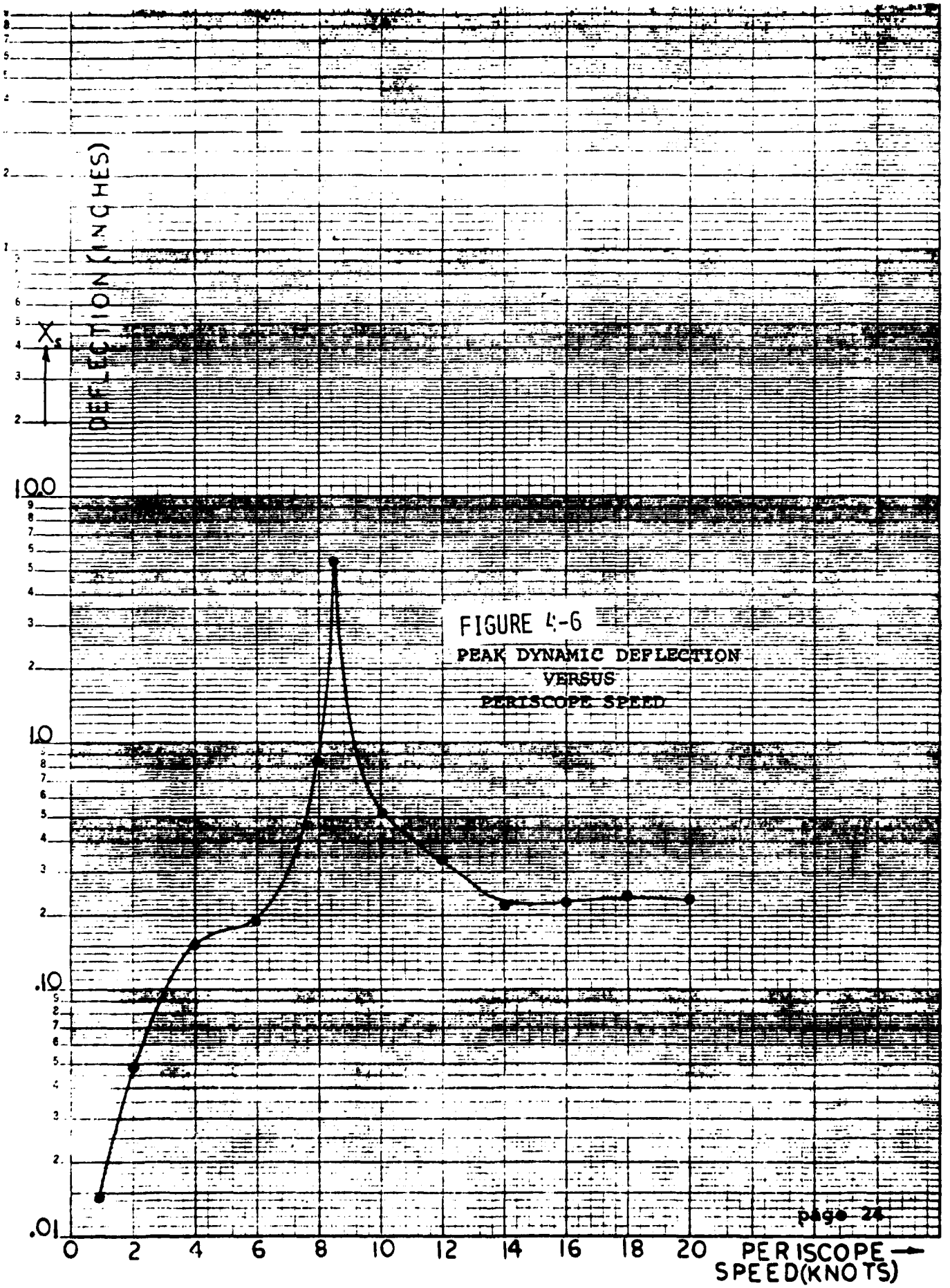

FIGURE 4-6
PEAK DYNAMIC DEFLECTION
VERSUS
PERISCOPE SPEED

page 24

4-2 STABILIZATION INVESTIGATION -- DESIGN CONCEPTS

The theoretical analysis in Paragrpah 4.1 provides an understanding of the forces on a periscope and the resulting deflections. Analyzing thses deflections, under both static and dynamic conditions using the type 16 periscope with a 19 foot mast extension as a model provides an order of magnitude of ranges for designing stablization concepts. This generalization of ranges permits the application of these concepts to a series of different periscopes at various mast extensions.

4.2.1 Single Axis vs. Two-Axis Correction

The first consideration is to determine the difference between single axis correction (along the viewing axis) and two axis correction (along the viewing axis and along a mutually perpendicular axis in the horizontal plane). A two axis compensation is obviously more complicated and requires more space, therefore, the following analysis is to determine the nature of the errors induced by limiting the compensation mechanism to a single axis.

The follow assumptions are made about periscope motion through a range of vehicle velocities:

a) The static deflection occurs only in the fore and aft

direction due to steady viscous drag. There may be static deflection athwart ship induced by the periscope rotation causing a lift force producing static deflection at 90 degrees to the vehicle motion. The athwart ship static deflection is considered secondary to the fore and aft static deflection and is described at this time for consideration in future studies, but not included in this analysis.

b) That vibration occurs in the fore and aft direction as well as the athwart ship direction. It is assumed that the athwart ship vibrational amplitude and frequency is greater than the fore and aft vibrational amplitude and frequency.

To indicate the change in camera scene as a function of periscope position, Figure 4-7 shows the monitor display at discrete positions versus a plan view of periscope tip excursions. In this figure the camera position is held fixed in the same direction as the vehicle and the scene displayed on the monitor is the horizon at various periscope positions. The display shows the scene uncompensate for motion and for single axis compensation along the viewing axis. A two axis compensation would indicate the horizon as a horizontal line across the center of the monitor for all periscope positions. This analysis is idealized to consider the compensation system error as zero.

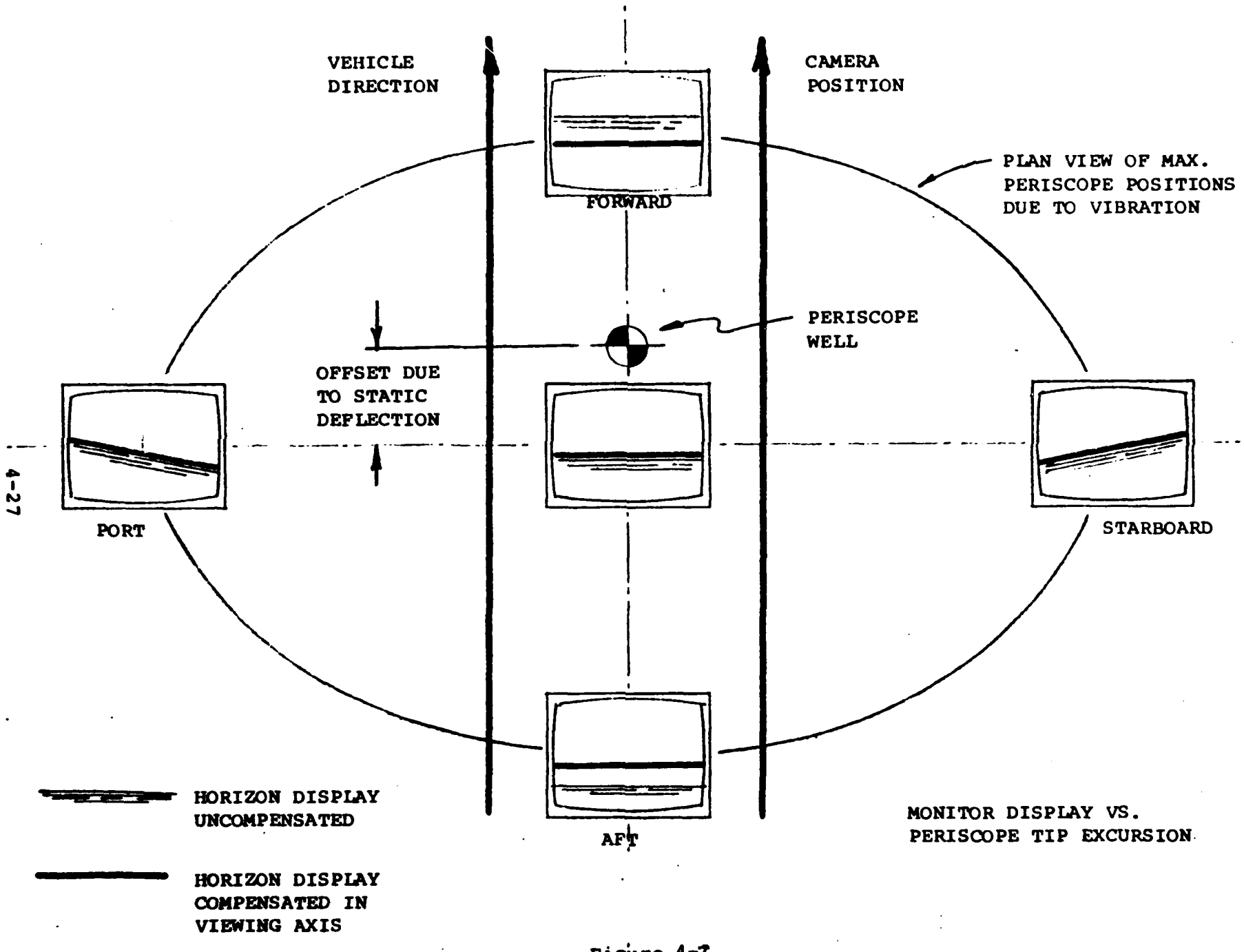
VEHICLE DIRECTION
CAMERA POSITION
PLAN VIEW OF MAX. PERISCOPE POSITIONS DUE TO VIBRATION
FORWARD
PERISCOPE WELL
OFFSET DUE TO STATIC DEFLECTION
PORT
STARBOARD
AFT
HORIZON DISPLAY UNCOMPENSATED
HORIZON DISPLAY COMPENSATED IN VIEWING AXIS
MONITOR DISPLAY VS. PERISCOPE TIP EXCURSION

Figure 4-7

The display for an uncompensated periscope camera shows the view of the horizon is subjected to both vertical translation and rotation. The magitude and frequency of the translation and rotation is a function of vehicle velocity. If the vertical angular velocity of the periscope tip is within the range of the CCD camera to sense the scene, then the resulting panoramic display will show undulations of the horizon at various frequencies. If the angular velocity exceeds the CCD camera range for sensing, then a loss of picture information will occur. The single axis correction serves to keep the horizon view stable at the center of the screen, however, the scene is still subjected to rotation. This compensation will thereby reduce the apparent vertical angular rotation and increase the operational range of the CCD camera.

Figure 4-8 shows the monitor display versus periscope tip excursion when the camera position is held fixed at a position is held fixed at a position 90° from the vehicle motion. A new series of monitor scenes are developed and the analysis is the same as previously stated. A variety of displays are generated as the camera rotates from o to 360 degrees and the vibrational amplitudes change as a function of vehicle velocity, making the mathematical analysis extremely difficult. Therefore it is suggest the analysis be based on test stand data, where the CCD camera is subjected to rotation and translation during the scanning period. By

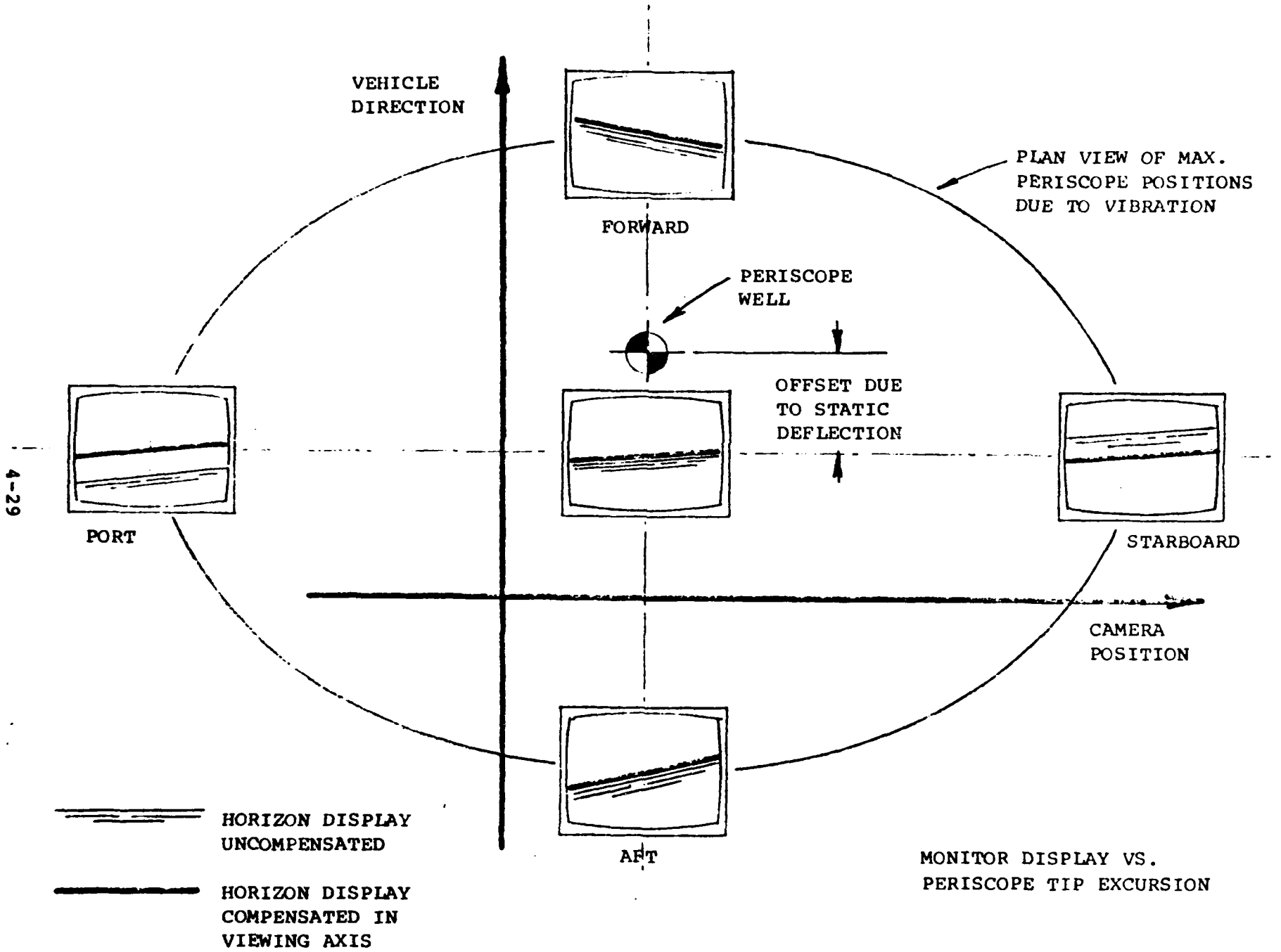
VEHICLE DIRECTION
FORWARD
PLAN VIEW OF MAX. PERISCOPE POSITIONS DUE TO VIBRATION
PERISCOPE WELL
OFFSET DUE TO STATIC DEFLECTION
PORT
STARBOARD
CAMERA POSITION
AFT
HORIZON DISPLAY UNCOMPENSATED
HORIZON DISPLAY COMPENSATED IN VIEWING AXIS
MONITOR DISPLAY VS. PERISCOPE TIP EXCURSION

Figure 4-8

varying the amplitude and frequency the range of camera performance can be determined. By analysis this range of performance can be correlated to vehicle velocity.

4.2.2 Sensor Considerations -- Stabilization System

An objective of this study is to control the smallest optical path element for compensation of periscope motion, by rotating the element as a function of the periscope angular position as a result of bending. The direct method of compensation consists of sensing the angular deflection of the periscope tip and using the signal to position the optical element to an equal angle in the opposite direction. The indirect methods consist of sensing either the angular velocity or the horizontal linear acceleration of the periscope tip and relating these measurements to the periscope angular deflections. Single integration of the linear acceleration is not recommended as a systems approach, because large commulative errors are encountered. A systems approach based on peak amplitude detection and/or frequency monitoring would seem to be more reasonable.

a) Angular Measurement - The range of frequency response

required precludes the use of pendulus transducers for sensing vertical. A two-degree of freedom gyro may be used to establish a vertical reference and provides signals which can be used to position an optical element for motion compensation. While this direct approach, angular measurement, is most desirable the trade-off factor is the space required for this system. The system consists of the gyro and a position servo for compensation. The cperational considerations are that the vertical reference must be established for the gyro wheel is brought up to speed and the time to establish this reference is a function of the power available.

b) Angular Velocity Measurement - The angular velocity can be measured by using a rate gyro as the sensor. The rate gyro is spring-constrained gyro which is smaller and less complex than the position gyro. The relationship between the angular velocity and the angular position of the periscope tip must be determined, for a particular periscope, to provide the "calibration" for the compensation system. The frequency response of the angular gyro is a function of the gyro range, i.e. the higher the range the higher the natural. Calculations, based on the type 1[illegible] periscope with a 14 foot mast extention, indicate that rate gyros has sufficent dynamic range to be considered as a method of compensation.

c) Linear Acceleration Measurement - The third method for compensation considered uses the linear acceleration of the periscope tip to determine angular position. As in the case of the rate gyro, the relationship between linear acceleration and angular position of the periscope tip must be determined to provide the "calibration" for the compensation system. The linear accelerometer uses various principles of transduction such as the piezoelectric type, strain gage, etc.. These transducers are small and exhibit a high degree of reliability, therefore should receive primary consideration as a sensor for the compensating system. The disadvantage may be the complexity of the circuitry required to relate the linear acceleration to the angular position.

4.3 RECOMMENDATIONS

This section describes areas of further investigation of the periscope camera compensation system as a logical extension to this study.

a) Motion Analysis - As a result of a search for pertinent technical papers, several references were identified but not received (see section 5.0 additional references). These papers should be reviewed to provide a more complete understanding of periscope motion, which is essential to the development of a compensation system.

b) Sensor Selection - The three sensors described in this report as potential sensors for compensation, should be evaluated as part of the total system, consisting of sensor, servo circuitry and servo drive. A mathematical systems error analysis and the predicted behavior in this report, will provide a range of performance for the various approaches. The space requirement for each system will establish a size versus performance criteria for system selection.

c) Dynamic Testing - To test sensor performance under dynamic conditions a test stand should be developed to simulate the motion of a periscope tip at various velocities and various mast extentions. To simplify this test stand, rather than vibrating a 14 foot mast, consideration should

be given to a four-bar linkage arrangement which will reduce the size of the test stand and provide greater versatility.

d) Utilizing the CCD Camera View for Compensation - The CCD camera view of the horizon contains the compensation information of vertical translation and rotation of the scene (see Figures 4-7 and 4-8). Further study of this approach is required to determine if this information could be used to a) compensate the picture motion directly in the camera system, or b) provide the sensing for mechanical compensation of an optical element for stabilization. The sensing of the horizon may be accomplished by using a second camera consisting of four vertical line arrays across the field of view and viewing the same scene as the primary camera. The four line arrays would provide the data to logically determine the horizon line. If one array was sensing an anomaly, such as a ship on the horizon, then the remaining three arrays would be use to determine the true horizon line.

e) Simulation of Picture Motion - The testing of the CCD camera performance under conditions of vertical translation and rotation of the scene, during the scanning operation, is essential to determine the degree of accuracy required of the compensating system. The Panoramic Scanning test stand contains manual adjustments to provide translation and rotation. It is recommended that automatic

drives be installed to provide translation and rotation at various amplitudes and frequencies for camera testing. The maximum amplitudes and frequencies can be extrapolated from this current study to simulate various vehicle velocities and mast extentions of the Type 16 periscope.

f) Prediction of Performance Under Operating Conditions

A next phase of study should include the prediction of performance of the compensated CCD camera based on final periscope selection and operating conditions. This study would estimate the velocity ranges (probably off-resonance) in which optimal camera performance can be expected.

SECTION V
DISPLAY RECORD STUDIES

5.0 DISPLAY/RECORD STUDIES

Much work related to display studies is reported in the system tradeoff section (Paragraph 6.2) of this report. More investigation into the matter of an appropriate Dislay/Record system for the panoramic scanner than contained therein, however, was conducted during the program. Many candidates for both real time display and hard copy recording were studied. Three display candidates were also built and tested as part of the scanner hardware system, the most complex of which was funded by Fairchild internal R&D funds. All work indicated strongly that both a "real time" viewing system for tactical scenarios as well as a record mode for "relaxed time" surveillance-reconnaissance scenarios were required. The following paragraphs in this section describe the display/record systems studies during the program. An additional display/record technique, i.e., "stop action" video disk recording was discussed in the referenced LOPATCH proposal recently submitted.

5.1 "REAL-TIME" DISPLAY

The "real-time" display for a CCD panoramic scanner must transform strip mode imagery into a full frame display suitable for viewing and quick reaction by a human observer. In addition to the falling raster and X,Y,Z display techniques constructed for the program, many other display candidates have been studied "on paper", each with its own particular advantage.

5.1.1 "Ping-Pong" Scan Converters

A simplified scheme for displaying the continuous panorama as a succession of frozen frames can be accomplished using two scan

converters. Incoming CCD video lines fill a scan converter memory. While this scan converter is continuously read out into a TV monitor, the second scan converter records the next frame's worth of CCD lines. When the second converter is full, the monitor is switched to its output video. In this way, an observer of the monitor sees successive one-frame pictures which remain stationary for about 0.7 second (depending on panoramic scan rate) and are then replaced by a new picture representating an area of the panorama immediately adjacent to the first. The disadvantage of this scheme as opposed to a falling raster is in the human factors. Switching from successive frames at a rate of 0.7 second each wil' be highly disconcerting to an observer. In addition, targets may occur at the edge of the picture, in the next picture they will be at the opposite edge. This arrangement makes detection amidst excessive noise quite difficult. The use of three or more scan converters could allow successive images overlapped by 1/3 to 1/4 but the frame fall-through rate of 0.7 second, dictated by the panoramic scanning consideration, will result in a very "jerky" picture. The scan converter idea however, is a cost effective, simple display solution.

5.1.2 High Resolution Storage Monitor

High quality storage monitors with good grey scale are currently available for use in medical electronic applications where pictures with resolutions as high as 1000 x 1000 elements are generated in X, Y scan fashion by X-ray or acoustic detectors. These pictures may be slowly recorded, one line at a time, on the monitor, and retained there for study as a full picture is generated. The problem with applying such a technique to the panoramic scanner is that much more than 1000 x 1000 elements of resolution is required to display the entire scanned panorama. For the tactical situation,

however, some recording compromises can be made, e.g., just those pixels surrounding the horizon may be recorded. These could be detected electronically and recorded in bands on the 1000 x 1000 element monitor. Figure 5-1 illustrates such a technique. The entire panorama is slowly built up on a single monitor in 20 bands, each representing a 0.9^{o} by 18^{o} portion of the horizon. The observer sees the entire safety search scan at one time and he has time to react to tactical requirements. In the example shown, 39 pixels from each CCD video line are selected for viewing. These pixels will subtend four hundred vertical feet at a distance of four nautical miles when using a two-inch focal length lens.

Figure 5-2 illustrates a variation on the same technique appropriate for use in a sector scan sweep of only 30^{o} when using an eight-inch lens for precise object recognition. Here, as many as 210 pixels from each CCD line can be selected and retained on the display. Each band covers 6^{o} of the 30^{o} panorama.

5.2 HARD COPY RECORD AND DISPLAY

In appropriate scenarios, a record/playback capability is necessary in the panoramic scanner. This function would give the submariner the ability to play back and review in "relaxed time" the imagery acquired in the rapid scan pan. This quick look and study function can provide information under all prevailing light conditions from daylight to starlight. Furthermore, for a system requirement greater than 2500 lines, the hard copy provides the means for fully utilizing the information obtained.

The number of pixels chosen for the Periscope E-O System will determine the optimized display and record methods. This number could conceivably vary over a range from 256 to 4096 depending on the

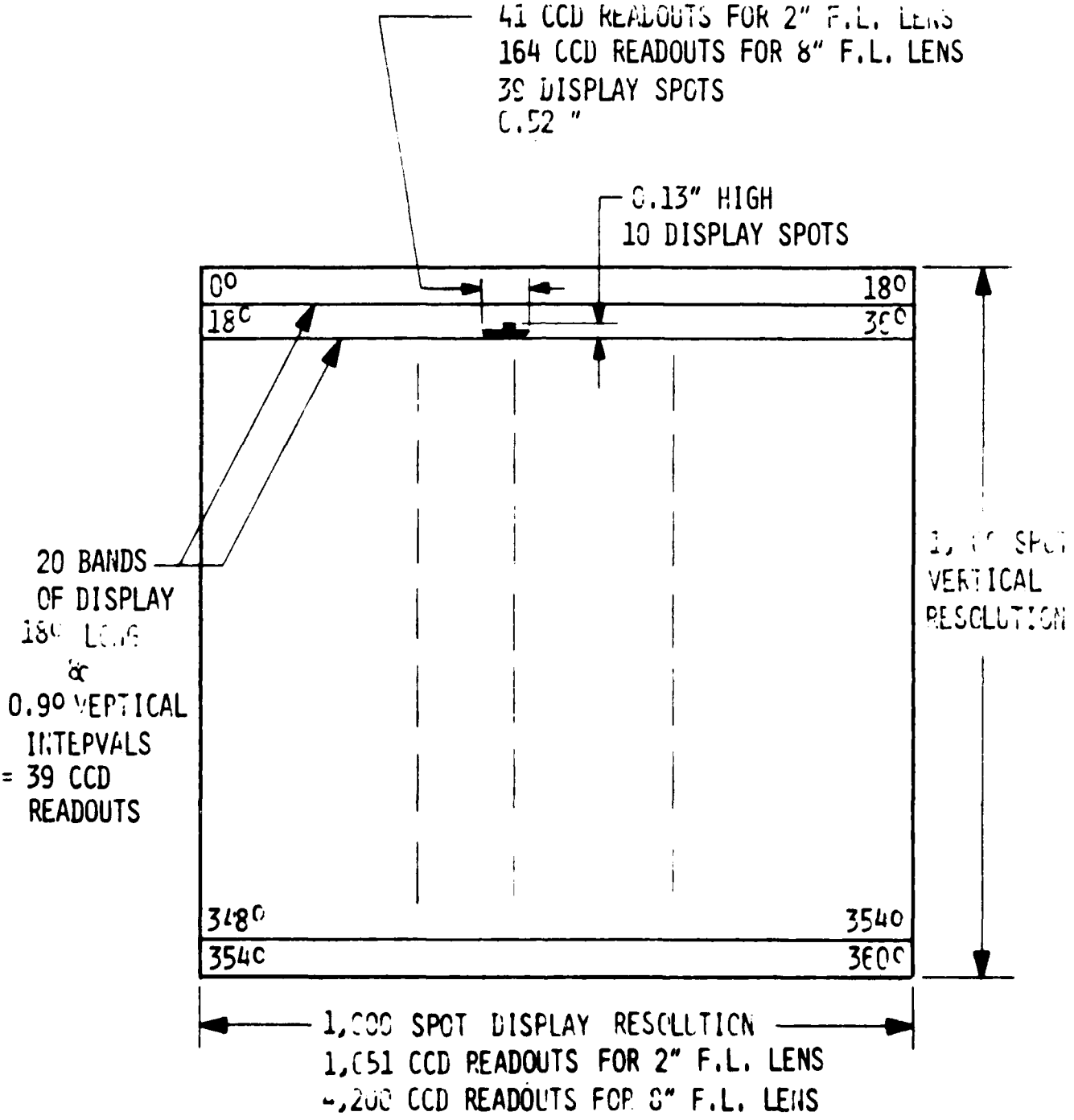

FIGURE 5-1

COMPATIBILITY OF 20 LINE DISPLAY RESOLUTION AND CCD RESOLUTION FOR 400 FOOT LONG X 100 FOOT HIGH TARGET AT 4 N. MILES

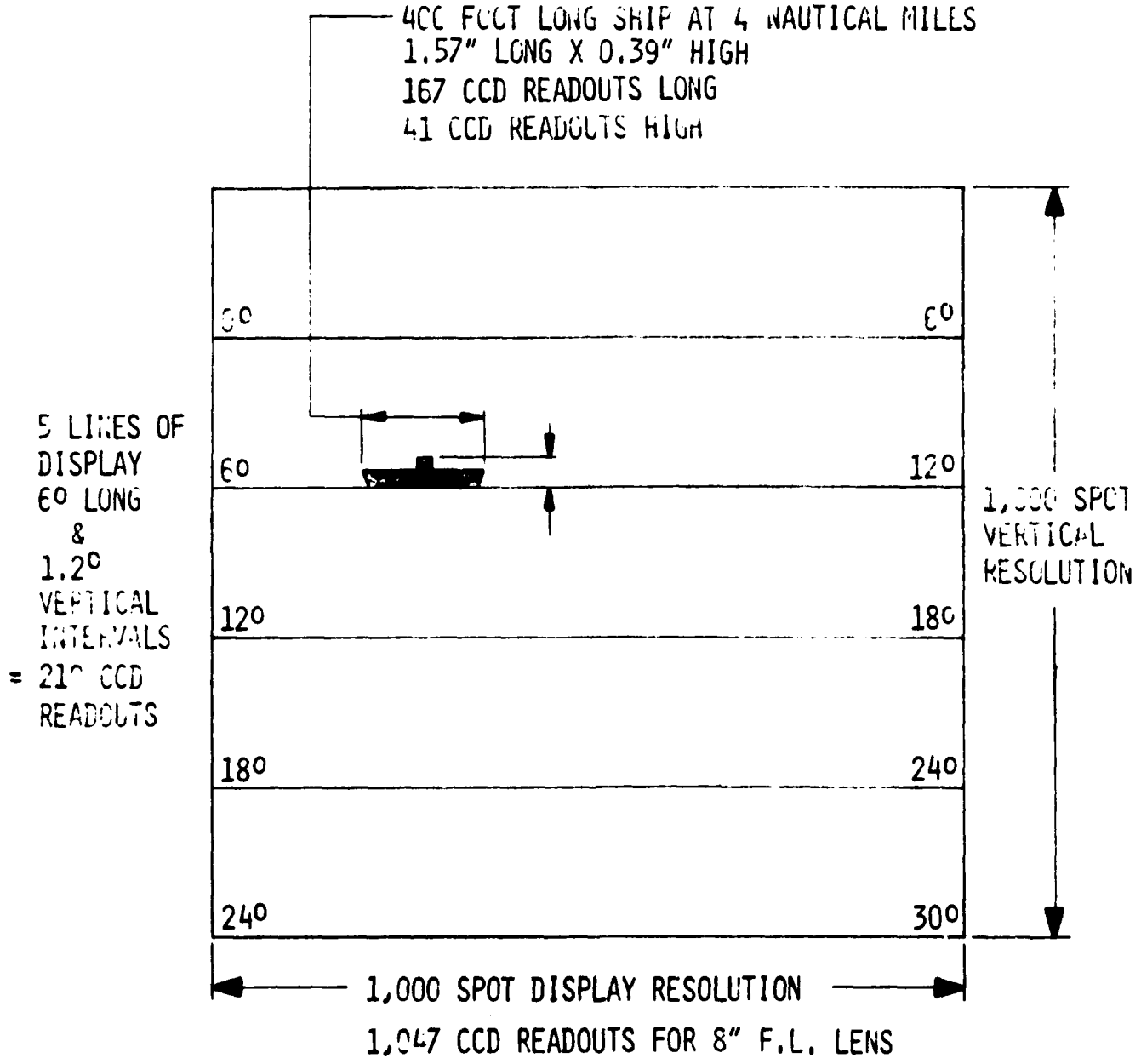

FIGURE 5-2 COMPATIBILITY OF 5 LINE DISPLAY RESOLUTION AND RESULTS WHEN SCANNING 30° SECTOR IN 10 SECONDS TO MAINTAIN LOW LIGHT LEVEL CAPABILITY WHEN USING 8" F.L. LENS

finalized system requirements. Record and display solutions, appropriate to various numbers of pixels, are therefore discussed here.

The record and display systems selected as most appropriate for this application all fulfill the basic criteria of rapid access to the data, small size-weight-power requirements, and highly reliable operation on a day-to-day basis. These recorder possibilities include:

a) Acousto-optically deflected laser beam recording using dry silver film.

b) Light emitting diode printing using dry silver film.

c) Electron beam recording using ESR-1 direct writing film.

For resolutions above 2500 pixels the hard copy recording systems become most attractive. Direct view monitor displays can't handle greater resolution information without some form of zoom mode. With a hard copy system, detailed looks at the entire scene are possible.

5.2.1 Laser Beam Recording

Laser beam recorders using acousto-optical deflection have recently appeared in practical small-sized operating equipment. A block diagram of an acousto-optic laser beam recorder is shown in Figure 5-3.

An incoming laser beam is scanned across the film and modulated with video information. An acousto-optic modulator and predeflector accepts input video and drives the beam. A secondary travelling wave lens system refocuses the deflected laser spot on the film plane.

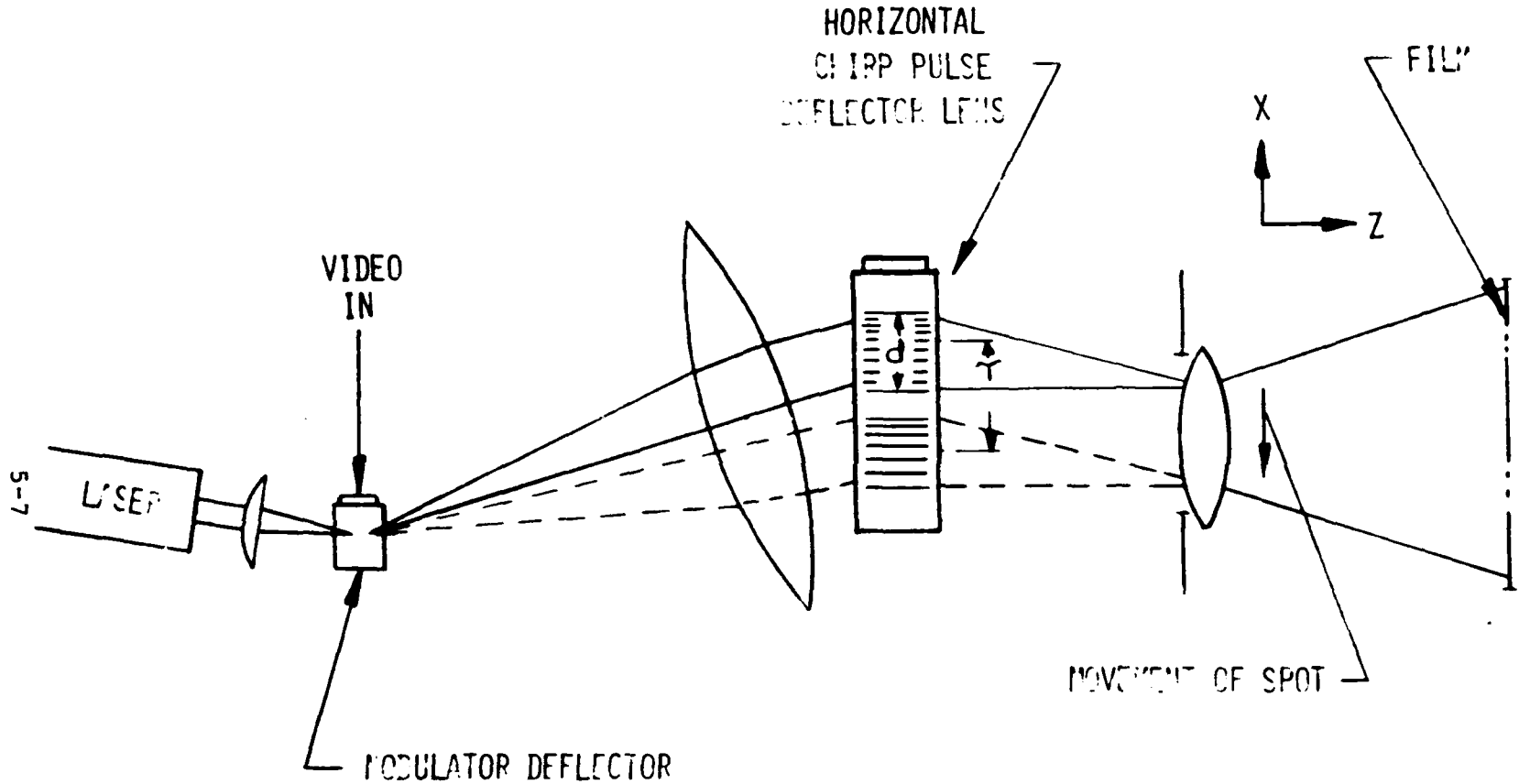

$$= \tau \Delta f$$

$$d \leq \tau$$

FIGURE 5-3 ACOUSTO OPTIC LASER BEAM RECORDER

A laser facsimile machine is made which prints 2048 elements across an 8 1/2" page of dry silver paper. Scan rates are kept low to maintain compatability with telephone lines but line rates up to 15 KHz are possible at data rates to 25 MHz. Console size is typically 19" x 16" x 20". Dry silver film immediately processed by a heated platen, eliminates the need for chemical processing and provides access to the processed film within 10 to 20 seconds after exposure. An image size of 0.001" per pixel allows the use of 70 mm film for up to 2500 pixels. A magnification of 5 times would provide enlargement for comfortable viewing.

Exposure of the dry silver film to a density of 2 requires 1000 ergs/cm^2. If 0.001 square inch of film is exposed for each pixel, the laser power required to expose the film can be expressed as a function of field-of-view and the number of pixels. Assuming an optical efficiency of 25% for the recorder, the locus of points for 15 mw and 10 mw He Ne laser powers as a function of field-of-view and number of pixels are presented in Figure 5-4. Comparing this curve with Figure 6-1 (see System Studies discussion in Section 6) it is seen that 15 mm of laser power is just sufficient to expose film using 2500 pixels and a 36^o field-of-view.

5.2.2 Light Emitting Diode Printers

Light emitting diode printers have potential for this application. In this type recorder the output from each sensor chip would be fed to its corresponding LED Module. An array of these modules equal in number to the CCD chips would then form the total recorder. Such a parallel operating system reduces both band width and exposure of each element. A LED recorder using a 128-element module is currently under development by a major manufacturer. The recorder uses proprietary light pipe techniques to transmit the LED

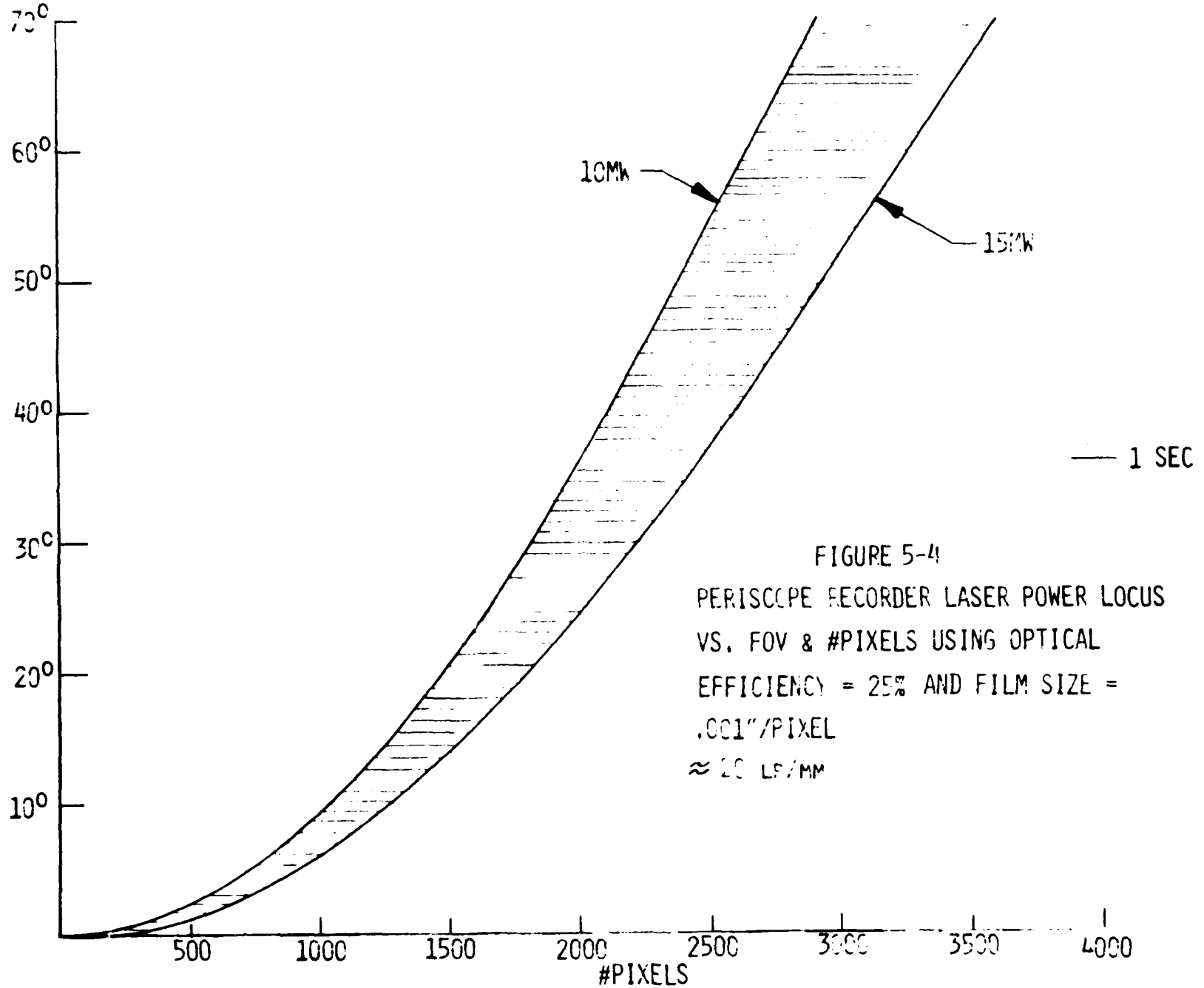

FIGURE 5-4

PERISCOPE RECORDER LASER POWER LOCUS VS. FOV & #PIXELS USING OPTICAL EFFICIENCY = 25% AND FILM SIZE = .001"/PIXEL

≈ 20 LP/MM

light pulses to the film plane. Preliminary calculations indicate that the LED recorder can expose the dry silver film.

5.2.3 Electron Beam Recording

An electron beam recorder also represents a potential solution to this display problem. The recorder may be thought of as a CRT recorder with the film inside the vacuum chamber. A block diagram of a typical electron beam recorder is shown in Figure 5-5. It has a three stage vacuum pumping system. The film chamber has a mild vacuum which is easily pumped and maintained. The extremely high vacuum required for the electron gun and beam path is valved off from the film chamber when film is loaded or removed. Pump-down for operation requires less than five minutes. The electron beam from the gun is deflected by a magnetic system and may paint either a frame or line scanned picture. Kodak ESR-1 film is directly exposed by the electron beam and no further development is necessary. When a ten second scan is completed, the film is removed through an airlock. Calculations indicate that 70 mm ESR-1 film can be exposed with a 0.001" beam producing over 2500 lines for the 36^{o} field-of-view case. The flexibility of the electron beam recorder is its most important attribute; scan rates and pixel size changes are easily accommodated. The film is available virtually as fast as with the laser and LED recorders. The main EBR deficiency is logistic, i.e., operating vacuum must be maintained at all times.

Table 5-1 contains a list of the various recorder manufacturers surveyed during the course of these display configuration studies. Table 5-2 gives specifications and details for several EBR films as well as dry silver film.

Using information pertinent to the state-of-the-art for the various

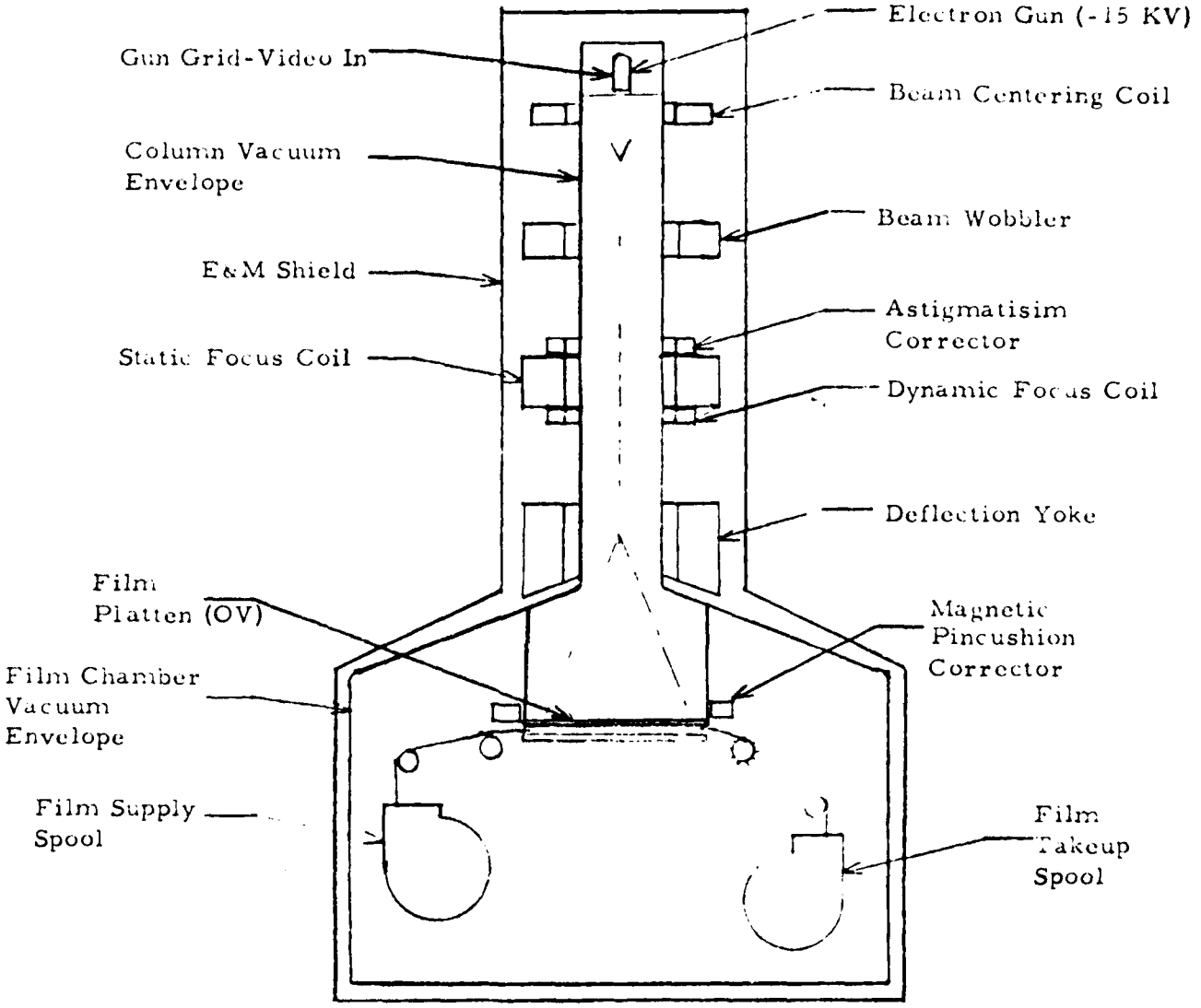

FIGURE 5-5

ELECTRON BEAM RECORDER

ELECTRON OPTICAL SCHEMATIC

TABLE 5-1

RECORDER MANUFACTURERS

LASER RECORDERS WITH MECHANICAL SCANNING

R.C.A.
GOODYEAR
EPSCO

LASER RECORDERS WITH A/O SCANNING

ISOMET
HARRIS
ANDERSON (DATALIGHT)

ELECTRON BEAM RECORDERS

EPSCO
IMAGE GRAPHICS

LIGHT EMITTING DIODE RECORDER

ACTRON

TABLE 5-2

EBR FILMS

So 219	Fine grained Handle in bright yellow safelight Exposure capability 15.6 cm^2/sec (for a density = 2) (100 NA beam) Has conductive coating D-19 5 min at 68°
So 438	Fine grained - 600 lp/mm Somewhat more light sensitiye' Exposure capability 62.5 cm^2/sec. No conductive coating
ESR - 1	Direct electron recording (no development) D max ≈ 1.5 magenta color Not light sensitive No conductive coating Exposure capability 6.25 cm^2/sec (100ua beam) Exposure capability 150 cm^2/sec (2.5ua beam)
3M Dry Silver Electron Beam Sensitive	Heat developed No conductive coating Relatively slow
Electron Resists	
So 214 Reversal	

DRY SILVER FILMS

3M 7869 Film	Red Sensitive Exposure required is 225 ergs/cm^2 Red Sensitive
3M Dry Silver Paper	Exposure required is 175 ergs/cm^2

hard copy recording systems a tradeoff study between systems, against a predefined set of panoramic scanner parameters was performed.

Table 5-3 illustrates the predefined scanner characteristics. A 6° x 360° FOV is assumed along with a line of pixels 2048 long. The same table also lists a series of film size possibilities. These film formats all require a specific spot size in the scanning systems to achieve the resolution of 2048 pixels per line. These resolutions are also listed in the table.

Table 5-4 shows the results of the tradeoff study. Three recorder types are compared against the system requirements. Three requirements for exposure capability are listed. They represent use of 5", 70 mm and 35 mm films respectively. The EBR cannot achieve the exposure required for 5" film The acusto-optic recorder cannot handle the bandwidth or the 5" film. The mechanical LBR can handle the required line rate but a spinner speed of 74,000 RPM is necessary. The tradeoff chart also indicates approximate prices for the three choices as well as relative sizes. Choices of any system will ultimately depend on real scanner requirements, including cost, space, performance, etc.

TABLE 5-3

SYSTEM DEFINITION FOR PERISCOPE SCANNER

FIELD OF VIEW	6° x 360°
PIXELS/LINE	2048
WORST CASE SCAN TIME (360°)	10 SEC
LINE SCAN RATE	12.3 KHz
PIXELS/SEC	25×10^6
VIDEO BANDWIDTH	$\frac{25 \times 10^6}{2} \times 1.25 = 15.6$ MHz

FILM POSSIBLITIES	EXPOSURE RATE
9" USING 8.5" x 60 = 42.5'/SHOT	= 2797 CM^2/sec
5" USING 4.5" x 60 = 22.5'/SHOT	= 783 CM^2/sec
70 MM USING 60 MM x 60 = 3.6M/SHOT	= 216 CM^2/sec
70 MM USING 50 MM x 60 = 3M/SHOT	= 150 CM^2/SEC
35 MM x 60 = 2.1M/SHOT	= 73.5 CM^2/SEC
35 MM USING 25 MM x 60 = 1.5M/SHOT	= 52.5 CM^2/SEC

FILM SIZE	SPOT SIZE	LP/MM
9"	≈ 111 UM	4.5
4"	≈ 50 UM	10
70 MM	≈ 30 UM	14.6
50 MM	≈ 25 UM	20.0
35 MM	≈ 17 UM	29.2
25 MM	≈ 12 UM	41

TABLE 5-4

PERISCOPE LBR - EBR TRADEOFF STUDY

	EBR	MECHANICAL SPINNER LBR	ACOUSTO-OPTIC LBR
15.6 MHz Bandwidth	Yes	Yes	Yes
2048 Pixels/Line	Yes	Yes	Yes
12.3 KHz Scan Rate	Yes	Yes (74,000 RPM)	Yes
25 MHz Pixel Rate	Yes	Yes	No
619 cm^2/sec Exposure	No	Yes	No
150 cm^2/sec Exposure	Yes	Yes	Yes
52.5 cm^2/sec Exposure	Yes	Yes	Yes

Suggests not possible with Acousto-Optic LBR
Possible with 25 mm EBR using S0438 film
Requires removal for development and a light table/microscope viewer
Possible with 50 mm EBR using ESR-1 film

Using four 512 devices in parallell you can reduce scan rate by using a four a beam LBR.

	EBR	MECHANICAL LBR	NO LBR
Cost Qty 1	$150K	$150K	$50K→150K
Size	2 Relay Cabinets	2.5 Relay Cabinets	1.5 Relay Cabinets

SECTION VI

6.0 SYSTEM DEFINITION STUDIES

System definition studies conducted during the course of the program included tradeoff studies, optical/mechanical layouts relating to type 16 periscope, and preliminary performance analyses.

6.1 TRADEOFF STUDIES

A series of system studies were performed during the course of the Periscope Program. These studies helped to define important variables and serve to aid in visualizing potential modes of scanner operation. The studies were also intended to help define operational areas in which the periscope scanner would have most application. At the time of this writing, the evolution of Fairchild's system studies of the panoramic scanner has far outdistanced much of the preliminary studies. This work, while sometime drifting astray, in retrospect, is what crystallized today's viewpoint and is presented for completeness in this section. Fairchild's latest conceptions regarding the optimum scanner configuration, is presented in our referenced LOPATCH Proposal.

6.1.1 Operational Assumptions

The specific display configuration is dependent on the operational requirements which will be addressed in the proposed Phase II program. Several parameters are assumed, however, for the following discussions. Consider that a limiting resolution of 12 feet per pixel pair at 4 nautical miles (24,000 feet) has been selected based on "detection" criteria. Also assume the following: The integrating CCD arrays being used have an element pitch of 20 um

(.0008"), the quick up-scan-down time is set at 10 seconds (36°/second) and both "real time" and "relaxed time" display modes are desired.

6.1.2 Real Time Display

The number of pixels and the lens field of view combine to determine the periscope sensor resolution. Figure 6-1 shows a plot of lens field of view in degrees vs. number of pixels for fixed resolutions of 10, 12, and 13 ft/pixel pair. The shaded area between these loci represents a potential range of operation for the CCD Periscope camera. These curves represent fixed focal lengths of 3.8", 3.15", and 2.9" respectively. The resultant line rates are also fixed for each curve at 3016, 2513, and 2320 lines per second. In turn, the fixed focal lengths result in fixed array exposure times of 0.04, 0.051 and 0.055 sec. respectively. In addition, similar curves are plotted for resolution of 20 and 60 feet per pixel pair.

Using a constant rotational scan rate of 36°/sec. and, as variables, the field of view and the number of pixels, plots of constant bandwidth at 1 MHz and 5 MHz are presented in Figure 6-2. The shaded area between these curves represents a good operating range for most TV type displays and a comfortable range for recorders. An examination of Figures 6-1 and 6-2 shows compatibility when less than 3000 pixels are used. Bandwidth is approximately:

$$BW = \frac{360^\circ \quad \text{No. Pixels}^{\,2}}{(\text{FOV}^\circ)\ (10\ \text{sec})\ \ (2)}$$

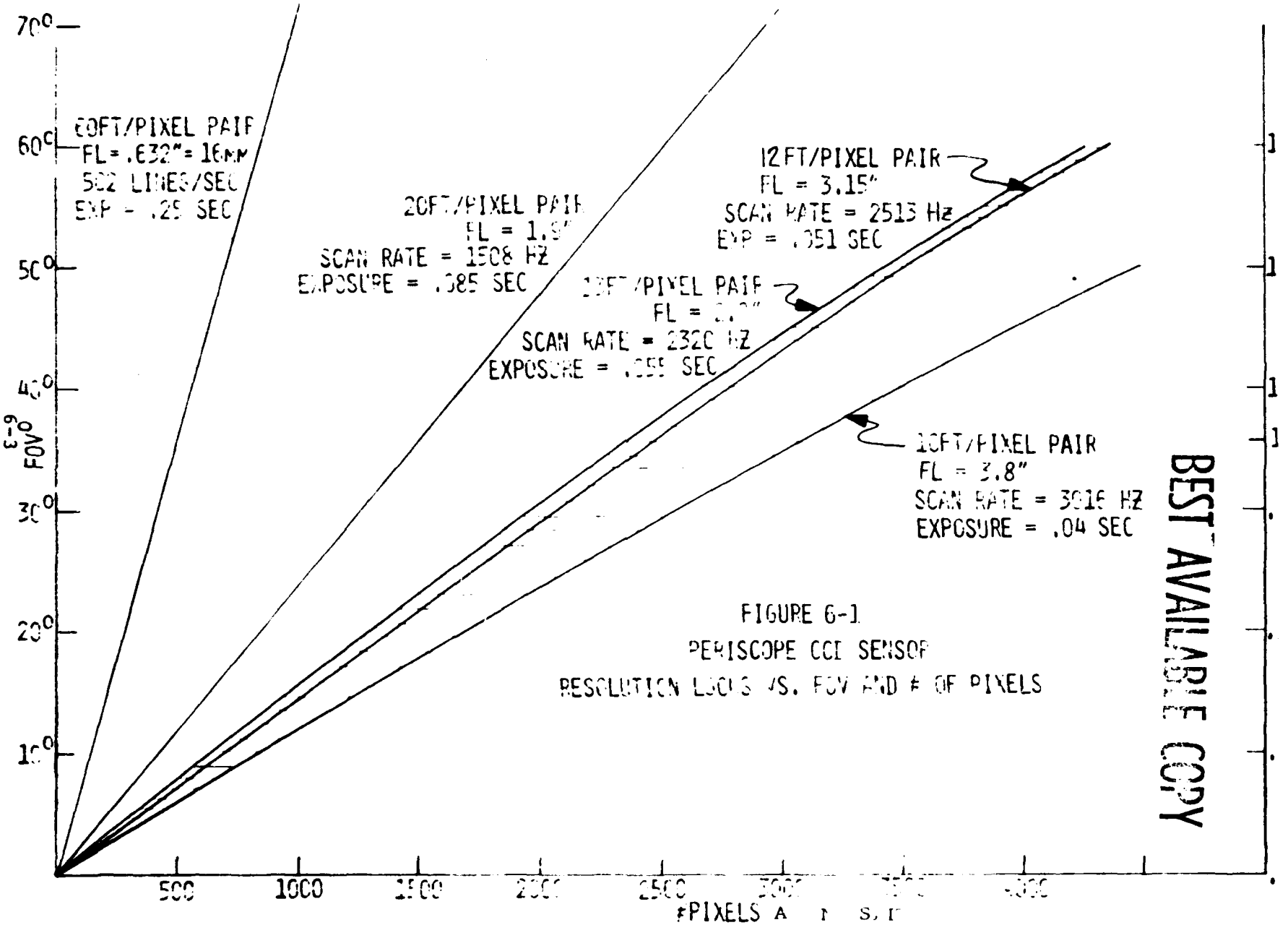

FIGURE 6-1

PERISCOPE CCI SENSOR

RESOLUTION LOCUS VS. FOV AND # OF PIXELS

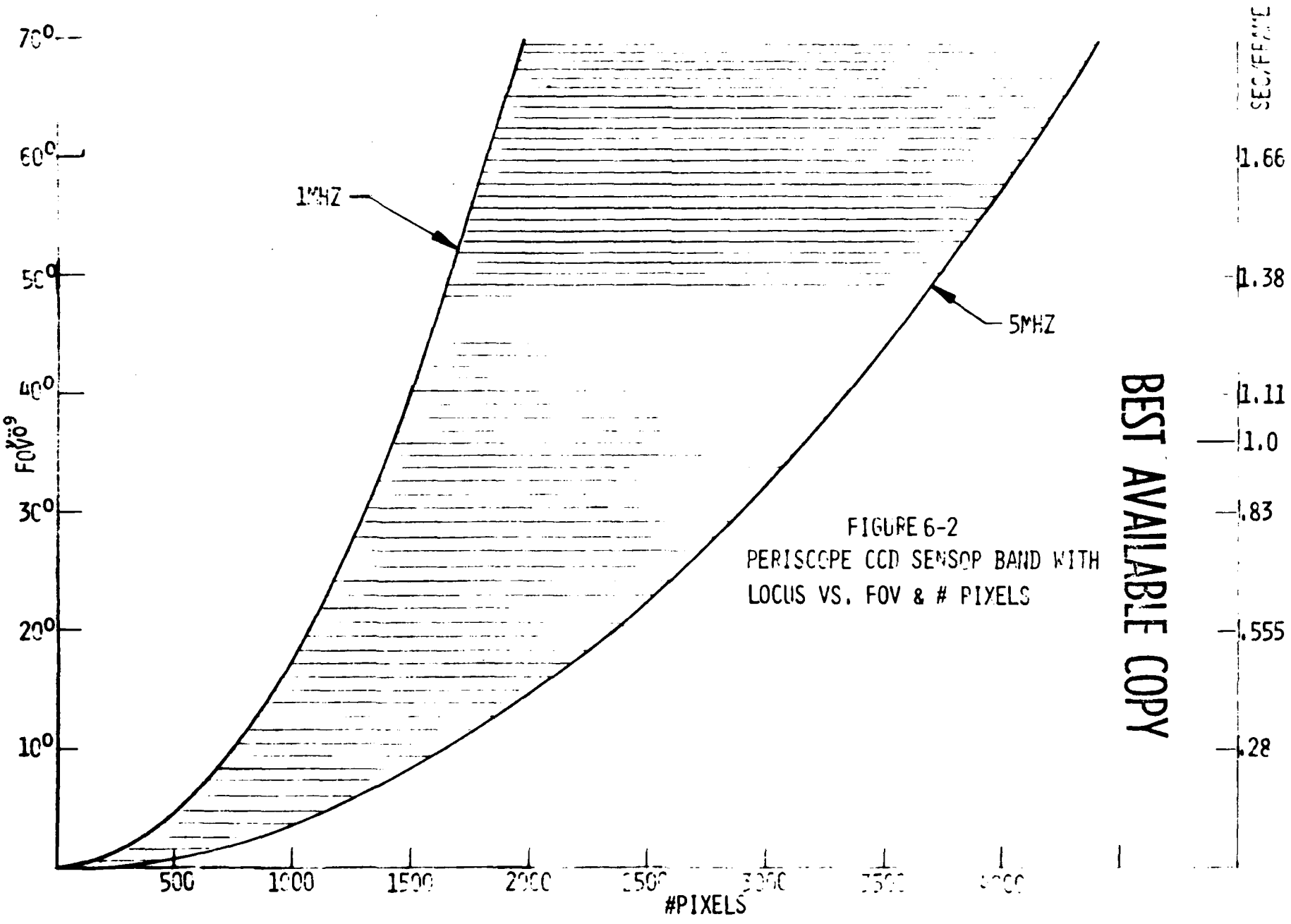

FIGURE 6-2
PERISCOPE CCD SENSOR BAND WITH
LOCUS VS. FOV & # PIXELS

where:

BW = data rate in Hz
FOV° = sensor field of view in degrees
No. Pixels ^{2} = the number of pixels/square frame

The number of integrations in the example is 128.

The right hand scale of Figure 6-2 shows the frame time, in seconds per square frame as determined by the field of view. As seen, a 36° field of view is required to achieve a frame "fall through" time of one second as well as CCD arrays of 2500 elements and over.

The real time direct view system, therefore, dominated by the "fall through" time of approximately one second and an approximate 2500-3000 line CRT display capability, establishes the field of view at about 36°.

As we have seen from this example, a resolution requirement (12 ft./pixel pair at 24,000 ft.) results in a fixed focal length of 3.15", a fixed line time of 2513 lines per second and a fixed array exposure time of .051 second. Increasing the number of pixels is seen to increase the field of view and the bandwidth requirements. Increasing the field of view increases the time per square frame.

Based on experience with the Fairchild prototype falling raster display it is estimated that an observer can detect targets on the horizon in about one second. The presence of the horizon helps to orient the observer and facilitate this search time. One second also corresponds to the frame time for a periscope observer with a 36° . V scanning the horizon at the proposed rates.

In order to achieve a one second frame time a 2500 element array and display scheme is necessary for the 12 ft./Pixel pair case. (Fig. 6-1) The observer sees the video from a 36° field of view with 2500 elements of resolution. To fully utilize this display, human factors must also be considered. The human eye can resolve 0.3 milliradians. If a 15-inch working distance from the monitor is used, the proper monitor size becomes about 12-inches. From 15 inches the monitor subtends a 40° angle.

Several monitor types are currently made with circular screens of 7" diameter and a .002" spot size. With a 5" square inscribed in this circular monitor, 2500 lines resolution performance is possible. A 2.5 X magnifier viewer would be required, however, to exactly simulate the 12-inch monitor examples discussed.

Different combination of scanner parameters have also been examined. The curves shown in Figures 6-3 and 6-4 deal, in general, with the system implication associated with using fixed focal length lenses of 2" and 8". Figure 6-3 plots target range versus resolution for each focal length; the effects of the horizon are neglected.

Figure 6-4 plots the number of pixels (each 20 μm) required to achieve vertical coverage of 500 and 100 feet as a function of target range for each focal length. At four nautical miles, when using a 2 inch lens, only 50 pixels are required to achieve a 500 foot field of view.

The curve in Figure 6-5 makes more assumptions. Here 1024 pixels/line are assumed as well as 128 lines of integration, 36° per second scan rate and 4 nautical mile range to target. The curve relates a) sensor field of view; lens focal length; and feet per pixel pair to b) array integration time, time for 1024 x 1024 frame and the required pixel clock frequency. From this data the effect of varying

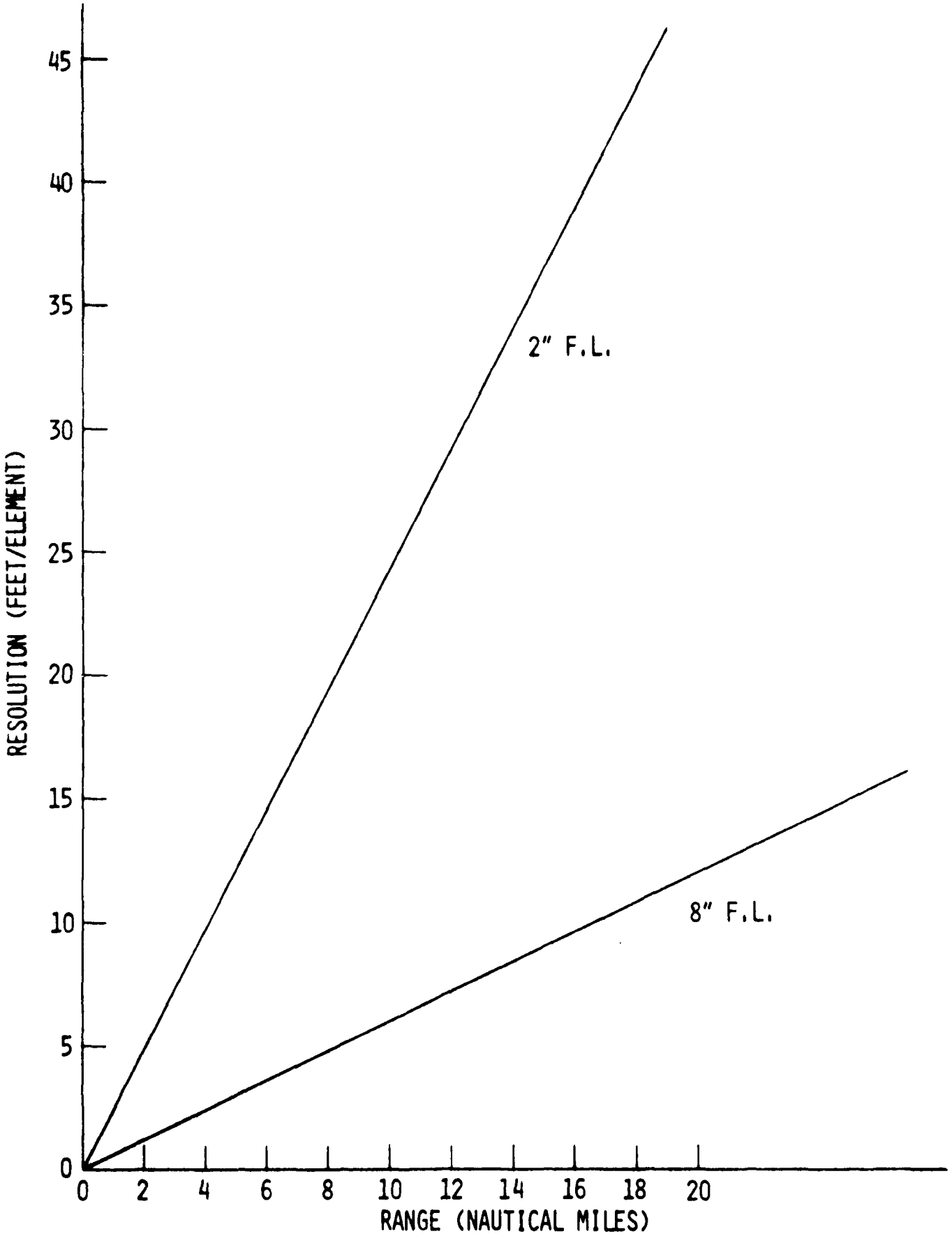

FIGURE 6-3 SYSTEM HORIZONTAL & VERTICAL RESOLUTION

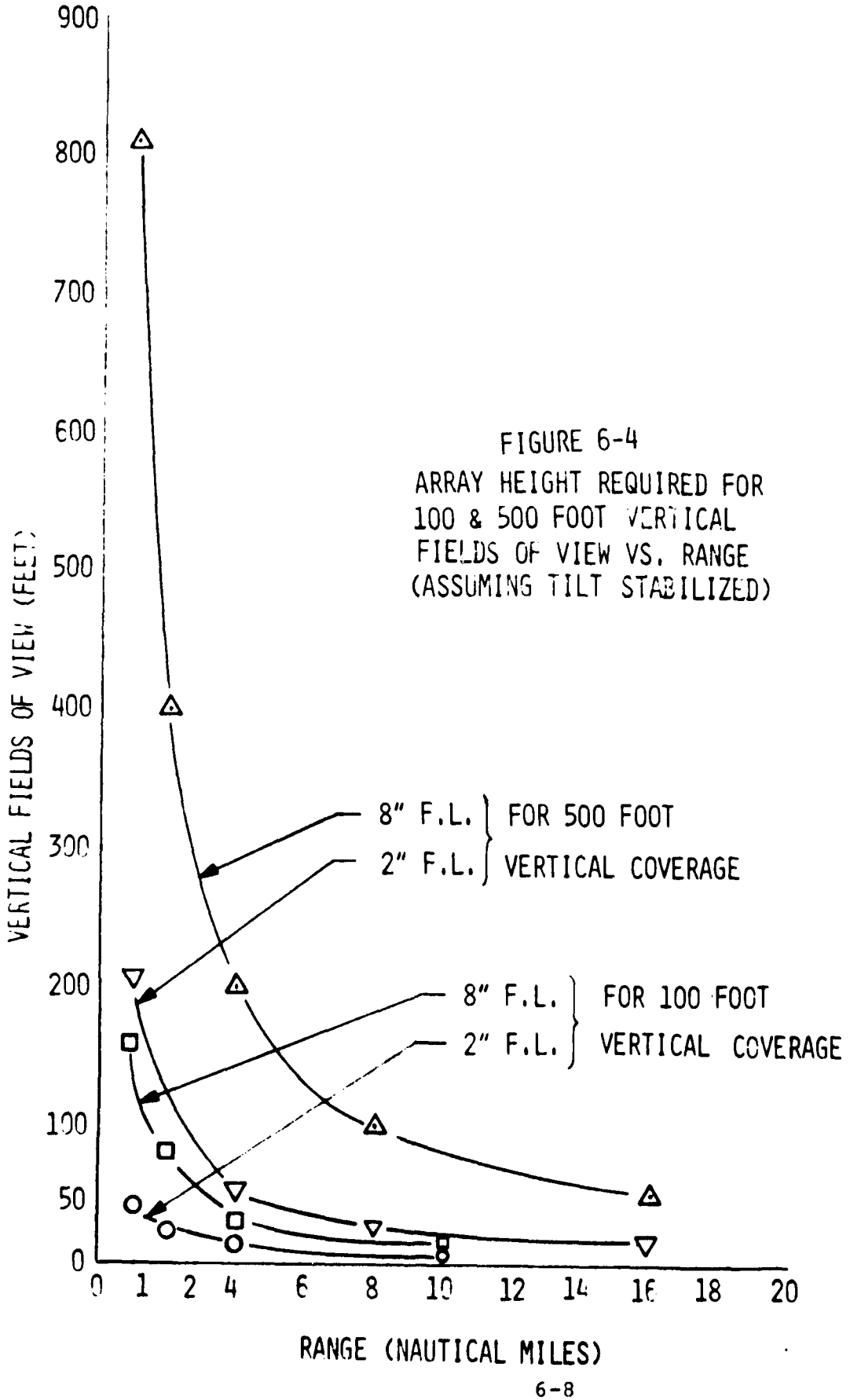

FIGURE 6-4
ARRAY HEIGHT REQUIRED FOR
100 & 500 FOOT VERTICAL
FIELDS OF VIEW VS. RANGE
(ASSUMING TILT STABILIZED)

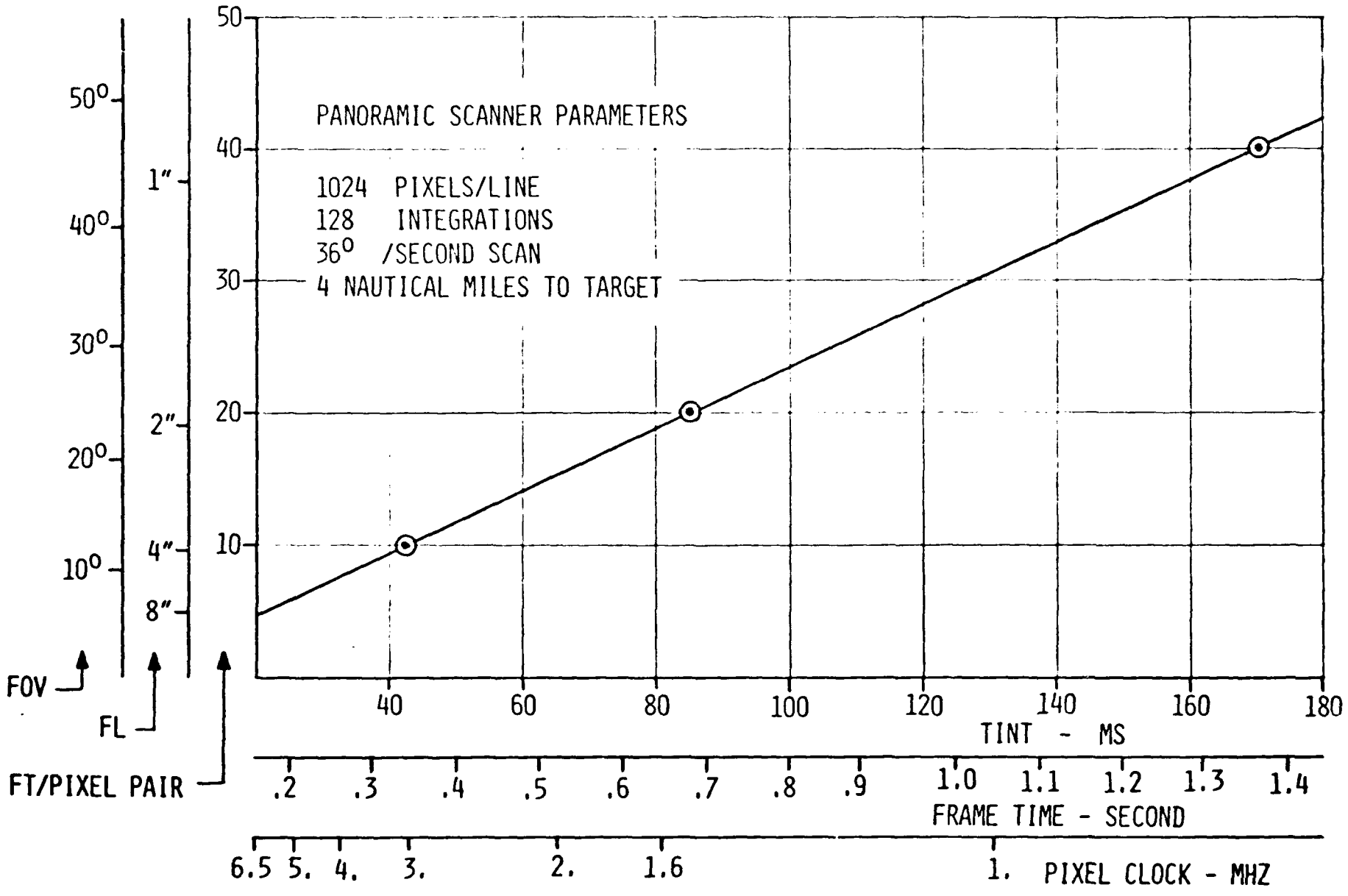

FIGURE 6-5 SYSTEM PARAMETERS

any of the six parameters can be determined. For example, increasing lens focal length increases the required bandwidth, reduces integration time, reduces the frame fall-through time, increases resolution and decreases the field of view. This figure represents a good tradeoff chart for a typical CCD scanner application.

6.2 OPTICAL/MECHANICAL CONFIGURATION STUDIES

In the early phases of the CCD Periscope Program several layout investigations were performed in package volumes that would mount on top a periscope mast as shown in Figure 6-6. These investigations generated three basic approaches that were labelled a) independent window (non-folded optics) b) common window (non-folded optics) and c) independent window (folded 20 focal length optics). Simplified representations of these configurations are shown in Figure 6-7. The layouts for the three cases are shown in Figures 6-8, 6-9, and 6-10.

Each arrangement was determined to have large implications in terms of mechanical constraints posed by the periscope. These investigations, therefore, were directed to be curtailed at this point until clarification of contraints were resolved.

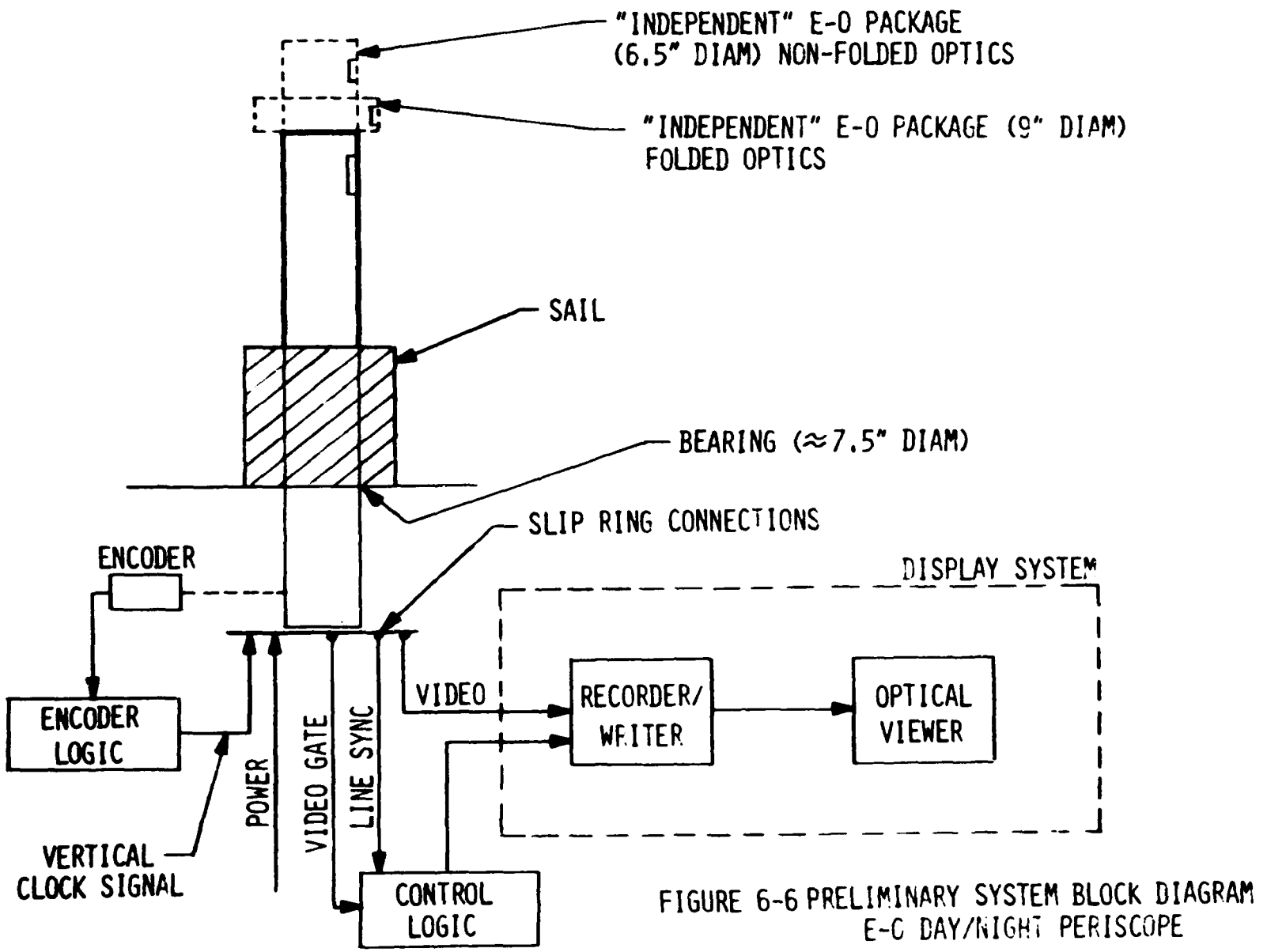

FIGURE 6-6 PRELIMINARY SYSTEM BLOCK DIAGRAM
E-O DAY/NIGHT PERISCOPE

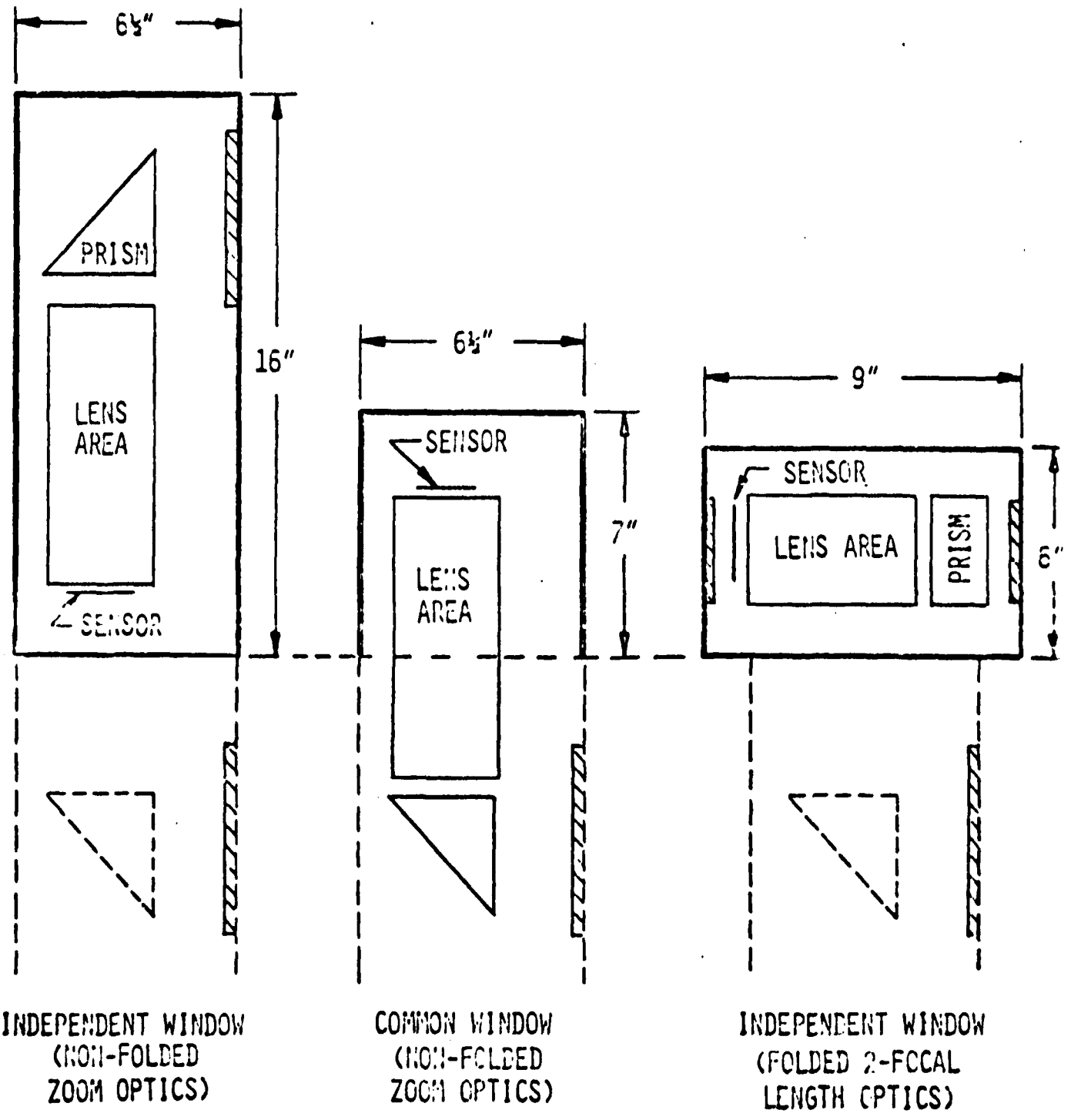

FIGURE 6-7 SIMPLIFIED COMPARISONS OF SEVERAL PRELIMINARY CONFIGURATIONS

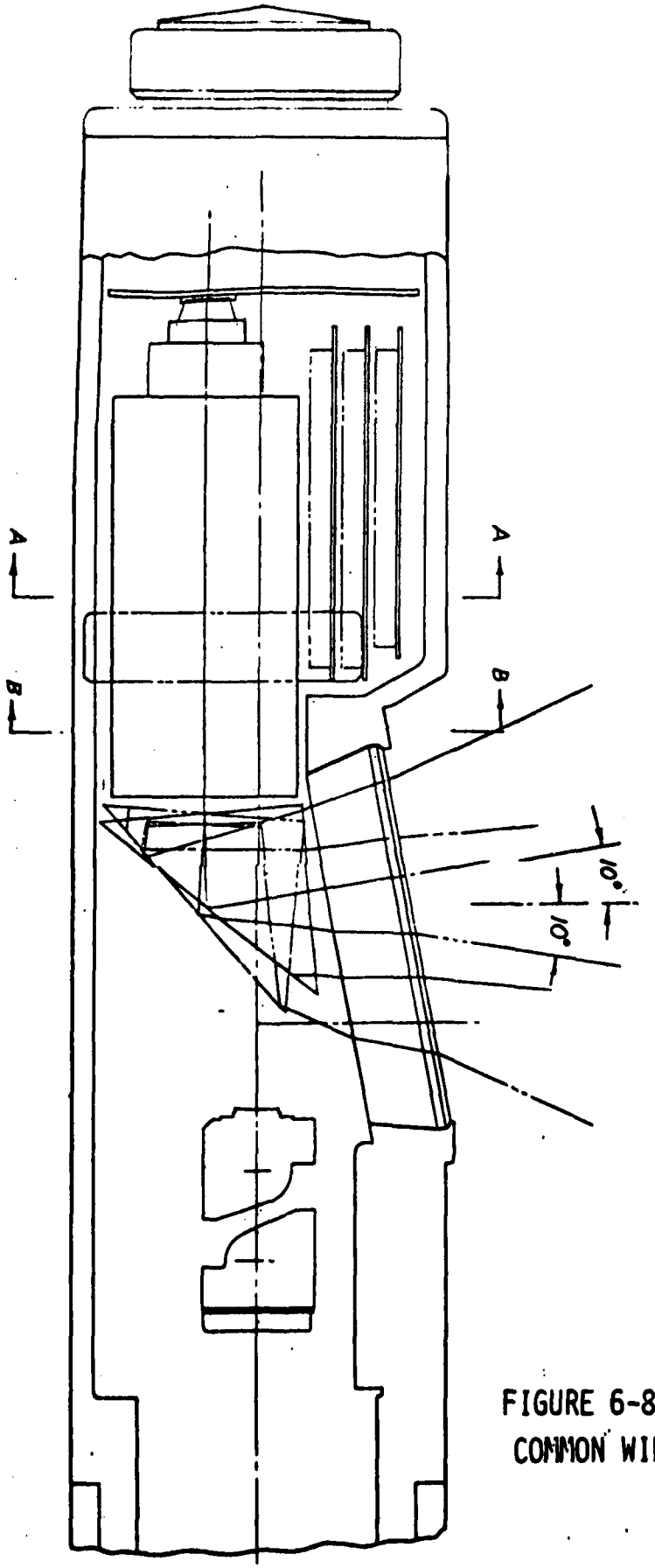

FIGURE 6-8
COMMON WINDOW CONFIGURATION

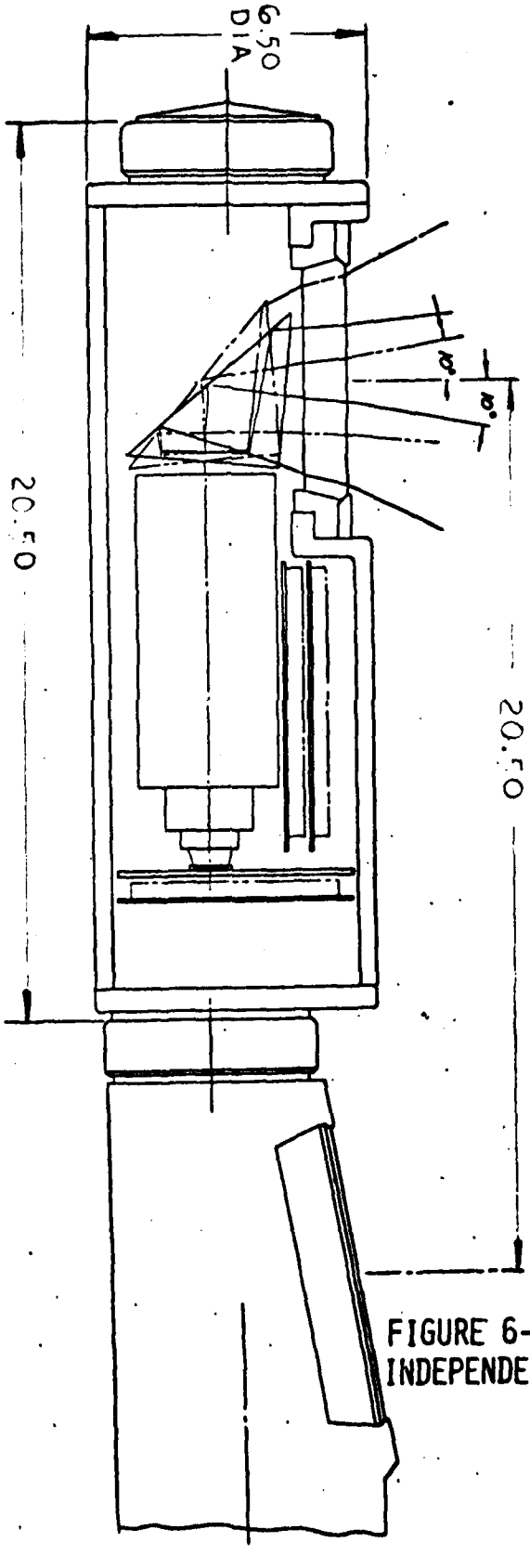

FIGURE 6-9
INDEPENDENT WINDOW CONFIGURATION

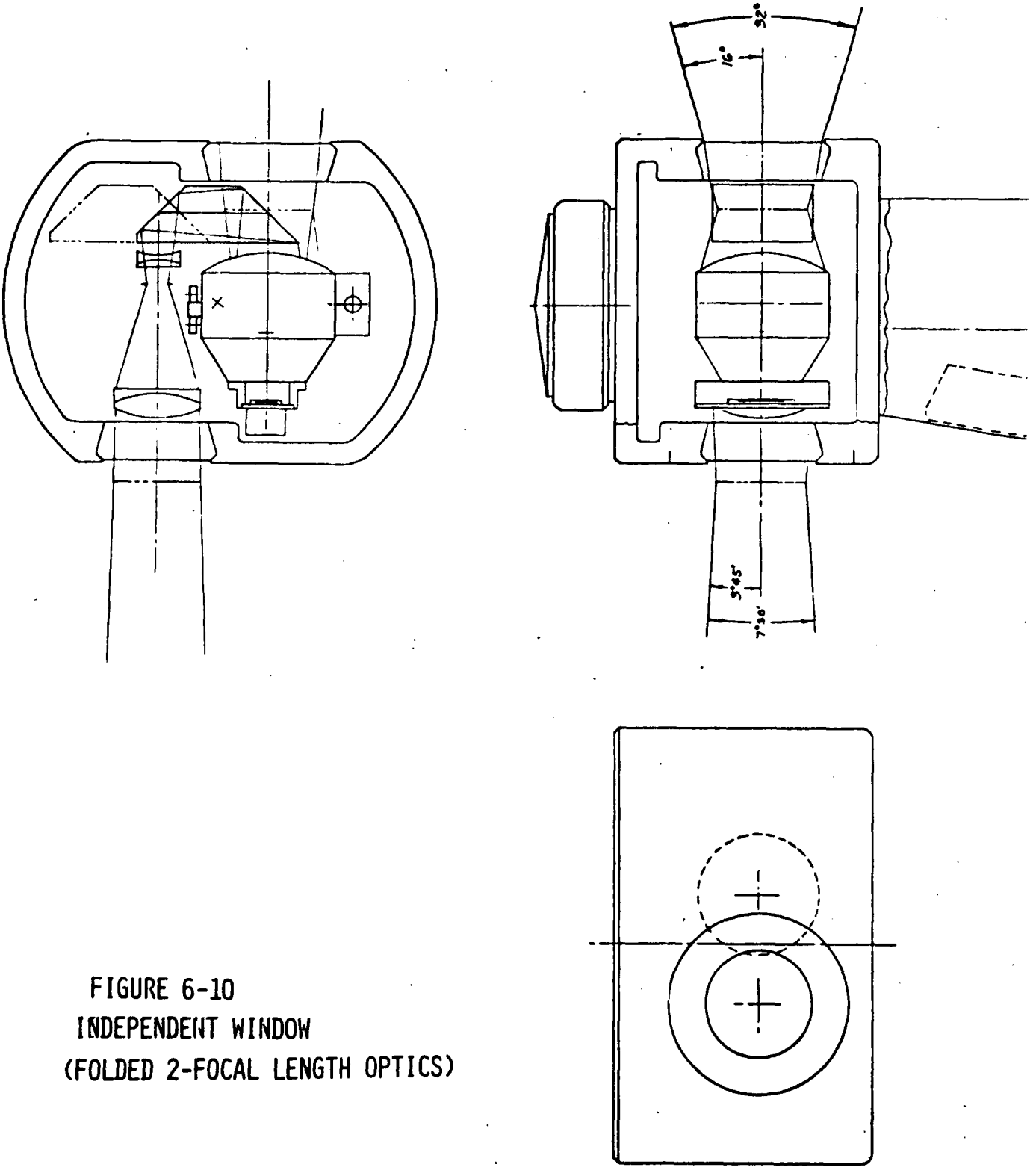

FIGURE 6-10
INDEPENDENT WINDOW
(FOLDED 2-FOCAL LENGTH OPTICS)

References

1) Kilcullen, A. F., 1970 Rewson Periscope Vibration Study. Naval Ship Research and Development Center.

2) Anonymous. Underway Vibration, Stress and Deflection Evaluation Test of Type 8B Submarine Periscope [Summary of Ref. # 3].

3) Anonymous, 1967. Underway Vibration, Stress and Deflection Evaluation Test of Type 8B Submarine Periscope. Sperry Piedmont Co.

4) Anonymous, NUSC, Underway Vibration Tests on Type 15B Periscope Aboard the USS Gato [Summary of Basic Report].

5) Pepi, J. S., 1973. Approximate Stress/Rate Functions for Fully and Partially Submerges Mast.

6) Pepi, J. S., 1973. Investigation of Raising Mast Between 8 and 20 Knots When Completely Submerged.

7) Project Order PO-9-0012. An Electrical Analog Technique for Periscope Response Calculations, March 19, 1969.

8) Ippen, A. T. (Editor), 1966. Estuary and Coastline Hydrodynamics. McGraw-Hill, New York, N. Y., 744 pp.

9) Agerschou, H. A. and Edens, J. J., 1966. Fifth and First Order Wave-Force Coefficients for Cylinderical Piles. Coastal Engineering: Santa Barbara Specialty Conference, Santa Barbara, 1965, pp. 219-248.

10) McCormick, M. E., 1973. Ocean Engineering Wave Mechanics. John Wiley and Sons, New York, N. Y., 179 pp.

11) King, R., 1974. Vortex Excited Structural Oscillations of a Circular Cylinder in Steady Currents. Sixth Annual Offshore Technology Conference, Dallas, 1974, pp. 143-154.

12) Wotten, R. L., 1969. The Oscillations of Large Circular Stacks in the Wind. Proc. Institution of Civil Engineers, 43: 573-598.

13) Laird, A. D. K., 1966. Forces on a Flexible Pile. Coastal Engineering: Santa Barbara Speciality Conference, Santa Barbara, 1965, pp. 249-268.

Additional References

Barnett, K. M., and Cermak, J. E., 1974. Turbulence Induced Changes in Vortex Shedding from a Circular Cylinder. Colorado State Univ. Report.

Bishop, R. E. D., and Hassan, A. Y., 1964. The Lift and Drag Forces on a Circular Cylinder in a Flowing Liquid. Proc. Roy. Soc. (London), Ser. A, 277: 32-51.

Borgman, L. E., 1965. Wave Forces on Piling for Narrow-Ban Spectra. Proc. A. S. C. E., Vol. 91. No. WW3.

Bretschneider, C. L., 1957. Evaluation of Drag and Inertia Coefficients for Maximum Range of Total Wave Forces. Texas A. E. M. Research Foundation Rept. No. 55-6.

Gaither, W. S., and Billington, D. P., 1964. The Dynamic Response of Offshore Structures to Time Dependent Forces. Proc. Ninth Conf. Coastal Engr., Lisbon, 1964, pp. 453-471.

Keulegan, G. H., and Carpenter, L. H., 1958. Forces on Cylinders and Plates in an Oscillating Fluid. J. of Research, 60:5.

King, R., Prosser, M. J., and Johns, D. J., 1973. On Vortex Excitation of Model Piles in Flowing Water. J. of Sound and Vibration, 29 (2): 169-188.

MacCamy, R. C., and Fuch, R. A., 1954. Wave Force on Piles. U. S. Army Beach Erosion Board, Tech. Mem. 69.

Pierson, W. J. and Holmes, P., 1965. Irregualr Wave Forces on a Pile. Proc. A. S. C. W. Vol. 91. No. WW4.

Wang, H., 1970. Loadings on Large Piers in Waves and Currents. Proc. Twelfth Conf. Coastal Engr. Washington, D. C., pp. 1491-1512.